SPHERICAL TANKS FOR USE IN THERMAL ENERGY STORAGE SYSTEMS

By

Fahad A. Khan

A Dissertation

Submitted to the Faculty of

WORCESTER POLYTECHNIC INSTITUTE

In partial fulfillment of the requirement for the

Degree of Doctor of Philosophy

in

Mechanical Engineering

April 2015

APPROVED:

Professor Brian Savilonis Advisor	Professor Ivana Milanovic Committee Member
Professor John Sullivan Committee Member	Professor Fiona Levey Committee Member

Dr. Raghvendra Cowlagi
Graduate Committee Representative

Abstract

Thermal energy storage (TES) systems play a crucial part in the success of concentrated solar power as a reliable thermal energy source. The economics and operational effectiveness of TES systems are the subjects of continuous research for improvement, in order to lower the localized cost of energy (LCOE).

This study investigates the use of spherical tanks and their role in sensible heat storage in liquids. In the two tank system, typical cylindrical tanks were replaced by spherical tanks of the same volume and subjected to heat loss, stress analysis, and complete tank cost evaluation. The comparison revealed that replacing cylindrical tanks by spherical tanks in two tank molten salt storage systems could result in a 30% reduction in heat loss from the wall, with a comparable reduction in total cost.

For a one tank system (or thermocline system), a parametric computational fluid dynamic (CFD) study was performed in order to obtain fluid flow parameters that govern the formation and maintenance of a thermocline in a spherical tank. The parametric study involved the following dimensionless numbers: Re (500-7500), Ar (0.5-10), Fr (0.5-3), and Ri (1-100). The results showed that within the examined range of flow characteristics, the inlet Fr number is the most influential parameter in spherical tank thermocline formation and maintenance, and the largest tank thermal efficiency in a spherical tank is achieved at Fr = 0.5.

Experimental results were obtained to validate the CFD model used in the parametric study. For the flow parameters within the current model, the use of an eddy viscosity turbulence model with variable turbulence intensity delivered the best agreement with experimental results. Overall, the experimental study using a spherical one tank setup validated the results of the CFD model with acceptable accuracy.

In memory of

Professor Oleg Faigel
(1936-2008)

Acknowledgments

I would like to thank my dissertation Advisor Dr. Brian Savilonis for his continuous help, patience, and positive feedback.

I am very grateful for my Master's Thesis Advisor and Committee member Dr. Ivana Milanovic who encouraged me to pursue my Ph.D. research and offered relentless advice and support throughout my journey.

I thank the rest of my Ph.D. dissertation committee members: Dr. John Sullivan, Dr. Fiona Levey, Dr.Cowlagi for taking the time to oversee my progress and provide suggestions and recommendations throughout my research.

Finally, I would like to extend my gratitude to all individuals who directly contributed to this work with their knowledge, insight, services, feedback, and editing: Dr.Adriana Herra, Dr. Ali NematBakhsh, Amir Ghasimi, Dr.Antoni Gil, Barbara Edliberti, Barbara Furhman, Bryan Choate, Dr.Chittaranjan Sahay, Abdulkarim Fattani, Abdulaziz Galib, Garth Blocher, Joao Baiense, Kristen Khan, Laura Hanlan, Mohammad Khan, Morteza Khalighi, Peter Hefty, Dr. Rafael Potami, Sam Nue, Sia Najafi, Dr. Sharon Wagner, Dr.Wael Khatib, Zach Taillefer.

Fahad Khan

Table of Contents

List of Figures vii
List of Tables ix
Nomenclatures x
Chapter 1 : INTRODUCTION 1
CSP Categories 3
Thermal Energy Storage for CSP 6
Research Motivation 9
Dissertation Overview 10
Chapter 2 : OVERVIEW OF CURRENT TES 12
Thermal Energy Storage (TES) 12
Thermal Energy Storage Media 14
Sensible heat storage mediums 14
Latent heat storage mediums (LHS) 16
Thermal Energy Storage Technologies 19
Salinity-gradient solar pond 19
Thermal energy storage in tanks 21
Heat pipe systems 31
Summary 35
Chapter 3 : SPHERICAL TANKS 36
Current Utilization in the Industry 36
Spherical Tank Utilization in TES 38
Technical Aspects of Spherical Tanks 40
Internal stresses and thickness calculation 40
Large vessel manufacturing 43
Heat transfer 45
Conduction from a spherical wall 47
External convection 47
Internal convection 49
Technical Aspects of Cylindrical Tanks 51
Internal stresses and tank shell thickness 51
Heat loss calculation in a cylindrical tank 52
Summary 56
Chapter 4 : COMPARING SPHERICAL TANKS TO CYLINDERICAL TANKS IN TES TWO TANK SYSTEMS 57
Two Tank Molten Salt TES 57
Current Limitations in TES Tanks 58
Cylindrical vs. Spherical Tanks for Two Tank TES 60
Other Structural Benefits of Spherical Tanks in TES 63
Tank Heat Losses 67
Cost Analysis 74
Summary 76
Chapter 5 : SPHERICAL TANKS FOR THERMOCLINE TES 78
Industrial Advantages for the One Tank Thermocline System 78

Literature Review on Stratified Tank Storage Systems 81
Relationship parametric numbers to tank efficiency and thermocline thickness..... 82
Thermal efficiency and inlet relationship (Thermocline Formation) 85
Thermal efficiency and tank wall relationship (thermocline stability)..... 87
Scaling issues in the thermocline tank system 89
Analysis: Thermocline Tank Numerical Modeling 95
Geometry and fluid domain 95
Mesh and mesh refinement 97
Boundary conditions and solver settings 98
Turbulence modeling and stability 100
Comparing Thermocline Thickness and TE in Spherical and Cylindrical Tanks of the Same Volume 105
Parametric Study of a Spherical Tank Thermocline System 111
Numerical Comparison of Three Common Types of Diffusers 113
Parametric Study Using a Plate Diffuser 120
Summary 121
Chapter 6 : EXPERIMENTAL WORK AND DATA VALIDATION 123
Equipment Specifications 123
Spherical tank 123
Circulating water bath 124
Inlet pump 125
Thermocouples 125
Inlet, diffusers and outlet 129
Data acquisition (DAQ) and LabVIEW program 131
Experiment Considerations 133
Procedure of the Experiment 136
Experimental and CFD Data Comparison 138
Comparing Gravity Current 139
Comparing thermocline thickness 143
Comparing exit temperature 147
Data discrepancy discussion 148
Summary 156
Chapter 7 : APPLICATION OF SPHERICAL TANK STORAGE IN DESALINATION 158
Fresh Water Scarcity and the Need for Desalination Capacity Increase 158
Types of Water Desalination Technologies 165
Direct solar water desalination (Solar Stills) 167
Humidification and dehumidification (HD) desalination 169
Multi stage flash (MSF) 170
Multi-effect evaporation (MEE) 172
Analysis: Spherical Tank Sizing for MED Powered by CSP 178
TES requirement and tank sizing 181
Tank storage size and cost function 182
Summary 190
Conclusions 191
References 195

List of Figures

Figure 1.1 Market share of renewable energies in the U.S. 1
Figure 1.2 Left: line focused collector, right: point focused collector [12] 4
Figure 1.3 Stirling engine power plant in Peoria, AZ [15] 5
Figure 1.4 Solar thermal storage systems classifications 8
Figure 2.1 Example of solar pond 20
Figure 2.2 Solar pond in El Paso Texas [47] 20
Figure 2.3 Thermocline hot storage tank during charging (right) and during discharging (left) ... 24
Figure 2.4 Packed bed TES during discharging 26
Figure 2.5 Active two tank system operation 27
Figure 2.6 Example of heat pipe system 32
Figure 2.7 Comparison between available TES systems [59] 34
Figure 3.1 Left: Spheroid, Middle: Pedesphere, right: Multicolumn sphere [74] 36
Figure 3.2 Example of a spherical tank for LPG [77] 37
Figure 3.3 Construction of large elevated spherical tank 45
Figure 3.4 Heat transfer through spherical tank for hot fluid 46
Figure 3.5 Liquid circulation boundary layer between two concentric spheres 50
Figure 4.1 Tank wall thickness reduction when replacing cylindrical tank with spherical tank 62
Figure 4.2 Shell volume reduction when using a spherical tank instead of cylindrical tank 62
Figure 4.3 Cylindrical & spherical tanks with side inlet 66
Figure 4.4 Heat transfer rates ratios Qs/Qc without the foundation (hot tank) 72
Figure 4.5 Heat transfer rates from cylindrical hot tank's bottom 72
Figure 4.6 Heat transfer ratios Qs/Qc without the foundation (cold tank) 73
Figure 4.7 Heat transfer rates from cylindrical cold tank's bottom 73
Figure 5.1 Coanda effect in using symmetry for tank simulation 96
Figure 5.2 Mesh sensitivity study 97
Figure 5.3 Unstructured mesh with wall inflation layers and inlet region refinement 98
Figure 5.4 Time step independent study 102
Figure 5.5 Momentum imbalance throughout the solution 104
Figure 5.6 Residual RMS Error Values 105
Figure 5.7 Thermocline region in cylindrical and spherical tanks at half the discharge 107
Figure 5.8 Spherical tank thermocline along the Y axis 108
Figure 5.9 Cylindrical tank thermocline along the Y axis 108
Figure 5.10 Spherical tank thermocline region movement at 50 s time intervals 109
Figure 5.11 Cylindrical tank thermocline region movement at 50 s time intervals 109
Figure 5.12 End of the dischange processs for cylindrical and spherical tanks 110
Figure 5.13 TE versus Froude number correlation 113
Figure 5.14 entropy production with a plate diffuser 115
Figure 5.15 Increase mesh element near the diffuser region 116
Figure 5.16 Temperature contours for: top left pipe inlet diffuser, top right circumferential diffuser, bottom left, radial diffuser, bottom right, plate diffuser 118
Figure 5.17 Increase of usable volume when using a radial diffuser in a spherical tank 119
Figure 5.18 Plate size and distance optimization 119
Figure 5.19 Froude number versus TE in a plate diffuser 120
Figure 6.1 Tank bottom hole cut for inlet diffusers 124

Figure 6.2 Acrylic tank 0.5 m Diameter 124
Figure 6.3 Circulation pump / heater (left), circulation bath (right) 125
Figure 6.4 Thermocline thickness via thermal film using two different sheets with different temperature ranges. 127
Figure 6.5 Thermocouple tree consisting of 15 J type thermocouples 128
Figure 6.6 Top cover of the tank with water outlet and thermocouple tree mount 128
Figure 6.7 Inlet pipe diffuser of 0.022 m diameter 130
Figure 6.8 Optimized plate diffuser 130
Figure 6.9 Tank top cover with thermocouple mount 131
Figure 6.10 LabVIEW front panel screenshot 132
Figure 6.11 Thermocouple tree, CJC and DAQ 133
Figure 6.12 Schematics for the experimental set up during the discharge 135
Figure 6.13 Two camera placement for gravity current capture 140
Figure 6.14 Gravity current side view using CFD 141
Figure 6.15 Photo of the gravity current taken by underwater camera 141
Figure 6.16 Picture distortion due to tank curvature 142
Figure 6.17 Irregular spread of gravity current 142
Figure 6.18 Measuring thermocline thickness using thermocouple tree at 2000s 144
Figure 6.19. Visualization of thermocline thickness and entrainment at 20, 40, 60, & 80 percent of the discharge 145
Figure 6.20 Thickness of Thermocline at 2000s in the pipe diffuser case 146
Figure 6.21 Thickness of Thermocline at 2000s in the plate diffuser case 146
Figure 6.22 Overlay of CFD and experimental data 147
Figure 6.23 Increased mixing due to exit geometry 149
Figure 6.24 Comparison of exit temperature after using syphoning 150
Figure 6.25 Exit temperature profile with eddy viscosity model 155
Figure 6.26 Comparison of experimental data, linearized CFD eddy viscosity model at the exit, and CFD Laminar model 155
Figure 7.1 World Desalination Capacities by Country 161
Figure 7.2 Desalination with renewable energy resources. Reverse osmosis (RO), mulistage flas (MSF), photovoltic (PV) eletrodyalsis (ED), multi-effect flash desalination(MED), mulistage vapor compression (MVC) 165
Figure 7.3 Desalination capacities by technology 166
Figure 7.4 Example of solar still 168
Figure 7.5 Basic CAOW HD cycle 170
Figure 7.6 Example of two stages MSE desalination 171
Figure 7.7 Four chamber MED unit 175
Figure 7.8 Schematic of Aquasol proposed plan [198] 180
Figure 7.9 Required water volume versus ΔT 183
Figure 7.10 HEX cost versus tube diameter 189

List of Tables

Table 1.1 Comparison between CPC types 5
Table 2.1 PCM properties 17
Table 2.2 Advantages and disadvantages of organic and non-organic PCMs [35] 18
Table 2.3 Advantages and disadvantages of two tank and one tank systems 30
Table 3.1 Average life span of common tanks 43
Table 4.1 Tank Specifications 64
Table 4.2 Maximum internal stresses on tanks 66
Table 4.3 Properties of the molten salt at cold and hot storage temperature 68
Table 5.1 Summary of literature on flow parameters' influence on thermocline storage systems 93
Table 7.1 HEX constraints with TES and MED 185
Table 7.2 HEX optimization parameters 189

Nomenclature

A	Area
C	Courant number = $\frac{u \cdot \Delta t}{\Delta x}$
C	Cost
Cp	Specific heat at constant pressure J/kg. K
Bi	Biot Number $Bi = \frac{h\,L}{k}$
D	Tank Diameter
E	Mixing factor
F	Normal force
F_r	Froude Number = $\frac{u}{\sqrt{[g\beta(\Delta T)D]}}$
Fo	Fourier number $= \frac{\boldsymbol{\alpha \cdot t}}{\boldsymbol{L^2}}$
Gr	Grashof number $\frac{g\beta(\Delta T)L^3}{u^2}$
H	Tank height
Nu	Nusselt number = $\frac{h \cdot L}{k_f}$
P	Internal Pressure
Pe	Peclet number = Re · Pr
Pr	Prandtl number = $\frac{u}{\alpha} = \frac{C_p \mu}{k}$
R	Thermal Resistivity
Re	Reynold′s number $= \frac{\rho UL}{\mu} = \frac{UL}{v}$
Ri	Richardson number = $\frac{PE}{KE} = \frac{gh}{u^2}$
S	Steam cost
T	Temperature
U	Overall heat loss coefficient
V	Volume
$\forall$	Shear stress force
Q	Heat transfer kJ
$\dot{Q}$	Heat transfer rate through the wall

I	*S*un irradiation constant W/m^2
Z	Tank mixing number
a	radial ratio r_e/r_i
d	Inlet diameter
e	Specific exergy
f	Friction factor
g	Gravity acceleration (9.8 m/s^2)
h	Specific Enthalpy (kJ/kg)
h	Convective heat transfer coefficient
h_{out}	External convection heat transfer coefficient
h_{fg}	Enthalpy of vaporization
k	Thermal conductivity
l	Distance between columns
$\dot{m}$	mass flow rate *kg/s*
ppm	parts per million
r	Radius
s	Specific Entropy
t	Tank wall thickness
thl	Thermocline
u	Velocity in x direction
x	Length of element
α	Thermal diffusivity, $\alpha = \frac{k}{\rho C_p}$
β	Volumetric thermal expansion coefficient
η	Thermal Efficiency
ρ	Mass density
v	Kinematic viscosity *($v = \mu/\rho$)*
v	Velcoity in the y direction
v	*specific volume*
Θ	Dimensionless temperature
σ_t	Circumferential (tangential) stress,

σ_m	Meridian stress,
σ_r	Radial stress
σ_S	Maximum allowable stress
σ_t	Tangential stress
δ	Boundary layer thickness
∞	Temperature of fluid

Subscript

L	Characteristic length
D	Characteristic diameter
a	Allowable
ave	Average
b	Middle of the cylinder
c	Cold
cap	Cap (spherical cap)
cyl	Cylinder
e	External
el	Electricity
f	Fluid
h	Hot
i	Inside
o	Outside
ref	Reference temperature
s	Surface
sh	Shell
sph	Sphere
t	Tangential
th	Thermal
thl	Thermocline

tu	Tube
w	Wall

Abbreviations

ANSYS CFX	Analysis systems computational fluids dynamic program
AISI	American Iron and Steel Institute
API	American Petroleum Institute
ASREA	American Society of Heating and Air-Conditioning Engineers
ASTM	American Society for Testing and Materials
BPE	Boiling point elevation
CAOW	Closed air open water
CFD	Computational fluid dynamics
CJC	Cold junction channel
CPC	Compound Parabolic Concentrator
CSC	Concentrated solar collectors
CSP	Concentrated solar power
DAQ	Data acquisition
DOE	Department of Energy
ED	Electro dialysis
ED	Electrolysis
EPRI	Electric Power Research Institute
FEA	Finite element analysis
FR	Flow Rate
GOR	Gain output ratio
GPM	Gallon per minute
HD	humidification and dehumidification
HEX	Heat Exchanger
HTF	Heat transfer fluid
HTF	Heat transfer fluid
HVAC	Heat ventilation and air conditioning
IEA	International Energy Agency

LCOE	Levelized cost of energy
LHS	Latent heat storage
LHS	Latent heat storage
LNG	Liquefied natural gas
LPG	Liquefied petroleum gas
LPM	Liters per minute
MD	Membrane desalination
MED	Multi effect desalination
MEE	Multi effect evaporation
MSF	Multi stage flash
NREL	National Renewable Energy laboratory
OAOW	Open air open water
OSW	Office of saline water
PCM	Phase changing material
PCM	Phase change material
PR	Performance ratio
PT	Parabolic trough
PV	Photovoltaic
RMS	Root mean square
RNG	Renormalization Group Theory
RO	Reverse osmosis
RSS	Reynolds shear stress
SCV	Spherical cap volume
SHS	Sensible heat storage
SPSS	Statistical Package for Social Science
STWD	Solar thermal water desalination
TE	Thermal efficiency
TES	Thermal energy storage
VC	Vapor compression
VI	Virtual instrument

CHAPTER 1 : INTRODUCTION

Climate change, increased prices of fossil fuels, and water and air pollution are all factors that have motivated industrialized countries to start investing in renewable energy resources and replacing existing fossil fuel based products with renewable alternatives. In 2011, the U.S. was ranked 7th in terms of percentage of electricity produced by renewable energy sources (2.7%). The U.S was preceded by: Germany (10.7%), the EU (6.7%), Italy (6.2%), Indonesia (5.7%), France (2.8%), and the U.K. (4.2%) [1].

In November 2006, the Washington Energy Independence Act was passed, mandating investor owned utilities to increase renewable energy generation from the current 3% to 15% by 2020 [2].

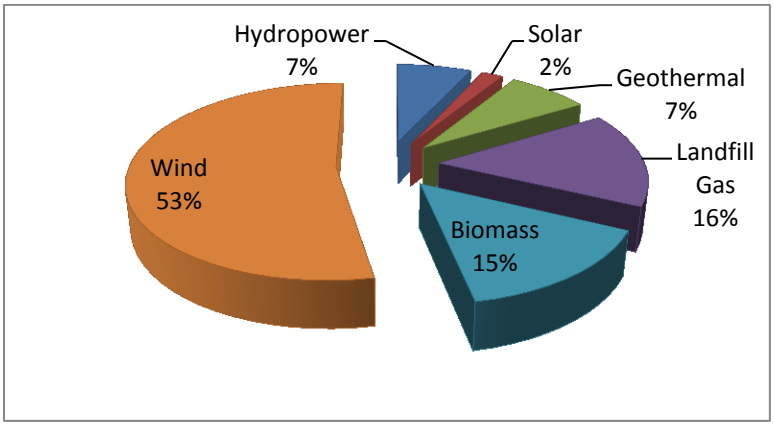

Figure 1.1 Market share of renewable energies in the U.S.

Solar energy is the least utilized, but fastest growing source of renewable energy in the U.S. The International Energy Agency (IEA) states that after 2060 solar energy

could provide one third of the world's power needs [3]. Solar energy is the most abundant energy source on the planet. Around 173,000 terawatts of solar energy continuously reach earth [4]. This power is ten thousand times the entire world energy needs. The sun radiates 1,354 W/m² to the top of the earth's atmosphere; this value is also known as the solar constant [5]. That amount of radiation is reduced at the earth's surface depending on the location and the time, ranging range from 0-1050 W/m². The variation of the solar radiation energy, and its relatively low energy density, are reasons why solar energy does not dominate the energy market.

Currently, the demand for solar energy is at an all-time high in the U.S., making the country the fourth largest solar energy market in the world. Solar energy is used in two forms: photovoltaic (PV) or concentrated solar power (CSP). Solar PV systems use semiconductors, materials to transform the photons in solar rays, in order to generate electrical power. CSP utilizes solar thermal power to generate steam, which is then used to operate a steam turbine and consequently generate electricity, or which can be used in other thermal applications. PV has the advantage of being able to operate even on a cloudy days as long as there is some sunlight, while CSP shuts down even in partial absence of sun [6]. However, CSP has the advantage of being able to store heat for continuous power generation, and it is also able to produce electricity on a large scale.

While the solar energy market is currently trending toward solar photovoltaic PV for power generation, due to decreasing cost of manufacturing, solar thermal power still has a tangible market share. CSP is utilized in heating, ventilation and air conditioning

(HVAC) applications, large scale power generation, which was launched in California's Mojave Desert in 2013, and is considered the world largest solar energy plant. The plant produces 377MW that serves 140,000 homes in California [7].

CSP Categories

CSP is categorized based on the type of solar collectors. Concentrated solar collectors (CSC) is categorized into three types, based on three kinds of solar collectors: parabolic troughs (line focused), dish engines (point focused), and power towers (point focused) also known as central receivers. The fourth type of solar thermal collectors, evacuated tube solar collectors, is not used in power generation due to low operating temperatures [8].

Typical concentrated parabolic collectors (CPC) in trough configuration have concentration ratio (also known as concentration factor) that are between 1.5 and 5 [9]. Concentration ratio is calculated as the aperture area divided by receiver area. Therefore having the CSP in a power tower formation significantly increases the concentration ratio due to the area of the mirrors ratio to the receiver area. Ivanpah solar CSP plant has a concentration ratio over 400 [10]. CPC's do not require sun tracking; however, tracking can improve the collector performance by up to 75 % [11].

Parabolic troughs (PT) arranged as in- line focused collectors, which concentrates solar radiation into a pipeline, are more economical and less technically challenging than point focused collectors; however they are less efficient and require more land space [12].

Figure 1.2 Left: line focused collector, right: point focused collector [12]

Advanced types of parabolic troughs with concentration ratios of 10-100 have the potential of providing operating temperatures of 100-400º C [13]. The performance of the parabolic trough depends on the ability to track the sun's movement, which requires a sophisticated control system in either one or two axes.

Along with the in-line focused and point focused collectors, the dish engine system is the third major type of solar concentrating collectors. This system consists of small mirrors installed in a dish shaped base where the receiver is at the dish focal point. Dish CPC have a concentration ratio that ranges from 600-3,000, and in some cases a concentration factor of 13,000 has been reported [5, 14]. With a dish CPC, concentrated solar thermal power has been used to operate Stirling gas engines.

Figure 1.3 Stirling engine power plant in Peoria, AZ [15]

Even though parabolic troughs currently dominate the CSP market of solar collection in electricity generation, the Dish-Stirling system is anticipated to surpass PT's in power generation, with a higher efficiency due to its higher concentration factor [16].

Table 1.1 Comparison between CPC types

Type	Concentration ratio	Tracking requirement	Temperature achieved
Line focused troughs	10-100	One axis	400-600° C
Point focused tower	500-1,000	Two axis	100-400°C
Dish System	600-3,000	Two axis	600-1500°C

Thermal Energy Storage for CSP

CSP has the disadvantage of dependency on solar radiation in order to operate. Since solar radiation is intermittent, thermal energy storage (TES) is needed to make up for the absence of sun and/or suboptimal weather. TES will enable the plant to run throughout the evening and thus increase its production rate and consequently its levelized cost of energy (LCOE).

Amongst the various types of energy storage, TES has the highest maturity, largest overall cycle efficiency, and the easiest placement [5]. TES improves CSP performance; however it comes with an additional capital and operation cost (pumps, pipes, tanks, storage medium, heat exchanger, and control system). Therefore, any improvements of the TES system economics will directly impact the LCOE.

TES was first utilized by the industry in the early 1980s and received notable attention in the 1990s [17]. Several TES projects have reduced energy costs and merited ASHRAE's Technology awards. However, there was a lack of attention focused on the use of TES in large scale application at that time. The stated reasons behind the lack of adoption of thermal storage systems in the energy sector include: operational risks, a large space requirement, complicated operation, high costs, and impracticality. Experts in the field of TES suggest that many of these reasons are not valid. Proper modeling and accurate economical calculations are in favor of using TES.

Solar thermal energy storage can be categorized into two types: sensible heat storage, and latent heat storage. In sensible heat storage, a medium is used to store the absorbed heat by increasing its temperature. The heat is released back to the system when needed either directly or through a heat transfer fluid (HTF) and a heat exchanger. Latent heat storage (LHS) depends on a phase changing material's (PCM) heat of fusion. Gas to liquid phase changes are not utilized in thermal energy storage applications.

Thermal storage systems can also be subdivided into active or passive. Active storage systems utilize forced convection, which transfers heat into the storage medium through a heat exchanger as part of the cycle's active loop. In passive systems, the storage material is isolated from the main loop and used when needed [18]. The passive storage systems mostly use solids such as concrete, graphite, or ceramics as storage media. In some cases a solid medium is coupled with the PCM, while the HTF is running through an internal piping system. In terms of system design and operation, storing sensible heat using a solid medium is less expensive than using liquids. In addition, solids such as concrete or ceramics provide higher heat transfer rates and cost less per kilogram than storing sensible heat in solar salt (the most common medium for tank storage systems). However, the practicality and implementation of thermal energy storage in solids on an industrial scale is still in the development phase.

Active storage systems are divided further into direct and indirect systems. The direct system uses the same material for storage and HTF, while the indirect system uses different materials for storage and HTF. Current indirect TES use mineral oil as the HTF

and solar salt as the storage material; a heat exchanger is needed to transfer the heat from the HTF to the solar salt tanks and vice versa. Direct TES have been favored in some solar plants since they eliminate the need for a heat exchanger, thus lowering capital and maintenance costs [18]. However, direct systems create some difficulties when using molten salt as the HTF, due to molten salt's high viscosity and melting temperature [6]. Moreover, mineral oil is not ideal for storing heat at high temperatures and has a relatively lower thermal capacity than molten salt; thus it is not preferred for storage. Figure 1.4 shows the classification of the thermal energy storage systems that are currently used by industry.

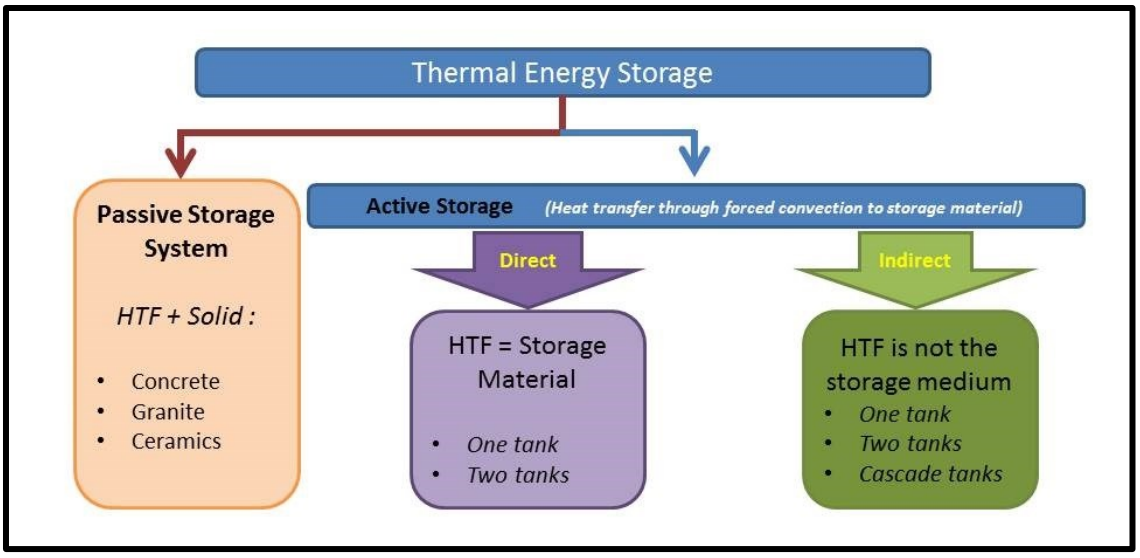

Figure 1.4 Solar thermal storage systems classifications

To date, according to the International Energy Agency (IEA), there is no cost effective compact thermal energy storage system [19]. In 2011, the U.S. Department of Energy (DOE) allocated 40% of its $9.9 million budget for concentrated solar power

(CSP) to sensible heat storage and 38% to PCM storage, due to their projected effects on reducing CSP energy costs [20]. The DOE report states that the current thermal storage cost is \$80-120/kWh_{th} based on daily storage cycle. This cost is targeted to be reduced to \$20/kWh_{th}.

A 2011 economics study reported that adding TES to a power generation plant increases its capital cost by 20-30%, which makes the project difficult to fund [6]. TES economics depends on the following four primary factors [21] : (i) thermodynamics such as efficiency, losses, and exergy; (ii) heat transfer rates in HTF materials (iii) fluid flow of HTF, storage material, and operating conditions; and (iv) other factors such as safety, environmental impact, and life cycle. Other secondary factors that affect TES performance when integrated into the system are: (i) mode of operation, whether active or passive; (ii) the type of storage (iii) climatic conditions; (iv) efficiencies of auxiliary systems; and (v) charging and discharging intervals.

Clearly there is much improvement and optimization that can be done on both the primary and secondary factors, which could influence TES system economics and overall thermal cycle efficiency.

Research Motivation

Currently, natural gas boilers are required as a backup for most CSP technologies. The use of TES is essential for CSP to be able to operate completely without fossil fuels Improvement of the current sensible heat storage systems is needed to make them more

thermally efficient and economically feasible. The literature review shows that some of the limitations of current sensible heat TES systems are related to tank shape.

Spherical tanks are used widely in nuclear cooling applications, water storage, and chemical plants. However, few thermodynamic analyses have been performed on spherical tank structures [22]. The current research will investigate the advantages and disadvantages of using a spherical tank for two tank and one tank TES systems.

Dissertation Overview

The remainder of the dissertation is organized as follows:

Chapter 2 provides a literature review of thermal energy storage systems, including types, applications, shortcomings, state of the art, and possible areas of improvements and research.

Chapter 3 investigates spherical tank utilization in the industry, explores the advantages and disadvantages, and provides the motivation and reasoning behind trying to use spherical tanks for thermal energy storage systems.

Chapter 4 involves a study of two tank storage systems with molten salt as the storage medium. Spherical tanks were investigated as an alternative to cylindrical tanks. Structural and thermal aspects of cylindrical tanks with varying *H/D* ratios (0.25 – 5) and spherical tanks of the same volume were compared.

Chapter 5 describes a computational fluid dynamic (CFD) study that compares the Thermal Efficiency (TE) of a one tank TES system (thermocline storage system) in a spherical tank to a cylindrical tank, to a thermocline storage system in a cylindrical tank of the same volume. A parametric study is then performed on a spherical tank during the discharge process, to determine the flow parameters that govern the thermocline formation and entrainment in a spherical tank. Furthermore, the CFD study investigates four different diffusers in order to determine which will deliver the greatest thermal efficiency in a spherical tank.

Chapter 6 further investigates the CFD study results provided in chapter 5. These results are validated through an experimental set up, by comparing thermocline thickness, tank thermal efficiency, and inlet gravity current, between the CFD and experimental data.

Chapter 7 provides a practical example of utilizing a spherical tank for thermal energy storage. A review of thermal desalination technologies is performed in order to demonstrate a possible integration of a spherical tank into a thermal desalination cycle. Spherical tank sizing and optimization, for coupling with CSP-powered multi effect desalination (MED), is performed.

CHAPTER 2 : OVERVIEW OF CURRENT TES

Thermal Energy Storage (TES)

Thermal Energy Storage (TES) is the missing link to sustainable and reliable power generation via solar thermal energy. The use of TES will improve the overall solar thermal system ability to handle sudden increases of demand at constant sun radiation, and improve the system economics by allowing larger production capacity [18].

The following case studies show the importance of having TES in solar thermal cycles at difference storage temperature ranges. An economical and feasibility study showed that in order to have a continuously operating solar thermal powered water desalination plant, it is economically essential to have a storage device for heat energy [23, 24]. Another study of a solar thermal power generation cycle showed that TES is needed in order to have continuous operation and also to maintain acceptable cycle efficiency. A study performed by Kearny et al. found that the use of high end TES operating at temperatures up to 450-500° C will increase the thermal efficiency of a Rankine cycle up to a total of 40% [25].

Currently, most solar thermal applications operate in daily and seasonal cycles, based on the sun's radiation power and duration. Most solar power generation plants depend on natural gas or fuel oil as a backup heat source [6]. TES can make up for the lost generation time due to the sun's absence during the night and also during bad weather conditions without the need for natural gas or fossil fuel back up. Currently, the

installation of TES is more expensive than having gas or fuel oil back up therefore it is not economically favorable. Research suggests that in order to give TES a competitive advantage over fossil fuel back up, there must be a change in energy policy. Carbon tax initiatives could make renewable energy resources competitive over traditional fossil fuel backups. Current thermal energy storage systems are able to operate between 293-393º C, with cycle energy recovery efficiencies of 96%- 97%. The cost is $80-$120 per kWh_{th} for installation and operation during the life span of the plant, which is estimated at 25 years [20].

The selection of the storage temperature and the mode of operation of the TES depend on the actual application for the system and the cycle requirements. Therefore, there is an area of future optimization for TES systems through the use of a combination of TES systems with different storage temperature in order to fulfill the cycle's thermal energy storage needs in order to improve the cost and performance of TES [26]. For example, in seawater thermal desalination, a simulation study showed that the storage system should be independent from the evaporation process and have its own dedicated solar collectors in order to have the maximum gain output ratio [27]. Other research suggests that for some power generation cycles, having a constant temperature heat source cannot be achieved by using sensible heat storage alone; therefore a combination of sensible and latent heat sources is required for such cycles [26].

The next section provides a brief overview on the two main TES storage mediums: sensible and latent, and the three main types of thermal energy storage: solar ponds, tank systems, and energy storage in pipe systems.

Thermal Energy Storage Media

Sensible heat storage media

High temperature (400-600º C) sensible heat storage tanks commonly use molten salts or mineral oil. Currently most tanks use molten salts because they are more economical and can operate at higher temperatures (up to 600º C) when compared to mineral oil, which has a maximum operating temperature of 300º C. In addition, molten salt is considered more environmentally friendly, and offers the best balance of capacity, economy, high temperature and thermal efficiency [28]. Molten salt storage tanks have been utilized in power generation plants since the 1980s to enable power cycles to run continuously without the need for fossil fuel back up. For power generation plants, the two tank molten salt storage system is considered the most economical and the simplest to operate [29].

Molten salts have various compositions and mixtures based on the required final material properties of the chemical salt. The desirable properties of molten salts are: low freezing temperature, low vapor pressure, moderate specific heat, low chemical reaction between the components of the salt, low corrosiveness with the tank, and low cost [30]. Nitrate salts have been preferred among chemical salts because they meet most of the

previous criteria and have been utilized in chemical plants for a long time, which establishes familiarity with its operation. Nitrate salts also have small corrosive effects on stainless steel and carbon steel [18]. The two leading molten salt products are *Solar salt* and *HitecXL*. Solar salt consists of 60% $NaNO_3$ and 40 % KNO_3, melts at 221^0C, is stored in the cold tank at 288^0 C, and costs approximately $0.49 per kg to purchase and approximately $5.8 to store the equivalent of 1 $kW_e \cdot h$. This last cost includes storage tank and operational costs [18].

For low to medium temperature storage (80-250º C), water, brine, mineral oil, and synthetic oil are the most common storage media. However, for medium heat storage below 100º C, water is the preferred storage material due to: (i) low cost, (ii) non toxicity, (iii) high thermal capacity, (iv) relatively low vapor pressure, and very high capacity rate for charge and discharge [31-33].

Sensible heat storage is also performed in solids such as reinforced concrete, granite, solid NaCl, cast iron, cast steel, silica fire bricks and magnesia fire bricks with a temperature storage range between (200-1200º C) [18]. This system is also known as a passive storage system. Solid storage systems include pipe systems for HTF to run through for heat exchange with the solid. Solid medium storage systems have the advantage of: (1) low cost of the storage medium and installation, (2) improved heat transfer rate between the solid medium and HTF, and (3) long cyclic degradation. The disadvantages are: (1) complicated heat exchange system required for the storage medium and piping system, and (2) long term heat capacity degradation of the storage

medium. In TES systems, the term passive refers to storage in solid medium and active refers to liquid storage medium where the storage medium itself circulates within the TES.

Latent heat storage mediums (LHS)

Latent heat storage is usually achieved by the utilization of a phase change material (PCM). PCM storage systems take advantage of the material's heat of fusion released by a phase change from solid to liquid and vice versa. PCM materials are characterized by high storage density and smaller temperature differences between storage and release temperature [34, 35].

The selection of PCMs depends mainly on their melting temperatures. Materials with melting temperatures below 15º C are used for cooling cycles, materials with melting temperature between 15º and 90º C are suitable for solar heating applications, and materials with melting points above 90º C are utilized in absorption refrigeration cycles [36]. Commercial paraffin is the most studied PCM and has a melting temperature of 55º C. Paraffin has the storage density of 200 kJ/kg and it is relatively inexpensive. For industrial scale power generation processes higher melting point PCM are required. Table 2.1 summarizes the PCM thermo-physical, chemical and kinetic properties highlighted by Buddhi [37]:

Table 2.1 PCM properties

PCM required properties	
Thermo-physical Properties	**Chemical Properties**
The melting point should be equal to the required operating temperature High latent heat of fusion per volume in order to reduce the size of the storage High specific heat C_p High thermal conductivity Small volume change with phase change	Complete reversibility per cycle of phase change No/low degradation rate with cycles No/low corrosiveness with the container No toxicity Not flammable or explosive
Kinetic Properties	
Nigh nucleation rate High crystallization rate	

Zalba et al. reviewed the properties of most phase change materials that have been studied from 1983 to 2003 [38]. PCMs are divided into organic and inorganic. For solar energy power generation PCM storage, organic and inorganic materials with melting points above 300º C have been the focus of study. Some of the researched materials with melting points between 300-550ºC are: pure salts, salt eutectics, metals and metal eutectics [19]. Table 2.2 highlights the major advantages and disadvantages of organic and non-organic PCMs.

Table 2.2 Advantages and disadvantages of organic and non-organic PCMs [35]

Phase Change Materials			
Organic		**Inorganic**	
Advantages	**Disadvantages**	**Advantages**	**Disadvantages**
Non corrosive Chemically stable Low vapor pressure No sub-cooling	Lower thermal conductivity Flammable Significant change in volume with phase change	Higher latent heat Non flammable Higher thermal conductivity Lower cost	More corrosive Susceptible to sub-cooling Decompose Improper re-solidification [39]

The HTF operating temperature is also a deciding factor of the storage system operating temperature. Currently, synthetic oil with operating temperature of 400º C is the most common HTF for solar collectors.

All PCMs have the disadvantage of low thermal conductivity. Therefore, much experimentation and research has been done on PCMs to improve their thermal conductivity. Some of those efforts are encapsulations with metallic casings of various shapes, and mixing the PCM with metallic parts.

Techniques to counteract the issues of low conductivity of PCMs and enhance the heat transfer coefficient are an active area of research in terms of size, geometry, cascading, and use in packed bed TES [39-41]. Cascading LHS is a technique that is used to improve the TES performance. Cascading uses different types of PCM and different storage sizes, and has the potential of improving the economy and thermal performance

of the TES [42-44]. PCM encapsulation can be done on a micro scale, to be used in slurries along with HTFs, especially in HVAC systems [21]. Another technique to improve the conductivity of PCM is the impregnation in metal foam, which has the potential of increasing the thermal conductivity by 180 times [45].

Thermal Energy Storage Technologies

Salinity-gradient solar pond

Salinity –gradient solar pond technology utilizes a vertical saltwater gradient in a technique in which the density of the water is increased by salt content. The top layer contains relatively fresh water. The middle layer has medium salinity and acts as an insulation layer. High salinity (denser) water is located at the bottom of the pond, and it can store heat up to 100º C. The pond bottom is lined with black material so that it can absorb solar radiation thus heating the water in the pond [46]. The heat is extracted from the bottom of the pond without disturbing the upper layers.

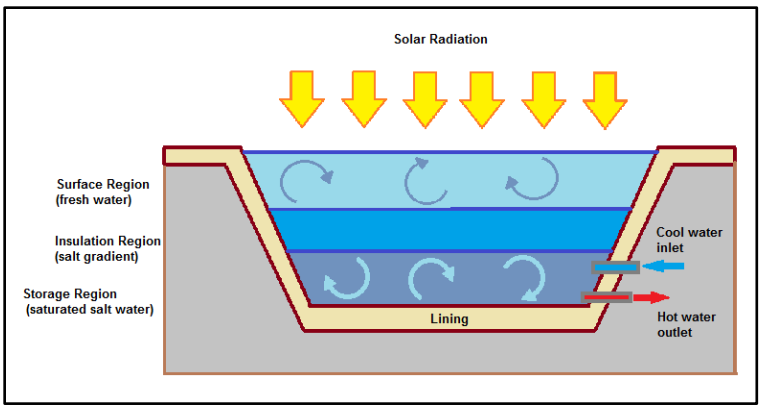

Figure 2.1 Example of solar pond

Figure 2.2 Solar pond in El Paso Texas [47]

The useful heat extracted from a solar pond can used for water desalination or to operate a power generation cycle. The utilized heat is evaluated on an annual basis to be between 10-15% of the total heat collected in the pond [13]. Increasing the size of the pond will increase the percentage of useful heat, due to reduction of losses at the rim of the pond. Since brine discharge is always associated with water desalination process,

solar ponds are a suitable approach for useful disposal of brine and also as medium to store heat for later use.

One of the largest solar ponds in the USA is located in El Paso Texas. At the time of a productivity evaluation in 1998, the pond had a surface area of 3355 m^2, generated 70 kW_{el} from an organic Rankine cycle, sustained temperatures higher than 90º C, and produced 80,000 gallons of fresh water [46]. Another successful 210,000 m^2 solar pond project is located in Israel near the Dead Sea that produces 5 MW of electricity using a Rankine cycle [48]. Small scale solar pond electricity production ponds have not been economically feasible for power generation [49].

Thermal energy storage in tanks

Thermal energy storage using latent heat or sensible heat is most successfully achieved by containment within a storage medium in tanks. Sensible heat storage with fluids is done in either one tank or two tanks. The two tank system uses one tank or a set of tanks for the hot fluid, and one tank or set of tanks for the cold fluid. There are three variations of the one tank sensible heat system: (1) a fully mixed tank, where the incoming and resident fluids are mixed and the temperature is averaged, (2) a thermocline system, where the resident fluid and the incoming fluid have minimal mixing and a thermocline layer is formed to act as a barrier during the entire charge or discharge, and (3) a one tank packed bed, where filler materials in forms of rocks or encapsulated PCM are used in the tank to act as the storage medium or stabilize a thermocline system.

One tank storage system

Fully mixed tank

One tank systems can be either stratified (thermocline and packed bed) or fully mixed. In a fully mixed one tank storage, the inlet temperature and the storage temperature are allowed to fully mix; therefore the tank output temperature is lower than the original storage temperature. Thermal energy storage in a fully mixed one tank is simple and reliable [50, 51], yet it has significantly lower thermal efficiency than a stratified tank (thermal efficiency is defined as the ratio of the energy extracted from the tank divided by the energy input).

Fully mixed TES systems are mostly utilized in HVAC applications, such as large scale underground seasonal storage tanks for homes and industrial buildings. [33, 52]

Stratified one tank system

In a stratified tank storage system, charging and discharging is done with certain flow criteria, which lead to high tank stratification and low mixing between hot and cold fluid. The buoyancy effect forces the hotter portion of the fluid to rise to the top of the tank and the colder fluid to sink to the bottom, forming thermally stratified layers throughout the tank. Filler material can be utilized in the one tank system in a packed bed configuration to reduce the cost of the storage fluid, improve tank stratification, and increase the thermal storage capacity (by using filler material as an additional storage medium) [18].

In a well-designed storage tank with a high degree of stratification, a thermocline region is formed. A thermocline is a relatively thin layer of fluid in which the fluid temperature changes markedly with depth. This interface layer between hot and cold layers also acts as a partition between the cold fluid at the bottom and the hot fluid at the top, thus maintaining a highly stratified tank.

In nature, thermoclines occur in lakes and oceans and separate the high surface temperature water from the cold deep water. The separation is density based; hence it also occurs between waters with different levels of salinity. A thermocline can be produced in a storage tank and used as a barrier between the cold and hot fluid. A tank undergoing charging or discharging with certain flow criteria (temperature difference, mass flow, and turbulence) can form a thermocline that separates the incoming fluid from the stored fluid. This thermocline is carried along throughout the entire charge or discharge process. Thermocline formation and maintenance result in a high degree of stratification and low mixing, leading to an increase in the tank's thermal efficiency.

In thermocline storage systems designs, there are two main desired traits: low mixing during the charging and discharging process, and a stable thermocline region. Low mixing results in minimal volume occupied by the thermocline region and consequently, a higher thermal efficiency. A stable thermocline region refers to constant volume occupation by the thermocline region after forming. Thermocline region volume increases occur due to heat loss from the tank wall and circumferential heat transfer along the wall between the cold and hot regions of the fluid.

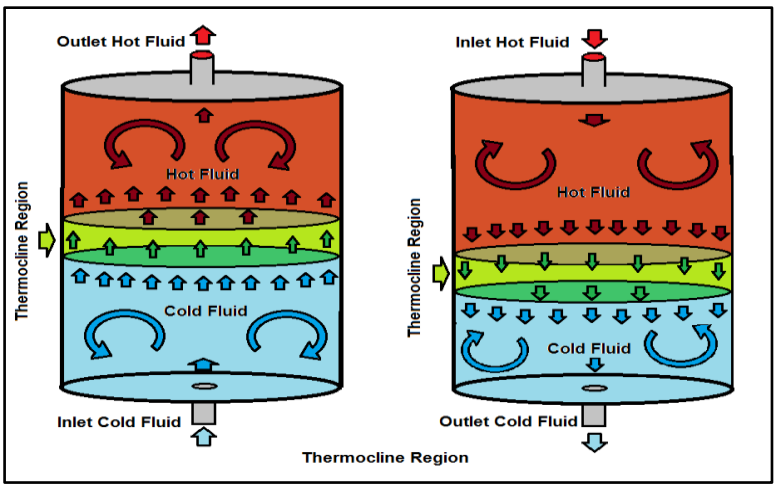

Figure 2.3 Thermocline hot storage tank during charging (right) and during discharging (left)

In a thermally stratified tank, the charging process takes place by pumping hot fluid into the tank from the top of the tank while the colder fluid is withdrawn from the bottom simultaneously at the same flow rate. The discharging process reverses the charging as shown in Fig 2.3. The cold fluid is pumped from the bottom this time and hot fluid is withdrawn from the top of the tank. A well-designed tank is capable of maintaining stratification throughout the entire charging and discharging processes, as well as during pauses in charging or discharging.

The degree of stratification and the thermocline stability in a one tank thermocline system is directly related to the tank geometry, inlet shape, and charging/discharging flow parameters [53]. Mixing in the inlet and outlet regions depends on inlet flow dimensionless numbers, such as Reynolds, Grashof, Froude, and Richardson [53-56].

Packed bed

A packed bed system is similar to a thermocline system. However, in the packed bed system the tank is filled with porous filler material. The tank can be filled completely or partially with filler material.

The filler material is used to stabilize the stratification and reduce the required amount of storage medium [18]. Using filler material is also desirable when molten salt is used, because molten salt is relatively expensive with a heat storage capability that degrades with time [57]. Alternately, the filler material can be used as the main storage medium, for charging and discharging [58].

Some of the filler materials used in packed bed storage tanks with molten salt are quartzite rock and silica. They are used because they can withstand operating with molten salt at a high storage temperature, and they have no chemical reactions with the salt [59, 60]. The interaction of the filler materials along with their geometry, and their heat transfer rate with the molten salt can affect the stratification of the tank and the performance of the TES [28].

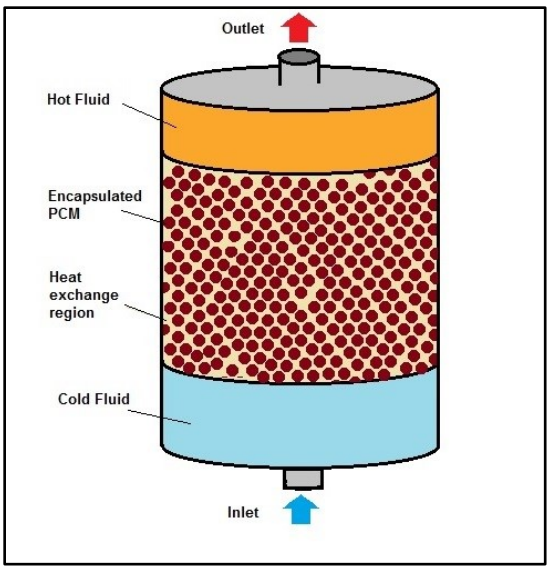

Figure 2.4 Packed bed TES during discharging

Two tank storage

A two tank storage system consists of two tanks: one tank contains the high temperature fluid and the other tank contains the cold fluid. Some configurations include a set of tanks for hot storage fluid and another set of tanks for cold storage fluid. The two tank system can be used in direct or indirect storage systems [18]. The operation of an indirect two tank system is illustrated in Fig.2.5. The solar collectors are used to heat the storage media coming from the cold tank. Heat is extracted from the hot tank and used to generate steam for the steam turbine. In this configuration, the system is continuously active during the cycle. Other cycle configurations have an isolated loop for the TES system to be used only when needed.

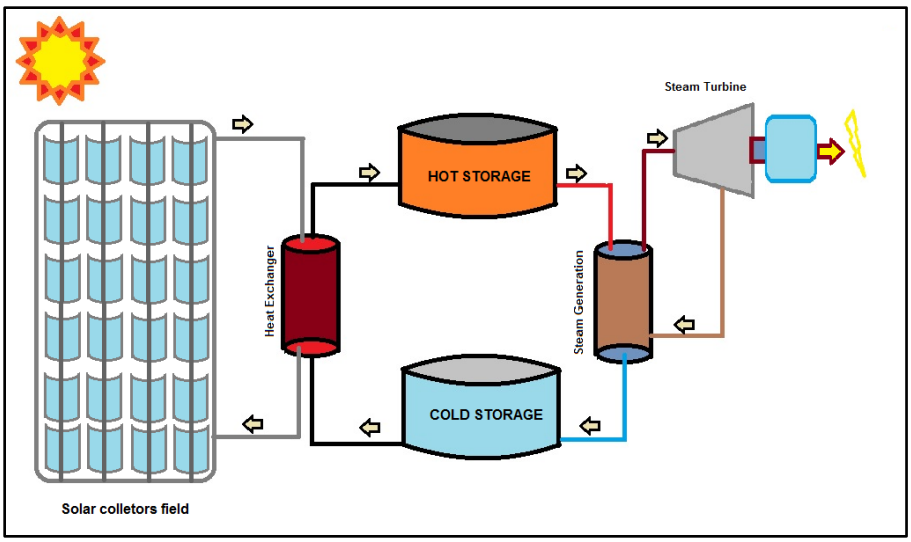

Figure 2.5 Active two tank system operation

Currently, two tank systems consist of cylindrical tanks with an ellipsoid roof. The tank design criteria (dimensions and building material) are dependent on the application and thermal energy storage requirements. Large cylindrical tanks are constructed from pre-fabricated metal segments that are welded, heat treated, and tested on site, similar to the storage tanks used in hydrocarbon storage. However, since these tanks are storing fluid at temperatures much higher than the ambient, they require additional foundation and wall insulation to reduce heat losses.

In the two tank storage system, mixing between hot and cold fluid is avoided, which improves the heat storage efficiency. Some of the issues concerning two tank storage systems are the high capital cost, maintenance and operation, and the risk of the molten salt freezing in the pipes. Herrmann and Kearney reviewed the literature in 2002 on thermal energy storage for parabolic trough power plants and concluded that the two

tank molten salt is the most thermally efficient yet the least economical storage systems [61]. Even though the two tank storage system increases the capital and maintenance cost, it is preferred due to: its relatively simple operation compared to the one tank system, low mixing between hot and cold fluid, and the mitigated risk of one tank failure [29]. National Renewable Energy laboratory (NREL) recommends using the indirect two tank storage system for solar thermal power generation plants [6].

An optimization study on tank design for molten salt thermal storage performed by Gabbrielli and Zamparelli [29] concluded that TES tanks must have the following capabilities: (i) to withstand the hydrostatic pressure of molten salt, (ii) to resist vacuum pressure, (iii) to resist over pressure (iv) to pump from the bottom (since pumping from the side will introduce a weak point in the cylindrical wall), (v) minimal heat loss from the side wall, and (vi) resist reaction with the storage fluid.

Advantages and disadvantages of one and two tank TES systems

The one tank thermocline system is recognized for its high reliability and high performance that can match tanks with physical separators between hot and cold fluids [62]. A study performed by Taylor et al. suggests that using a thermally stratified liquid is more effective than using a packed bed thermal storage system [63].

On the other hand, the one tank system has a more complicated charging and discharging processes than the two tank system or a fully mixed one tank system, due to

constant switching between the inlet and outlet. In addition, the tank has to be symmetrical in order to ensure interchangeability of the inlet and outlet [64].

In terms of the tank capacity, a one tank system requires a higher unpumpable volume of liquid, which is reserved for the thermocline region, than a two tank system or a fully mixed one tank system. The main advantage of a one tank system over a two tank system is the cost reduction caused by eliminating the need for a second tank, which reduces the cost of the storage system by at least 35 percent [65]. The advantage of a thermocline tank storage system over the fully mixed one tank system is a higher thermal efficiency of storage fluid.

According to the National Renewable Energy laboratory (NREL), a sensible heat storage system with a liquid medium in two tanks is the most practical and the most economical thermal energy storage system. Consequently, in high temperature energy storage for power generation, two tank systems are the most dominant in the market [6]. An economics study showed that the usage of two tank molten salt storage and CSP increased the annual capacity factor from 30% to 55% with 12 hours of storage [66]. The annual capacity factor is the percentage of the actual power generated throughout the year to the potential power generation.

However, a stratified one tank storage system is an attractive alternative due to the promising cost reduction associated with an additional tank and the potential of achieving acceptable thermal efficiency. Satisfactory thermal efficiency is accomplished by reducing the mixing between hot and cold fluids inside the tank [59]. Storing hot fluid in

a fully mixed tank reduces the tank's thermal efficiency by 30 - 60 % in long term seasonal energy storage applications where hot or cold fluid is stored for over 3 months [67].

The use of the direct tank storage system, where the HTF is the same as the storage medium, has the potential of cost reduction and performance improvement by eliminating the need for heat exchangers. The following table summarizes the advantages and disadvantages of one tank and two tank systems:

Table 2.3 Advantages and disadvantages of two tank and one tank systems

Sensible heat storage system	Advantages	Disadvantages
Two tank system	Mixing between hot and cold fluid is avoided Simple operation Higher thermal capacity Risk mitigation of tank's failure (there is a backup tank)	High cost of tank's construction Low resistance to internal pressure Pumping has to be from the bottom (for molten salt)[29] Heat losses from the top and bottom are high Size limitation due to practical *H/D* constraints
One tank system (stratified)	Eliminate the need for a second tank Reduction of used space	Mixing inside the tank reduces storage efficiency Heat losses from the walls and bottom deteriorate the stratification in the tank and lower the efficiency Thermocline region takes up 30% of the tank's volume More complex charging and discharging (requiring switching inlet and outlet)
One tank system (fully mixed)	Reliable operation Simple operation (no need for switching inlet and outlets) High flow rate	Low thermal efficiency compared to stratified tank

Heat pipe systems

Due to the high cost encountered in molten salt tank systems, heat pipe systems and PCM material storage systems have drawn attention in the last decade. Heat pipe systems use either or both sensible heat and latent heat storage. Various combinations, of solid material, PCM, shapes, and geometry have been studied in the solar energy field. Solid materials used in heat pipe systems are: ceramic, concrete, granite and other manufactured composite materials [68].

For heat pipe systems with solid materials, the HTF runs through pipes embedded in solid blocks, usually concrete or ceramic, in order to store sensible heat. Solid media storage has been under experimental study for parabolic trough power plants in Platforma Solar de Almeria in Spain but has not been placed into practice yet on an industrial scale [69].

Two systems, high temperature concrete and cast ceramic, have been tested with a maximum temperature of 390 ^{0}C and synthetic oil as the HTF running through cast iron pipes. Both systems were suitable for solar trough heat storage and both were able to withstand cyclical charge and discharge. The study also showed that the ceramics have superior thermal and mechanical properties to the high temperature concrete. However, the study favored high temperature concrete due to its low cost and convenience of handling.

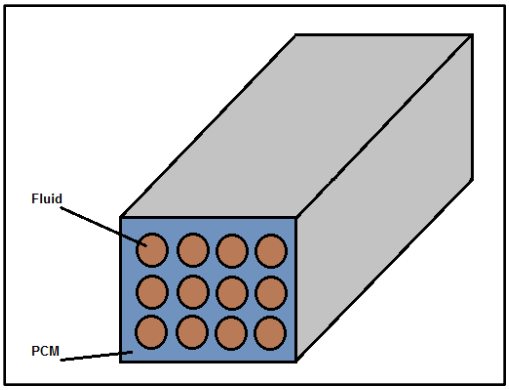

Figure 2.6 Example of heat pipe system

Numerous studies have been performed for sizing and material selection for heat pipe systems via numerical simulation or small scale experimental set ups [70, 71]. The heat pipe system is known for its flexibility of using both SHS and LHS and also being built in cascade configuration. The geometry of the pipes, pipe layout, and flow parameters inside the pipes to maximize the heat exchange between the HTF and the storage medium are also areas of interest in heat pipe systems [72].

The ability of heat pipe systems to use both LHS and SHS gives it the advantage of supplying HTF with constant temperature, which is required for some steam generation processes. Constant temperature is difficult to achieve by using sensible heat storage alone since sensible heat storage has a variable release temperature [26].

A pilot storage system that consists of a three part storage module has been successfully tested [73]. The system has the following specifications: sensible heat storage using two concrete modules, latent heat storage unit that uses $NaNO_3$ as a PCM,

operating temperature up to 400º C, pressure of 128 bars, and heat storage capacity of 1*MWh*. The small scale system was tested as part of a special cycle loop in a *Carboneras* power plant in Spain in 2010 and performed successfully. A similar large scale system is being planned for implementation in the same plant.

Figure 2.7, is adopted from Medrano et al. [59]. The figure summarizes the most recent thermal storage systems with their advantages and disadvantages. Industrial scale power plants favor using the two tank system due to the low mixing between the cold and hot HTF and high storage temperature. On the other hand, the two tank storage system has the drawbacks of high initial cost and the higher operation requirement due to the high freezing temperature of the molten salt, which requires keeping the pipes at a high temperature at all times.

	System		Positive	Negative	Recent applications
Active storage	Direct	Direct Steam Generation (DSG)	1. Simple plant configuration 2. Low cost for capital, operation, and maintenance 3.Eliminates the need for Heat exchanger (HEX) between the steam and the HTF.	1. Higher cost for piping system due to high pressure requirements 2. Need a backup heating system 3. Control issues due to change in solar radiation	PS10 and PS20 Abegoa, Spain,2007
		Two tanks	1. No mixing between hot and cold HTF 2.High temperature operation With high temperature HTF , smaller size storage can be used 3. Hazard mitigation in case of tank failure	1.High cost of : HEX, TES, tanks 2. Heating back up is required	SEGS II ,Degget, CA USA,1985
	Indirect	One tank	Lower cost due to : 1. One tank instead of two 2. Filler material can be used and substitute for expensive salt.	1.The high freezing temperature of salt requires keeping the system at high temperature 2. Mixing between hot and cold HTF reduces temperature output 3. Complicated design 4. Tank failure has no back up	Solar One, Barstow, CA ,1988
		Two tanks	1.Mixing between the hot and cold HTF is avoided 2. High temperature can help reduce the size of the storage 3. the possibility of freezing of the salt is decreased since HTF flows only between the tanks 4. provide back up in case of tank failure	Increased capital cost due to: a. Two tank construction b. More TES material is required c. HEX is required	ANDASOL II, Spain 2009 SOLANA,Phoenix,AR,US A 2011
		Cascade tanks	1. PCM storage capacity is utilized more efficiently 2.Uniform outlet temperatures	Increased cost due to: 1. More tanks 2. More PCM	Has not been done on industrial scale (only pilot scale)
Passive Storage	Concrete/ Ceramics		1. Low cost of material 2.Increased heat transfer rate	1.Increased cost due to HEX 2.Unstable over time	Experimental phase
	PCM + sensible		1. High storage capacity 2. Low cost	1. Low heat transfer rate 2. Low PCM thermal conductivity	N/A

Figure 2.7 Comparison between available TES systems [59]

Summary

Thermal energy storage is an evolving area of study. The benefits of using TES have been realized in power plants, desalination, and HVAC systems on small and large scale. TES systems are undergoing constant improvements in terms of economics, reliability, thermal capacity and configurations.

In considering solar thermal energy, the success of using the sun's heat as the sole source of energy depends largely on the TES system associated with the cycle, location, and mode of operation.

CHAPTER 3 : SPHERICAL TANKS

Current Utilization in the Industry

Spherical tanks are used in several applications such as water storage, nuclear cooling, and storage of liquefied gases such as liquefied natural gas (LNG) and liquefied petroleum gas.

Elevated water storage applications are common for municipal water storage. They are preferred over other types of elevated tanks because of the additional storage capacity, additional system pressure due to elevation (which is very useful for continuous pumping during power outages), improved aesthetics, suitability for different types of soil, resistance to seismic activity, maintenance facilitation due to complete surface exposure, and the efficiency of building material usage [74]. Elevated spherical water storage tanks come in three shapes: spheroids, pedesphere, and multicolumn spheres.

Figure 3.1 Left: Spheroid, Middle: Pedesphere, right: Multicolumn sphere [74]

Spherical tanks are also used for outer space applications due to complete tank drainage when compared to cylindrical tanks. Tank drainage is performed in outer space by injecting pressurized gas; this is a necessary practice in a zero gravity environment [75]. In addition, they are used in satellites and launch vehicles due to their high volume to weight ratio. In such applications, the sloshing inside the tank and the tank natural frequency at different fill levels are subjects of investigation [76].

The second most common utilization of spherical vessels in the industry is pressurized gas storage because they can withstand higher internal pressure and have fewer size limitations than cylindrical pressure vessels. A spherical tank with pressurized gas inside and a concrete foundation is shown in Fig. 3.2.

Figure 3.2 Example of a spherical tank for LPG [77]

Spherical tanks have high rigidity and durability. The performance of a 200 m^3 liquefied petroleum gas (LPG) tank with a wall thickness of 24 mm under 1.7 MPa

pressure was evaluated after it had been in operation for three years, revealing high resistance to micro cracking and shell deformation, with minimal wall thinning [78].

Ground level or buried spherical tanks are usually built using reinforced concrete, and they are used for water storage. A study performed on a thin shell spherical tank made with reinforced concrete proposed using a reinforced concrete sheet placed on an inflatable rubber membrane. The membrane is then inflated like a balloon before the concrete is fully solidified, in order to give the concrete sheet a dome (half a sphere) as the final shape. This technique to erect a dome has the potential to reduce the cost of materials and manufacturing associated with spherical vessels, thus making the use of spherically shaped concrete tanks more feasible [79]. The study included two types of spherical concrete tanks for water storage: buried and half buried. In a few African countries, such as Kenya and Uganda, brick cement spherical tanks are used for water storage. Spherical shapes are preferred for such applications because they require less building material and support, and are easier to construct [80].

Spherical Tank Utilization in TES

The use of spherical tanks for thermal energy storage has been limited to underground seasonal storage. A recent study proposed using spherical tanks for underground seasonal storage due to their rigidity [52]. The utlization of spherical tanks in thermal energy storage has been hindered by the associated manufacturing cost. However, spherical tanks are gaining interest and popularity due to their structrual attributes of lower heat loss and high resistance to internal pressure. Fiber glass and

polyethylene are promising alteranives to stainless steel because they facilitate the manufacturing of large spherical vessels through structrual reaction injection molding for fiber glass to reduces material and manufacturing cost. Curently, polyethylene underground cylindrical tanks are used for long term hot water storage [81].

Some materials such as Therminol VP-1 are considered good candidates to be used as storage media for TES. However, Therminol VP-1 has a high vapor pressure, and requires an increased tank wall thickness [82].

The merit of using a spherical shape for a thermal storage system is illustrated by comparing a cylindrical rock packed bed and a spherical liquid tank for thermal storage with the same volume [83]. Finite difference modeling was performed to obtain the spherical tank's charging rate and total energy stored. Data were compared to existing data for the rock packed bed. At the same rate of energy input, the spherical liquid tank had a much higher charging rate and a larger energy capacity per volume than the rock packed bed.

Currently there are no tanks designed especially for thermal energy storage systems. For the two tank system, hydrocarbon cylindrical tanks are used with a modified foundation and added wall insulation to mitigate heat transfer to the ambient. When storing molten salt at high temperature, multilayers (up to five layers of insulation bricks) of foundation have to be prepared before the tank is installed [29].

Technical Aspects of Spherical Tanks

Internal stresses and thickness calculation

Spherical tanks are considered thin walled vessels when the wall thickness is very small compared to the other tank dimensions. The thin wall assumption is valid when all of the following parameters are satisfied: (1) the thickness is less than 0.1 of the tank radius R, (2) the pressure inside the vessel is more than the pressure outside, (3) the pressure analysis considers only the internal pressure, (4) the calculation involves only the shell and excludes any stress concentration at an opening, support, or connection.

There are three stresses acting on the inside wall in a spherical tank. The internal pressure forms three types of stresses: circumferential (tangential) stress $\boldsymbol{\sigma_t}$, meridian stress $\boldsymbol{\sigma_m}$, and radial stress $\boldsymbol{\sigma_r}$. The meridian stress and the tangential stress are equal because the circumference and the meridian are the same [84]. Assuming a true sphere, $\boldsymbol{\sigma_r}$ and $\boldsymbol{\sigma_t}$ are calculated using the following formulae:

$$\boldsymbol{\sigma_r = \frac{p}{a^3-1}\left[1-\left(\frac{r_e}{r}\right)^3\right]} \qquad \textbf{3.1}$$

$$\boldsymbol{\sigma_t = \frac{p}{a^3-1}\left[1+\frac{1}{2}\left(\frac{r_e}{r}\right)^3\right]} \qquad \textbf{3.2}$$

where $\mathbf{r_e}$ is the external radius, **r** is the location where the stress is to be calculated, **p** is the internal pressure, and $a = {}^{r_e}/_{r_i}$. The maximum value of stress occurs in the internal fiber of the shell $r = r_i$; the previous expressions can be reduced to:

$$\sigma_{ti} = p \cdot \frac{\frac{a^3}{2}+1}{a^3-1} \qquad 3.3$$

$$\sigma_{ri} = -p \qquad 3.4$$

Considering the maximum allowable stress σ_s, and the internal diameter D_i, the required wall thickness t at a given internal pressure p can be calculated as:

$$t = \frac{D_i}{2}\left(e^{\frac{p}{2\sigma_s}} - 1\right) \qquad 3.5$$

In pressure vessels, the internal pressure is uniform along the entire inner surface and the hydrostatic pressure is negligible due to the low density of LPG and LNG, which is not the case in thermal storage systems using liquids such as molten salt or water.

Spherical tank support is designed based on the weight of the stored product and the location where the tank will be placed. A Pedesphere tank, where the tank is placed on a pedestal, is suitable for locations with low seismic activity in order to avoid the inverted pendulum effect during an earthquake. Other types of support include a column support where the tank is supported by a number of columns at either the equator or below the equator of the tank. Ground support with full or partial burial is common for water storage tanks where additional hydrostatic pressure is not required.

The number of supporting columns required for the tank is chosen based on the storage product weight and also the estimated wind and seismic activity:

$$n = 2F/\forall \qquad \textbf{3.6}$$

Where n is the number of columns, $\boldsymbol{F}$ is the normal force on the side of the tank and $\forall$ is the shear force exerted on the tank. The number of columns is also related to the tank diameter and distance between each of the supports [85]:

$$l = \sqrt{Dd/2} \qquad \textbf{3.7}$$

Where l is the distance between columns, D is the tank diameter, and d is the column diameter. The connection of the support columns and the tank is called the support belt. Spherical tank support is thoroughly investigated in locations where seismic activities are expected. A Finite element analysis (FEA) performed on a spherical tank during a seismic event suggested that the spherical tank support legs behave more like a frame than an inverted pendulum, providing flexibility for the tank to move in the horizontal direction more than the radial direction. This results in less possibility of fracturing individual legs due to bending stress. Therefore increasing the number of columns and reducing their individual diameter is preferred. The study also suggests that number of supports, materials, and external and internal diameters are a function of the weight of the stored product and location [86].

Typical tank life depends on the stored material, building material, temperature of operation, weather conditions, and periodic maintenance. Average life span of some common tanks is listed in Table 3.1[87]:

Table 3.1 Average life span of common tanks

Type of Tank	Number of years
Concrete tanks	30-55
Steel oil storage	25-20
Stainless steel with chemical storage	15-30
Steel pressure tanks	20-25
Elevated steel water tanks	30-40

Large vessel manufacturing

Small to medium scale spherical tanks are made from pre-cast segments that are individually welded and then treated in heat treatment ovens. Large vessels are constructed on site from pre-fabricated segments that are welded and treated on location individually. The complete tank has to be heat treated and hydro-tested (filled with water and then pressurized by air) on site. Welding of grouped segments is shown in Figure 3.3.

The cost of spherical tanks is usually estimated based on the weight of the vessel. Meanwhile the cost of cylindrical tanks is based on the volume. Therefore, the cost estimate of a spherical tank varies depending on the shell thickness. The material used in making the shell alone can lead to a cost variance of plus or minus 20 % [88]. The use of

a spherical tank instead of a cylindrical tank can cut the material used by half. This saving in material has to be considered during the tank shape selection.

The traditional manufacturing process of spherical tanks is responsible for the cost associated with spherical tank construction. However, there are several patents for innovative construction methods that have promising cost savings on welding, casting, and treatment of spherical tanks [89-93]. The low and infrequent demand of spherical tanks hinders putting some of these methods into practice. Recently, the boom of liquefied natural gas LNG led manufacturers to invest more in cheaper methods to construct pressure vessels for storing and transporting LNG gas, which consequently will lead to cost reduction in spherical tank construction.

Figure 3.3 Construction of large elevated spherical tank

Heat transfer

When a spherical tank is used in a TES system, either for cold or hot storage, heat transfer to or from the ambient occurs due to a temperature difference between the storage medium and the ambient. Based on the surrounding air temperature or ground temperature, conduction to the ground or external convection to the atmosphere can take place causing the tank to lose or gain heat over time. The duration of storage, location, and tank support are all factors in heat loss calculations and insulation requirements. Duration of storage can range from 6 hours in CSP summer back up to 4 months in seasonal hot water storage. The geographical location influences the external convection through wind and conduction to the ground.

Finally, the type of spherical tank support (multicolumn or pedestal) plays a major role in the heat loss mode (convection or conduction) in the lower portion of the tank. Therefore, the choice of support has to be accounted for in the design in order to minimize heat transfer and make decisions on insulation methods.

Figure 3.4 shows the heat transfer from a spherical tank containing hot storage fluid to the ambient through four thermal resistances: internal convection resistance, wall conduction resistance, insulation conduction resistance, and external convection resistance. The heat transfer considers only the wall and neglects conduction through supporting columns. Modifications are to be done in order to include tanks supported on the ground, buried or partially buried.

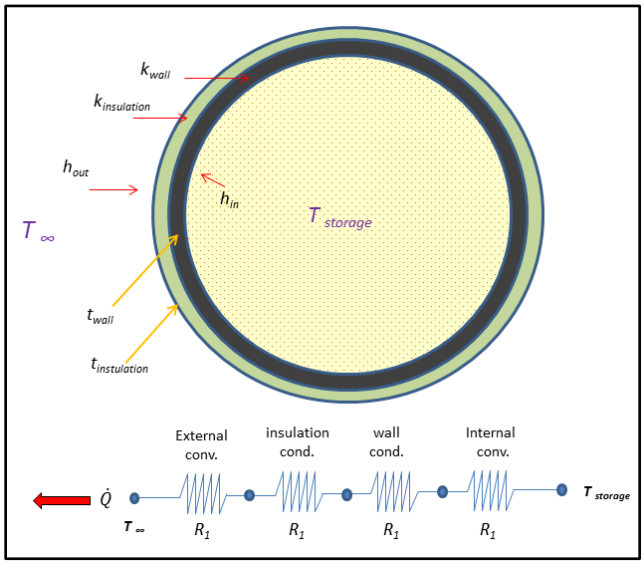

Figure 3.4 Heat transfer through spherical tank for hot fluid

Conduction from a spherical wall

Conduction heat transfer through a spherical vessel is calculated using the following equation [94]:

$$\dot{Q} = \frac{4k\pi r_1 r_2 (T_h - T_c)}{t} \qquad \textbf{3.8}$$

Where $\dot{Q}$ is the heat transfer rate through the wall, k is the tank thermal conductivity, r_1 is the internal radius, r_2 is the external radius, T_h and T_c are the hot and cold temperatures for the storage and ambient, which can alternate based on a hot or cold storage system, and t is the wall thickness. Based on eq. 3.9, the wall thermal resistance for the wall and the insulation layer can be calculated as [94]:

$$R = \frac{t}{4k\pi r_1 r_2} \qquad \textbf{3.9}$$

External convection

External convection from the tank takes place by either forced convection due to wind or natural convection if the wind is negligible. The Whitaker relationship can be used to calculate forced convection over a sphere for the range of Reynolds numbers (*Re 3.5- 80,000)* and Prandtl numbers between *0.7- 380* given by [95]:

$$Nu_{Sph} = \frac{hD}{k} = 2 + [-.4Re^{1/2} + 0.06Re^{2/3}]Pr^{0.4}(\mu_{\infty}/\mu_s)^{1/4} \quad \textbf{3.10}$$

The calculation of the natural convection coefficient for spherical shaped vessels has been an area of interest due to their industrial application. Few theoretical and experimental studies provide an approximation of Nusselt number based on the sphere diameter Nu_D and Rayleigh number [96]. For natural convection from outside the spherical tank, Churchill recommended the following relationship for Rayleigh numbers less than 10^{11} and Prandtl number larger than 0.7 [97]:

$$\overline{Nu}_D = 2 + \frac{0.589Ra_D^{1/4}}{\left[1+\left(\frac{0.469}{Pr}\right)\right]^{9/16}}^{4/9} \quad \textbf{3.11}$$

Where Ra_D is the Rayleigh number evaluated at the sphere's outer diameter. The external convection heat transfer coefficient h_{out} from Nu_D as:

$$h_o = \frac{Nu \cdot k}{D} \quad \textbf{3.12}$$

Using h_o , the thermal resistance due to external convection can be calculated as:

$$R_o = \frac{1}{h_{out} \cdot A_{out}} \quad \textbf{3.13}$$

Where A_o is the external area of the tank.

Internal convection

There are only few thermodynamic studies performed on the flow inside a spherical vessel due to free convection [98]. Hutchins and Marschall performed a finite difference numerical analysis verified by experiment for the pseudo-steady state in order to calculate the natural convection inside a spherical tank [99]. The results showed that the Nusselt number can be correlated with the Rayleigh number (*Ra),* at Pr > 0.7:

$$\boldsymbol{Nu_D = 1.19 Ra^{0.2215}} \qquad \textbf{3.14}$$

The experiment was confined to *Ra* number between 10^5 and 10^{10}. The *Ra* number was calculated using the following equation:

$$\mathbf{Ra} = \frac{\boldsymbol{\rho \cdot g \cdot \beta \cdot D^3 \, (T_w - T_c)}}{\boldsymbol{k \cdot \nu}} \qquad \textbf{3.15}$$

Where g is the gravity acceleration, β is the coefficient of thermal expansion, T_w is the wall temperature and T_c is the temperature at the center of the sphere.

The flow of natural convection inside a sphere includes a circulation layer near the wall due to wall curvature; the circulation is caused by conduction heat transfer through the sphere, which creates a buoyancy force difference. This phenomenon was illustrated by an experimental study on PCM melting in a spherical container [100] and a mathematical simulation of unsteady natural convection on a sphere [98]. The thickness of the circulation boundary layer changes with the Rayleigh number and the temperature difference between the inside and outside of the sphere. Figure 3.5 shows the circulation

expected between two concentric spheres. The inside sphere is kept at a constant hot temperature while the outside sphere is maintained at a colder temperature.

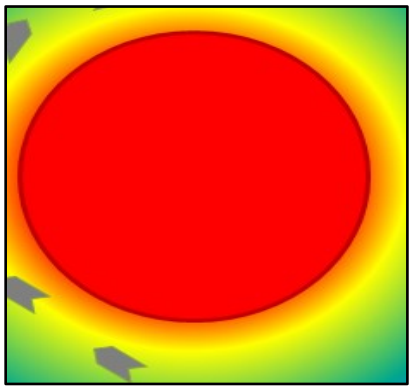

Figure 3.5 Liquid circulation boundary layer between two concentric spheres

Heat transfer rate calculations for spherical shape containers are more common for encapsulated phase change materials (PCMs) than for liquids inside spherical tanks. The sphere was acknowledged as the optimal shape for PCM containers in packed bed TES. Spheres have a low heat transfer rate to volume ratio, and they are easy to pack inside a packed bed tank. Saitoh compared the thermal performance of *n-heptadecane* $C_{17}H_{36}$ inside spherical and cylindrical enclosures [101]. The comparison showed that a spherical shape had the highest thermal storage performance due to thermal capacity, external flow contours, and porosity. Roy and Sengupta studied the melting of PCM inside a spherical tank and noted that natural convection heat transfer losses from the top and bottom of the sphere are significant [102].

Spherical shape tanks have technical and economic advantages over other tank shapes in terms of: possible material saving due to their high resistance to internal pressure, simple foundation construction and preparation, and reduction in wall heat transfer due to a low surface area to volume ratio.

PCM encapsulation in spherically shaped containers has proven to deliver the best result in packed bed storage systems proving the important role of container shape on its thermal capacity. The use of spherical tanks in TES system is currently limited to underground seasonal storage. Further investigation of spherical tank usage in two tank and one tank system is needed to examine their technical and economic feasibility as TES vessels.

Technical Aspects of Cylindrical Tanks

In the next chapter, cylindrical tanks for two tank storage system will be compared to spherical tanks of the same volumes in terms of shell thickness, internal stresses and heat loss from the wall and foundation. The following formulas will be utilized for the required comparison.

Internal stresses and tank shell thickness

There are three stresses acting on the inside wall in a cylindrical tank [84]. Those stresses are: (i) hoop (tangential) stress σ_t, (ii) radial stress σ_r, and (iii) longitudinal stress σ_a. Amongst these three stresses, only the longitudinal stress is constant throughout the wall. The calculation for stresses on the inside wall stresses are given by [67]:

$$\sigma_t = P_i \frac{r_o^2 + r_i^2}{r_o^2 - r_i^2} \quad \textbf{3.17}$$

$$\sigma_r = -P_i \quad \textbf{3.18}$$

$$\sigma_a = P_i \frac{r_i^2}{r_o^2 - r_i^2} \quad \textbf{3.19}$$

where P_i is the internal pressure, r_i is the internal radius, and r_o is the outside radius. At wall thickness $t/r_o \leq 0.1$, such as in this study, the cylinder is considered thin walled and the internal pressure is supported by the hoop stress and the axial stress that are calculated as follows:

$$\sigma_t = \frac{Pi \cdot r}{t} \quad \textbf{3.20}$$

$$\sigma_a = \frac{Pi \cdot r}{2t} \quad \textbf{3.21}$$

If the hoop stress is assumed to be constant on the entire side wall, the following equation for wall thickness is obtained:

$$t = \frac{pD_i}{2\,\sigma_{allowable}} \quad \textbf{3.22}$$

Heat loss calculation in a cylindrical tank

Conduction through the walls, roof, and bottom:

Conduction heat transfer from the tank's cylindrical side wall was calculated using the following relation as follows:

$$\dot{Q} = \frac{2\pi kL(T_1 - T_2)}{ln\left(\frac{r_2}{r_1}\right)} \qquad \textbf{3.23}$$

The heat transfer calculation can be used to calculate the wall thermal resistance (R):

$$R = \frac{ln\left(\frac{r2}{r1}\right)}{2\pi kL} \qquad \textbf{3.24}$$

Where k is the shell's material thermal conductivity, T_1 is the inside temperature, T_2 is the outside temperature, r_2 is the outer diameter, and r_1 is the inside diameter of the cylinder. The conduction at the top and bottom walls of the cylindrical tanks can be treated as regular conduction through a plane wall:

$$\dot{Q} = \frac{2\pi r^2 k(T_2 - T_1)}{t} \qquad \textbf{3.25}$$

With R equation:

$$R = \frac{t}{2\pi r^2 k} \qquad \textbf{3.26}$$

Where r is the inner diameter of the tank, and t is the wall thickness of either the top or the bottom (which have different thicknesses). The wall thickness will be the highest at the bottom of the tank, and the lowest will be at the top, which correlates with the hydrostatic pressure of the liquid inside the tank.

External convection

External convection for a TES tank varies based on the location where the tank is placed due to the variations in wind, and ambient temperature). To compare the tank's shell heat loss alone, no insulation was considered and natural free convection was assumed in this study. A location based forced external convection calculation and insulation thermal resistance must be estimated for an actual evaluation.

Natural convection from a vertical cylinder depends on *D/L*, the fluid's Prandtl number, and the Rayleigh number from [25]:

$$\overline{Nu_L} = \frac{4}{3}\left[\frac{7Ra_L\,Pr}{5(20+21Pr)}\right]^{1/4} + \frac{4(272+315Pr)L}{35(64+63Pr)D} \qquad \textbf{3.27}$$

However, for all the cylindrical tanks' *H/D* ratios taken in this study, the relation $D \geq \frac{35L}{{Gr_L}^{1/4}}$ was valid. Therefore the cylindrical tank wall can be treated as a vertical plate for Ra between 10^4 and 10^{13} [94], and the Nusselt number can be alternatively calculated as follows:

$$\overline{Nu_L} = \left[0.825 + \frac{0.387{Ra_L}^{1/6}}{\left[1+\left(\frac{0.492}{Pr}\right)^{9/16}\right]^{8/27}}\right]^2 \qquad \textbf{3.28}$$

The subscript *L* denotes the characteristic length, which is the height of the cylinder *H*. The top of the cylindrical tank can be treated as a horizontal plate with the hot surface area facing the top. The Nusselt number can be calculated using equation 4.20& 4.21:

$$\overline{Nu_L} = 0.54\, Ra_L^{0.25} \quad for \;\; 10^4 < Ra < 10^7 \qquad 3.29$$

$$\overline{Nu_L} = 0.15 Ra^{\frac{1}{3}} \quad for \;\; 10^7 < Ra < 10^{11} \qquad 3.30$$

The characteristic length equals the surface area divided by the plate's perimeter. In the case of a round flat plate, the surface area will be $\frac{R_o}{2}$ with R_o being the outside radius of the cylinder [94].

Natural convection inside cylindrical tanks

Natural convention inside the vessel will occur due to buoyancy caused by the difference temperatures in the layer close to the shell and the center of the vessel. The difference in temperature will lead to density variation in the storage fluid, which will cause the low density fluid to keep rising to the top of the tank. Lin and Akin performed an experimental study to calculate the pseudo-steady state natural convection heat transfer inside a vertical cylinder [113]. They found a characteristic length that provided the best results when compared with experimental results and other characteristic lengths relations:

$$L = 6 \cdot \frac{Volume}{Surfce\ area} = D\left[\frac{3\left(\frac{H}{D}\right)}{1+2\left(\frac{H}{D}\right)}\right] \qquad 3.31$$

They also found that for a Prandtl number above 5, the Prandtl number has no significant effect on natural convection and that only geometrical aspects and the

Rayleigh number influence natural convection inside the tank. The Nusselt number for vertical cylindrical tanks can be calculated using the following:

$$Nu = 0.519 \cdot Ra^{0.255} \qquad 3.32$$

The Rayleigh number is calculated using the temperature difference between the wall and the center of the cylinder:

$$Ra_L = \frac{\rho \cdot g \cdot \beta (T_s - T_b) L^3}{v \cdot k} \qquad 3.33$$

Summary

Technical aspects such as internal stresses for both spherical tanks and cylindrical tanks, which lead to tank construction material volume, will be subjected to comparison under the same storage volume of the same TES storage medium. Heat loss from each tank in a two tank storage system will be calculated for the hot and cold storage tanks in order investigate the amount of insulation and foundation required for each set of tank systems.

CHAPTER 4 : COMPARING SPHERICAL TANKS TO CYLINDERICAL TANKS IN TES TWO TANK SYSTEMS

Two Tank Molten Salt TES

Molten salt two storage tank systems consists of two tanks: One tank contains the high temperature molten salt, and the other tank contains low temperature (above the salt's freezing temperature) molten salt. Some configurations include a set of tanks for hot molten salt and a set of tanks for cold molten salt.

To date, the two tank system is the most dominant storage system in direct steam generation and solar power plants. Two tank systems have proven to be technically feasible and have been used in several CSP plants in the U.S and Europe. Even though there are several types of TES, the two tank system is the only system that is used commercially.

The advantages of the two tank system when compared to the thermocline one tank system are: (i) mixing between the hot and cold storage fluid is avoided, (ii) simple operation with no need to switch between the inlet and outlet, (iii) risk mitigation in case of tank failure [29], and (iv) higher storage capacity per tank due to lower unpumpable volume. Thermal capacity is defined as the amount of molten salt that can be drawn from the tank divided by the tank volume [82].

The disadvantages of the two tank molten salt system are: (i) high installation cost of storage estimated at 30-50 US$ per 1 $kW_{th} \cdot hr$ [103], (ii) high insulation cost for tanks, piping and foundations, (iii) cyclic degradation and corrosiveness of molten salt at high temperature and (iv) the need for a heating back up source inside the tank and for the piping system in order to keep the system temperature above salt melting temperature.

Current Limitations in TES Tanks

One-tank and two-tank molten salt storage systems share the common issue of high capital cost of the tank. Each tank costs 35% of the entire TES system [60]. One tank systems are considered in molten salt TES for the sole reason of eliminating the cost of a second tank, and saving floor space. Current molten salt storage tanks are cylindrical with an ellipsoid roof. The tank design and sizing depend on the plant's thermal energy storage requirements. These types of storage tanks are constructed, welded, heat treated and tested on site, similarly to the storage tanks used for hydrocarbon products [104].

A tank design optimization was performed on cylindrical tanks for molten salt TES of a 600 $MW\,h$ thermal storage tank for a CSP power plant. It concluded that TES tanks must have the following capabilities [29]: (i) withstand the hydrostatic pressure of molten salt, (ii) resist vacuum pressure (that could occur when the relief valve fails in the closed position and the salt suddenly cools), (iii) resist over pressure (that could occur when the heat exchanger fails), (iv) pumping is from the bottom (since pumping from the side will introduce a weak point in the cylindrical wall), (v) minimal heat loss from the

side wall , (vi) the roof must withstand the vacuum pressure and over pressure, (vi) wall material has to resist reaction with molten salt.

In an engineering study performed by Herrmann et al. of TES two tanks systems, the most economical design was found to be a cylindrical shell (also known as a tube shell) with a self-supporting roof [105]. The tanks are similar to the tanks used for oil storage, with added insulation to the walls and a modified 5 layer insulation for the foundation. In the same study, the pumping heads required for 1 to 15 hours of thermal storage at 10 *MWe* power generation rate, were 19.2-38.4 m. However, no pumps were identified as suitable for this application. The pump should draw suction from the bottom of the tank with a motor located on the top of the tank and connected through a long shaft. Recent market research to find such a pump shaft revealed that the maximum available length of pump shaft is 12 m. Moreover, the weight of the pump's motor and the motor's assembly has to be considered in designing the tank's roof structure.

Thermal energy storage tanks designers favor large *H/D* ratios because they provide a better thermal gradient in a one tank system [82]. In two tank systems, a large *H/D* is also preferred because it leads to lower heat transfer rates from the top and bottom of the tank. However, Pacheo et al. reported that that tallest tank that could be practically manufactured is 16 m. In addition, having a tank height exceeding the diameter will increase the cost by at least 35% to account for the added foundation measures and support [74]. In contrast, LPG spherical tanks have been constructed with various heights with excellent tank reliability record. Spherical tanks can have a diameter up to

22 m with variable wall thickness and braces to accommodate stress deformation and give the tank the required rigidity. The ability to increase the tank height and overcome the pumping limitation will lead to larger tank volumes and consequently more thermal storage hours per tank.

Therefore the current limitation of the two tank system cylindrical vessels are: low resistance to internal pressure, large heat loss from the bottom and top of the tank, tank height limitation due to pump availability, and low resistance to vacuum pressure.

This study investigates utilizing spherical tanks in molten storage system as an alternative to cylindrical tanks. Structural and thermal aspects of cylindrical and spherical tanks of the same volume are compared in order to determine possible economic savings or technical advantages.

Cylindrical vs. Spherical Tanks for Two Tank TES

In this part of the analysis, spherical and cylindrical tanks of the same volume are subjected to tank shell volume comparison based on the required shell thickness for each tank. The cylindrical tanks used for *Solar Two* plant are constructed of carbon steel ASTM-A516-70 for the cold molten salt and stainless steel 304 for the hot salt [106]. Stainless steel is used because molten salt tends to be more reactive with carbon steel at temperatures above 300° C. The same materials selection is used in this comparison of cylindrical and spherical tanks. The internal pressure acting on the tank walls is the hydrostatic pressure caused by the molten salt, which varies with liquid height inside the

tank. Because molten salt do not need to be stored under pressure, and there is no high vapor pressure acting on the internal walls or roof of the tank. Therefore, the only pressure acting on the tank walls is the hydrostatic pressure. Wall thickness is calculated using hydrostatic pressure and maximum allowable stress for each material with a safety factor of 2. The Safety factor equals the yield stress divided by the actual tank stress. Safety factor of greater than 1 is acceptable for regular tanks and for pressure vessel designs it is typically vary from 3.5 to 6 [107].

The tank material used in this comparison was Stainless Steel A304 with a maximum yield stress of 215 MPa and allowable stress of 100 MPa. The calculation was performed using thickness calculation formulas in chapter 3 with variable wall thickness based on the hydrostatic pressure. Figure 4.1 shows the average wall thickness reduction when substituting spherical tanks for cylindrical tanks of the same internal volume. Using the calculated shell thicknesses, the shell volumes of cylindrical tanks and spherical tanks are compared in Fig.4.2. This reduction in material could yield significant savings in cost and possibly increase the internal pressure resistance.

Recently, due to higher molten salt storage temperatures, hot molten salt storage tanks are equipped with flexible stainless steel AISI 321H liner in order to improve corrosion resistance to molten salt at temperature higher than 500° C [29] .

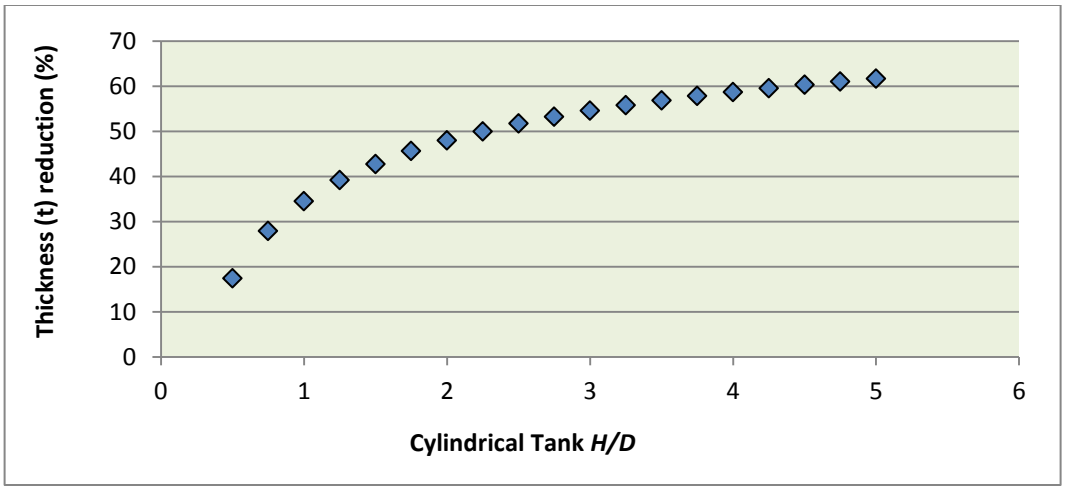

Figure 4.1 Tank wall thickness reduction when replacing cylindrical tank with spherical tank

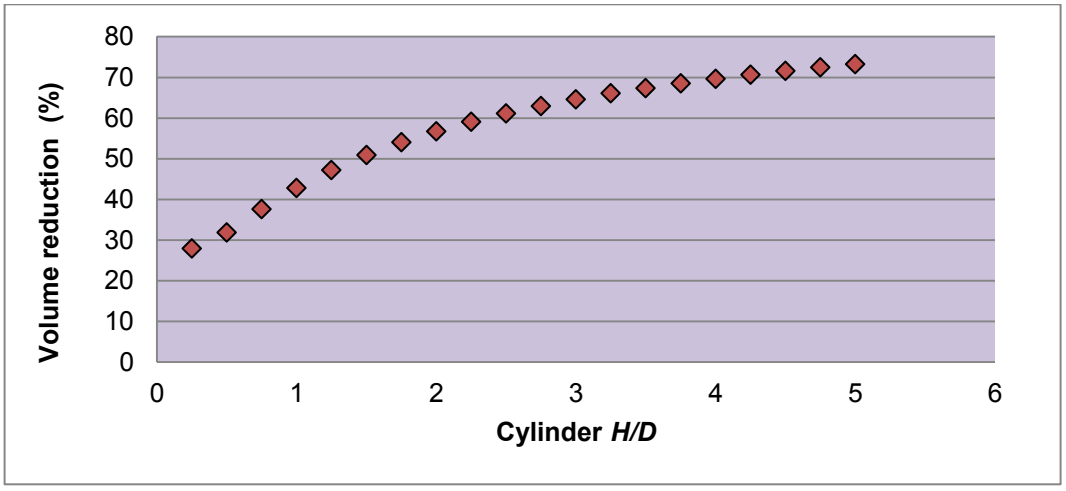

Figure 4.2 Shell volume reduction when using a spherical tank instead of cylindrical tank

The reduction of shell material was expected due to the spherical tank's high resistance to internal pressure. In LPG storage, a 50 % reduction in shell volume is expected when replacing a cylindrical tank with a spherical tank. However the higher density of molten salt in comparison to LPG required a thicker shell to accommodate the hydrostatic pressure of the molten salt even with the absence of high vapor pressure in molten salt.

Other Structural Benefits of Spherical Tanks in TES

In order to fulfill the requirement highlighted by Gabbrielli and Zamparelli [29], TES tanks have to withstand vacuum pressure and over pressure. Spherical tanks have been shown to have a higher resistance to internal pressure, hence their utilization in LPG storage. However, withstanding an over pressure of 20 bars (the typical operating pressure of a Rankine power cycle) would only be possible by increasing the shell thickness by at least a factor of 12. A relief valve would be the most suitable option for risk mitigation.

Tank height restriction is related to pump availability. The current type of pump that is used to withdraw molten salt from the tank is a cantilever (vertical) sump pump with specific bearing material to withstand the operational temperature and corrosiveness of molten salt at hot temperatures. Few studies have investigated the improvement of pump specifications to overcome the vibration and bearing shortcoming that comes with having a longer pump shaft [108]. However, the highlighted tank height restriction due to pump shaft length limitation, could be superseded by introducing side pumping into the

tank using a different type pump, the option is not possible in cylindrical tanks due to the possibility of shell weakening and introducing a critical stress point at the tank wall.

Finite element analysis was performed using ANSYS to investigate maximum stresses on tanks shells including side pumping. The goal of the analysis was to compare the maximum normal stresses acting on the tank's shell with side pumping for spherical and cylindrical tanks of the same volume. The volume chosen for this comparison is 4413 m^3, which was adapted from Gabbrielli and Zamparelli's recent optimized TES cylindrical tank with *H/D = 0.5*. The corresponding tank dimensions for spherical and cylindrical tank are provided in table 4.1.

Table 4.1 Tank Specifications

Tank's Dimension	Cylindrical	Spherical
Height (m)	11.20	10.18
Diameter (m)	22.40	10.18
Shell thickness at the top (m)	0.0002	0.005
Bottom Shell thickness (m)	0.0100	0.0300
Safety Factor	2	
Density of salt (kg/m^3)	1900	

The tanks were modeled using stainless steel A304 material properties with a hydrostatic pressure acting on the inside of the tank at the given operating temperature of 550° C to account for thermal expansion. The cylindrical tank was assumed fixed at the

bottom, and the spherical tank was supported by fourteen columns with 1m diameter and 0.05 m thickness. A side inlet was placed on the side of the tank with an opening of 30 cm, and the outlet of the tank was placed at the bottom, assuming gravitational draining as shown in fig 4.3. The maximum shear, principal, and normal stresses were identified for each tank and are compared in table 4.2.

The maximum principal stress and maximum shear stress in the cylindrical tank were located on the side inlet opening. The maximum normal stress was found on the top joint of the side shell and the roof. Spherical tanks showed lower stresses and the maximum principal stress was found below and above the support joints due to local deformation. The FEA analysis showed no shell weakening effect on the spherical tank's shell due to the side inlet.

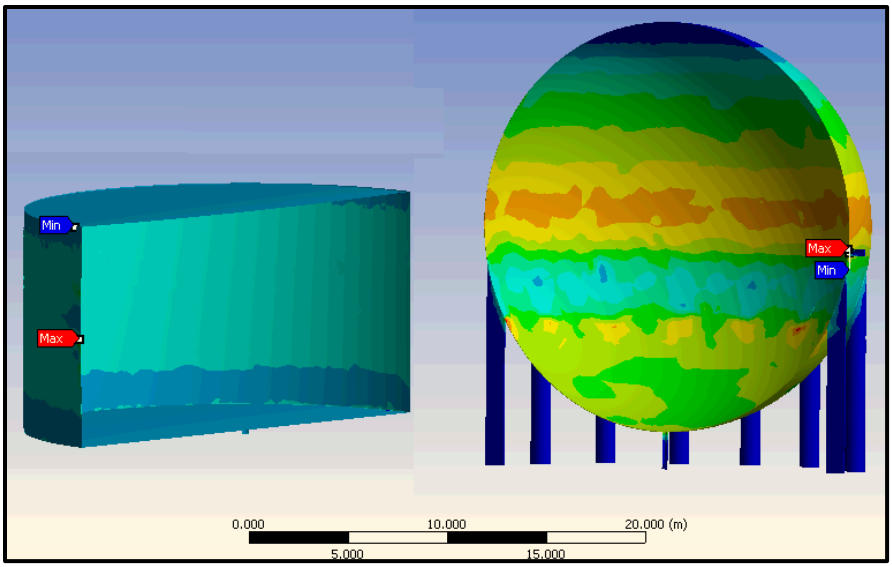

Figure 4.3 Cylindrical & spherical tanks with side inlet

Table 4.2 Maximum internal stresses on tanks

	Spherical Tank	Cylindrical Tank
Maximum principal stress (MPa)	111	1700
Maximum shear stress (MPa)	60	920
Normal stress (MPa)	92	1700

Tank Heat Losses

Heat losses from TES tanks are responsible for high insulation costs, auxiliary heating systems inside the tank to prevent the salt from freezing, and lost thermal energy that could be used for power generation. The *Solar Two* test reported 143 *kW* of thermal losses from the tanks, hot (550ºC) and cold (290ºC) [109]. Losses in a storage tank are caused by heat conduction from the storage fluid and the tank shell, natural convection inside and outside the tank, and insulation degradation.

In cylindrical tanks, the largest amount of heat loss occurs from the bottom of the tank, and the second major heat loss occur from the tank's roof. Using firebricks and foam glass at the bottom of the tank is common for insulation, and these are used in the *Solar Two* plant. The sides and roof were insulated with 46 cm and 30 cm thicknesses of mineral wool blankets respectively, and both were covered with 5 cm fiber glass board [110].

In 2004, Hermann et al. performed a cost study on the two system molten salt storage tank with different storage capacities and *H/D* between 0.25 and 0.75 [111]. The study showed insulation costs of \$360/ m^2 and foundation costs of \$600/ m^2 based on the storage required for a power generation of 10 MW_{el} in the *Solar Two* plant. In addition to foundation thermal insulation, a leak detection system is required in a large tank for temperatures more than 93° C to comply with American Petroleum Institute (API) 650 standards [112].

Insulation costs have decreased since the commission of *Solar Two* in the late 1990s. Currently, Aerogel insulation is being considered to replace the old insulation in *Solar Two*. Aerogel is an advanced insulation material with low bulk density and thermal conductivity 2-3 times less than ceramic fiber, as low as $0.016 W/m \cdot K$. New manufacturing technology has lowered the cost and made it possible to consider Aerogel for molten salt storage tank insulation. Therefore, it is more economical to insulate a spherical tank with exposed bottom walls than to insulate a cylindrical tank on the ground with multilayer firebrick insulation.

In the next section, thermal resistance from conduction, internal convection, and external convection were calculated using heat loss formulas provided earlier in chapter 3 in order to compare the heat transfer rates from spherical and cylindrical tanks of the same volume. Table 4.3 provides the fluid thermodynamic properties used for the calculation of the internal convection of molten salt in the cold and hot tanks.

Table 4.3 Properties of the molten salt at cold and hot storage temperature

Salt Property	290° C	550° C
Density (kg/m^3)	1905.5	1740.2
Specific Heat *Cp* (J/kg K)	1492.9	1537.6
Thermal Conductivity *k* (W/m K)	0.5475	0.4981
Absolute Viscosity μ (Pa.s)	0.00318	0.0011
Coefficient of thermal expansion β (1/K)	3.397×10^{-4}	3.719×10^{-4}

In calculating heat loss with conduction, an average thickness of the cylindrical wall was taken since the thickness will vary linearly with the height, based on the fluid hydrostatic pressure as shown in fig 4.9.

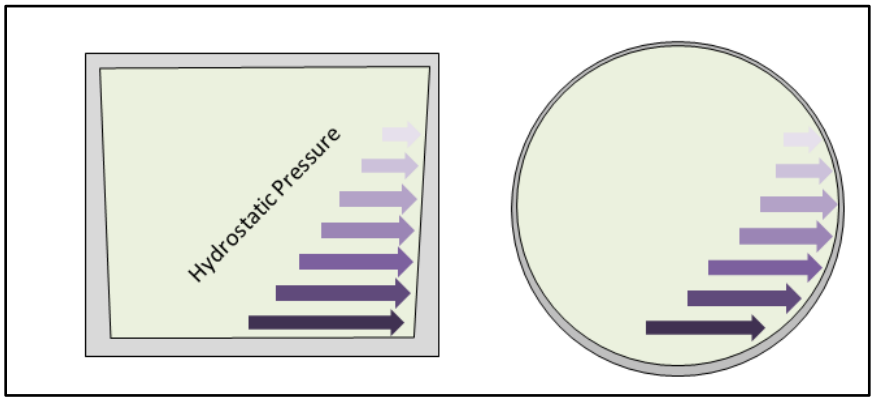

Figure 4.9 Tank shell thickness increase from top to bottom

Average thickness was considered in the calculation of the shell's thermal resistance. The shell thickness actually increases linearly with hydrostatic pressure similarly to the cylindrical tank. Since the overall shell of the spherical tank in this study was thinner than the shell thickness required by a cylindrical tank of the same volume, conduction thermal resistance in the spherical wall was significantly lower than the cylindrical shell's thermal resistance.

The Prandtl number for the molten salt in this study is larger than 7, however, the Ra number for both the cylindrical and spherical tanks was in the 10^{16} region, which indicates "hard turbulence" convection [114]. At higher Rayleigh numbers, it was necessary to use the power fit correlation provided by Niemla et al. [115]:

$$Nu = 0.02 \cdot Ra^{1/3} \qquad 4.1$$

The internal convective heat coefficient h_i was calculated similarly to the outside convection coefficient h_o, but in h_i calculation, the bottom of the cylindrical tank was included. The obtained thermal resistance through the total wall resistance was calculated by adding the three resistances:

$$R_{total} = Rconv_i + Rcond + + Rconv_o \qquad 4.2$$

Then calculation of the rate of heat transfer for each tank, hot and cold, based on temperature difference, was calculated using the relation:

$$\dot{Q} = \frac{\Delta T}{R_{total}} \qquad 4.3$$

Heat transfer rates were calculated for cylindrical tanks with variable *H/D* ratio and spherical tanks of the same volume. Comparisons were then performed. The cylindrical tank's diameter was kept constant at 22.4 m to coincide with the optimized diameter for TES cylindrical tank in [29] and *the H/D* ratio was varied between 0.25 and 5. The spherical tank diameter was calculated based on the cylindrical tanks volume to keep the same tank volume.

Hydrostatic pressure determined the wall thickness according to the liquid's height and density. Each of the thermal resistances were calculated for the hot and cold tanks for the corresponding fluid properties at the given storage temperature and tank shell material; stainless steel for hot tanks and carbon steel for cold tanks. Figures 4.10 to Fig.

4.13 show the heat transfer rate ratio of the spherical tank to the cylindrical tank with the same volume, and the heat transfer rate from the bottom of the tank without insulation for the hot and cold tank respectively.

The spherical tanks have at least 35% less heat transfer than the cylindrical tanks and that ratio increases with higher *H/D*. The rate of heat loss from the bottom of the tank increases as *H/D* increases, then starts to drop after *H/D* = 1.5. That is due to the effects of shell thickness, which increases with *H/D* ratio increase, and the characteristic length *H/D* on the conduction resistance and internal convection resistance respectively.

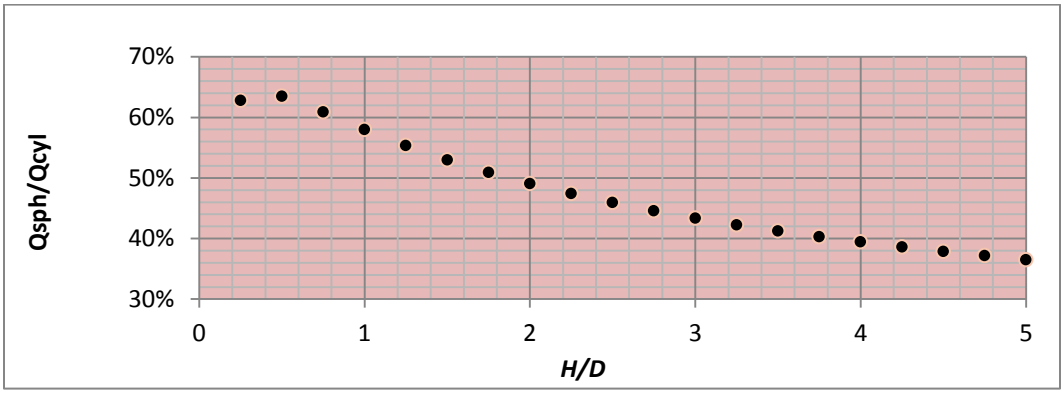

Figure 4.4 Heat transfer rates ratios Qs/Qc without the foundation (hot tank)

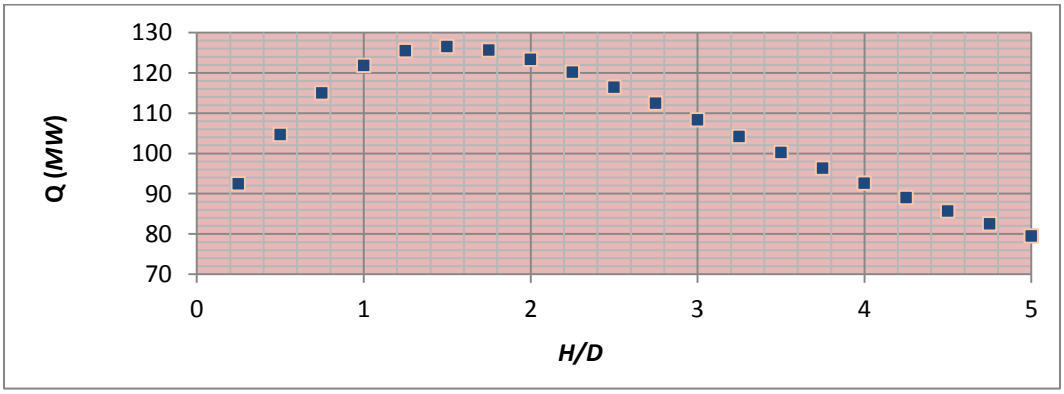

Figure 4.5 Heat transfer rates from cylindrical hot tank's bottom

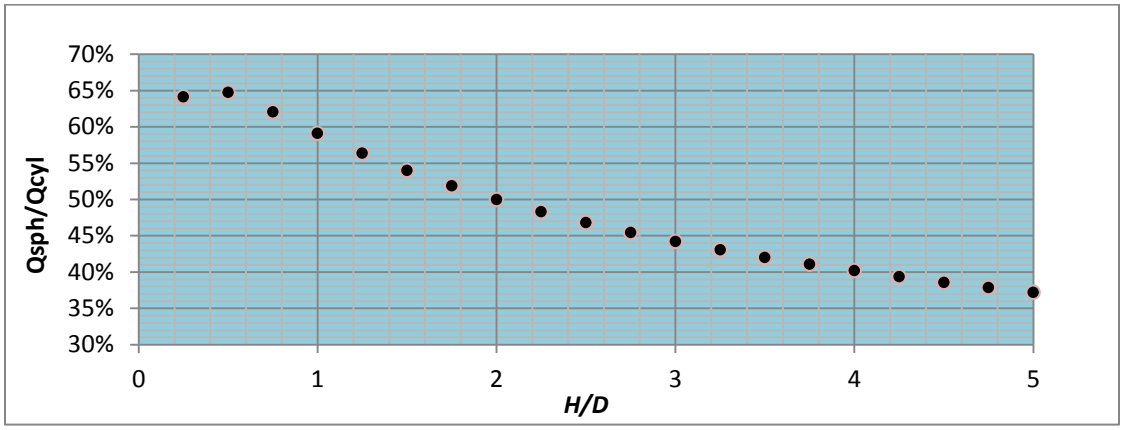

Figure 4.6 Heat transfer ratios Qs/Qc without the foundation (cold tank)

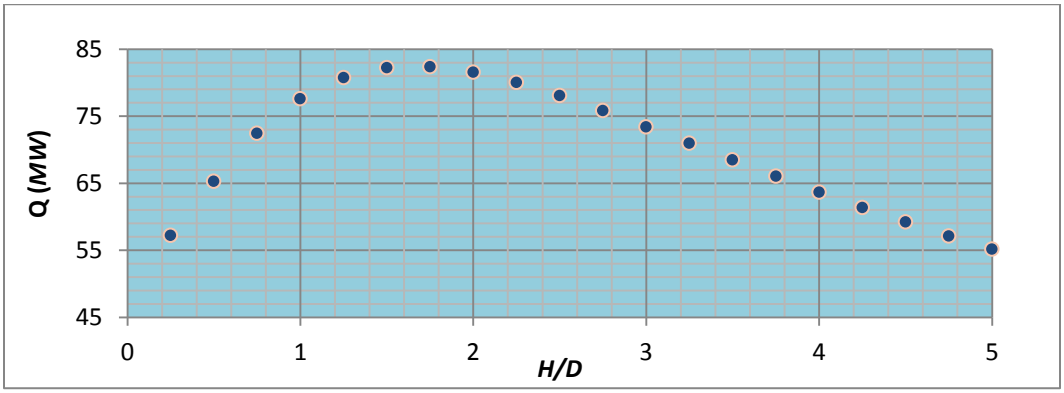

Figure 4.7 Heat transfer rates from cylindrical cold tank's bottom

The literature showed earlier that the maximum practical cylindrical tank height is 16 m [82] and the current utilized height of molten salt storage tanks of 11m [29] leads to $H/D = 0.5$. This establishes 35 % less heat transfer rate from the cylindrical tank's wall.

Cost Analysis

Economics is the main driver in TES's success as a substitute for fossil fuel back up in solar power generation. The cylindrical tank's capital cost is evaluated based on the volume of stored material. Cases with different *H/D* ratio were considered. In this part of the comparison, the diameter was held constant at 22.4 m, and the *H/D* ratio was varied from 0.15 to 0.8 to give a maximum height of 18 m. The type of tank considered is API compliant field erected vertical cone roof with a flat bottom. Field erected tanks are constructed on site by welding prefabricated metal sheets together after constructing the necessary foundations.

Spherical tank cost is evaluated based on the vessel's shell weight. The internal volumes of the spherical tanks were the same as those obtained from the varying *H/D* cylindrical tanks. The cost of the spherical tank based on the weight of the material used included the support columns weight. The cost evaluation of the two vessels types was calculated using *Matches,* which is a company that provides cost estimation tools in chemical energy, manufacturing and metallurgy [116]. The type of material assumed in the calculation was stainless steel 304, which costs more than carbon steel, but would be required for storage of the "hot" salt.

The tank's shape impacted the cost of insulation. Costs for insulation and tank foundation were adopted from Herrmann et al.'s study of *Solar Two's* storage tanks. The study showed an estimated cost of $\$360/m^2$ for insulation and $\$600/m^2$ for the foundation. Wall insulation with the same cost per m^2 was applied to the spherical tank, even though savings could have been realized with thinner insulation. The cost of foundation was added to the cylindrical tank, since it is a major requirement in order to mitigate the conduction from the bottom of the tank. Since the cylindrical tank's diameter was kept constant at 22.4m the added foundation cost was $271,000 for all the tanks. The accumulated tank cost comparison is shown in fig 4.9 as tank cost of each shape and total cost with the foundation and insulation.

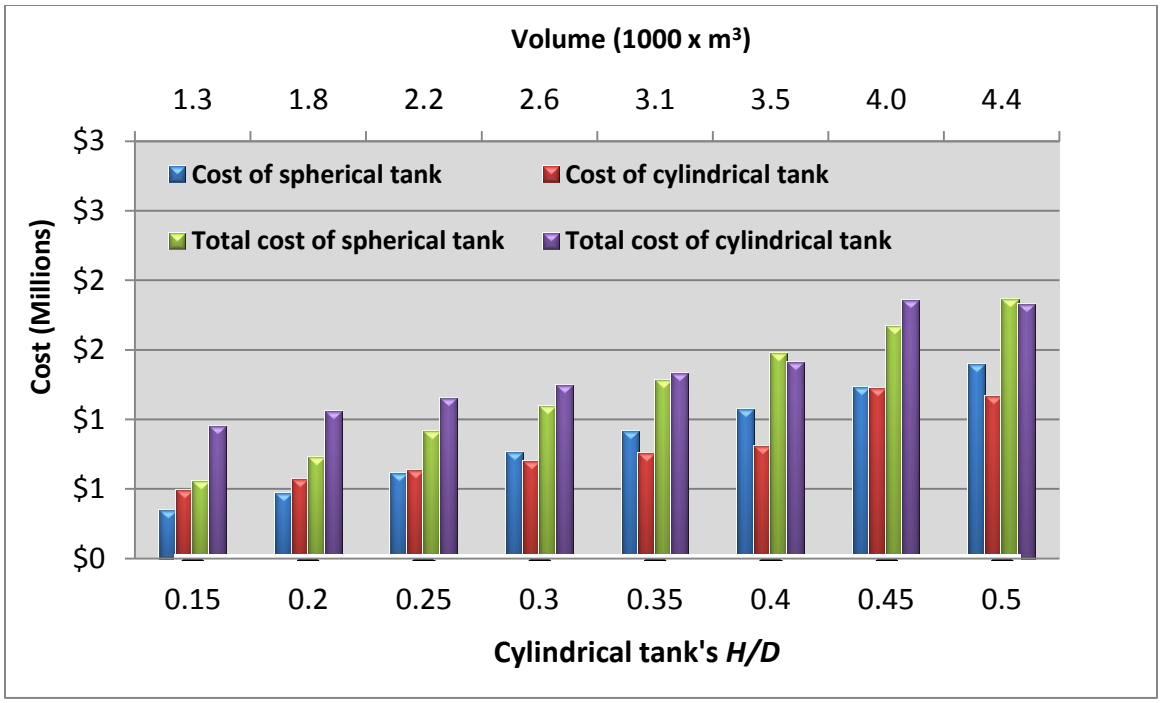

Figure 4.9 Spherical tank vs. cylindrical tank costs

The cost estimation for spherical tanks includes erection, structural support, and foundations. The cost depends largely on the spherical tank's wall thickness [87]. Spherical tanks show large total cost reduction when compared to cylindrical tanks.

Summary

In this study, the benefits of substituting spherical tanks for cylindrical tanks in molten salt TES systems were investigated. The comparison of the two tank shapes showed 35% less heat loss from the spherical tank's wall, requiring less insulation. The currently utilized coned-roof cylindrical tanks require involved and costly foundation

preparation to counteract the conduction heat loss from the bottom of the tank. By using spherical tanks, conduction heat loss from the bottom of the cylindrical tank is avoided.

The study showed that spherical tanks require less building material than cylindrical tanks (30 % at H/D = 0.5), and they can resist more internal pressure with less wall thickness, leading to a significant cost saving on building material.

Previous literature highlighted a cylindrical tank's height limitation due to pumping restrictions through the bottom of the tank via a long-shaft centrifugal vertical pump. This requirement limited the tank's height to the available length of pump shafts in the market and created an added design constraint of placing the pump motor on the tank's roof. Side pumping was not considered due to possible shell weakening in cylindrical tanks. The FEA part of this study showed that spherical tanks make side pumping possible with no risk of weakening the tank's shell, which gives them a pumping advantage over cylindrical tanks and consequently less size constraints.

Cost analysis showed that the substitution of cylindrical tanks with spherical tanks in TES applications results in 40 % reduction in cost due to saving in material, insulation, and foundation with the added advantages of overcoming the pumping limitation, size constraints, and increased resistance of internal pressure.

CHAPTER 5 : SPHERICAL TANKS FOR THERMOCLINE TES

Industrial Advantages for the One Tank Thermocline System

There are two types of one tank systems: stratified storage and fully mixed storage. In fully mixed storage, one tank is used, and the incoming fluid either hot or cold is allowed to fully mix with the stored fluid, which in turn lowers the output temperature. Fully mixed one tank storage is the simplest and most reliable thermal storage tank [50, 51], but it has the lowest thermal efficiency among sensible heat storage tank systems. In an evaluation study of solar power storage performance using a single stratified tank versus a mixed tank, the stratified tank saved 5.25% energy over a one year evaluation [117].

Stratified tank storage, also known as thermocline storage, utilizes a highly stratified tank for liquid storage. In this type of storage system, both cold and hot portions of the fluid are stored in the same tank. At certain flow parameters, a thermocline layer is formed during the charge and discharge processes, which acts as a barrier between the hot and cold fluid. Thermocline storage systems are more common for HVAC applications to store colder water for use in cooling buildings by utilizing using chiller systems where a thermocline system is used as the sole cooling system or to help offset energy costs during summer time [118]. In some cases, a seasonal storage system is used to store cold water from the winter to be used during the summer time [52].

A thermocline is a relatively thin layer of fluid in which the temperature changes markedly with depth. In nature, thermocline phenomena occur in lakes and oceans and separate the surface high temperature water from the deep cold temperature water. The separation is density based; hence it also occurs between waters with different levels of salinity. This density difference is governed by fluid diffusion and conduction properties.

In a storage tank, the thermocline layer also acts as a barrier between the incoming and the resident fluids by reducing mixing inside the tank. The buoyancy effect causes the higher density (colder) fluid to sink to the bottom of the tank while the lower density (hotter) fluid rises to the top of the tank, forming a thermally stratified layer in the tank.

The thermocline region is usually very stable and can be maintained by avoiding high mixing in the storage medium. Salinity pond storage systems maintain a thermocline region indefinitely. There are some injection techniques that can re-establish a thermocline region once a fully mixed condition occurs.

A well-designed tank is capable of maintaining stratification throughout the charging, idling, and discharging process. A thermocline system is recognized for its high reliability and high performance that can match tanks with physical separators between hot and cold fluids [62]. Taylor et al. suggests that using a thermally stratified liquid is more effective than using a packed bed thermal storage system [63]. Using stratified liquid as the storage medium reduces the entropy generation caused by heat transfer between solid and liquid and thus increases the second law efficiency. Moreover, systems

that rely on physical barriers, such as membranes or a labyrinth, introduce conduction across the barriers which increase the internal losses between the cold and hot region. A thermal efficiency of up to 90 % was obtained experimentally in a tank system without a physical barrier [118].

One the other hand, the thermocline system has a more complicated charging and discharging process than the two tank system due to the required switching between inlet and outlet for the charging and discharging. In addition, the mixing of hot and cold fluid inside the tank reduces the energy storage capacity. Moreover, the one tank system requires more unpumpable volume, which is the volume occupied by the thermocline region.

The main advantages of a thermocline one tank system are: the elimination of a second tank, which in turn reduces the storage system cost by about 35% [60], and when compared to the fully mixed one tank system, increases thermal efficiency by 40% [32].

Thermocline theory in storage tanks is limited to empirical correlation of specific cases [148]. The current literature shows that the thermocline is defined between two turbulent inlet and outlet regions and a stagnant region in between, where the thermocline will move upward or downward. Previous dye flow visualization studies elucidated that mixing in the inlet and outlet region due to flow characteristics, difference in temperature, and material thermal properties are responsible for thermocline volume occupation in a storage tank. Once the volume of the thermocline has been established, it remains constant throughout the charge/discharge. However, factors such as heat loss

from the tank and axial conduction through the thermocline might increase the volume in longer cycling storages.

Literature Review on Stratified Tank Storage Systems

Thermocline formation and movement in a tank are governed by the temperature difference between the resident and incoming fluid and the flow parameters inside the tank, which are dictated by: the inlet velocity, inlet shape, and tank geometry, and temperature difference. Haller et al. proposed the following influential factors on the stratification in storage tanks [56]: (i) tank size and tank aspect ratio *H/D* for cylindrical tanks, (ii) location and geometry of the inlet and outlet, and (iii) dimensionless numbers such as Peclet, Richardson, and Froude numbers. Nelson et al. [119] added to the previous factors: (iv) the operating temperature range, (v) thermo-physical properties of the storage fluid, and (vi) tank geometry and material.

A Buckingham Pi analysis performed by Musser and Bahnfleth [120] produced seven dimensional numbers of which five relate to the flow and two to the tank geometry. Not all the seven dimensionless numbers significantly influence the tank stratification level and the thermocline formation and movement. The following review will highlight the most commonly used dimensional numbers correlated to thermocline formation and movement in a storage system in cylindrical and rectangular tanks. Most of these studies rely on a parametric study followed by a statistical analysis to determine the correlation between the dimensionless number and the tank efficiency or the thermocline thickness.

Relationship parametric numbers to tank efficiency and thermocline thickness

There are several measures for thermocline storage system performance. These measures were established to evaluate the mixing that occurs inside the tank. Mixing inside the tank is responsible for lowering tank thermal efficiency by increasing the volume occupation by the thermocline region. Thermal efficiency is commonly defined as energy extracted from the tank divided by the initial energy stored.

The first correlation of tank efficiency that appeared in the literature is the mixing factor. The mixing factor (*E)* at the inlet region was used by Oppel et al. [50] to quantify the mixing inside the tank, which was determined to be responsible for lowering the tank efficiency. The study produced the following relation of the dimensionless inlet eddy conductivity factor:

$$E_{inlet} = a(Re/Ri)^{b} \qquad 5.1$$

Where in the modeled case "a" was calculated to be 4700 and "b" is 0.95. Each of the experimental five cases in the study had its own "a" and "b" values. A similar study identified the conductivity factor as the tank's mixing number. A study performed by Nelson et al. [119] deployed the same relation of eddy conductivity factor as the tank's mixing number *Z* for a cylindrical tank instead of a rectangular tank. The relation was formulated after a parametric study with variable tank's *Re* and *Ri* numbers was conducted:

$$Z = 1.68 \times 10^4 (Re/Ri)^{0.67} \qquad 5.2$$

As the value of *Z* approaches 1, the mixing in the tank is reduced, while at mixing number = 1 no mixing takes place at all. A higher *Z* value indicates high mixing in the tank, a Z value equals to 1 indicate a fully mixed tank. In both references [50, 119] , Reynolds's and Richardson number were calculated as:

$$Re = Vel_i \, D/\nu_{ave} \qquad 5.3$$

$$Ri = \frac{\Delta \rho g L}{\rho_{ave} Vel_i^2} \qquad 5.4$$

Where *D* is the tank's diameter, *L* is the tank's Length from the inlet to the outlet, Vel_i is the velocity inside the tank and ν_{ave} is the average viscosity of hot and cold fluid.

Lavan and Thompson [54] correlated the effect of *L/D*, the tank's *Gr* number, and the inlet's *Re* number. A least square fit of all the data is given by eq.5.5:

$$\eta = \frac{FR \cdot t}{V} = 1 - (e^{-0.067 Re_d^{-0.55} Gr_D^{0.35} (L/D)^{0.58}}) \qquad 5.5$$

Where *FR* is the flow rate, *t* is the time where *ΔT* drops to the assigned value of 0.9, which is when the temperature has dropped to 90 % of the original *ΔT*, and V is the volume of the tank.

This definition of efficiency at 90% of the original *ΔT* became the most popular measure of efficiency since 90 % extraction is the maximum theoretical energy extraction

based on an energy balance performed by Krane and Krane [121, 122]. Therefore the η_{90} is used in several papers and is calculated as defined by Berkel [123] as $\eta_{0.9}$:

$$\boldsymbol{\eta_{90}} = \frac{\boldsymbol{V_{0.9\Delta T}}}{\boldsymbol{V_{tank}}} \qquad \textbf{5.6}$$

Where $V_{0.9\ \Delta T}$ is the volume of fluid extracted from the tank until ΔT=0.9 of the original ΔT, and V_{tank} is the entire tank volume. For example, if the tank storage temperature was $50^{\circ}\ C$ and the inlet temperature is $10^{\circ}\ C$ then ΔT equals $40^{\circ}C$ and therefore 90% of ΔT = 36. Consequently $V_{0.9}$ will equal the volume extracted until the exit temperature drops by 4 degrees to $46^{\circ}\ C$. This volume will be divided by the total tank volume indicating the η_{90} of the storage tank.

Thermocline thickness is another measure of tank stratification. Even though it does not provide good quantitative results for comparison [120], it is commonly used in thermocline storage design. Thermocline thickness measurement is only useful when the temperature on each side of the thermocline is constant, which is usually valid when the tank wall is adiabatic. The thickness is measured using the value of dimensionless temperature Θ as:

$$\boldsymbol{\theta} = \frac{\boldsymbol{T - T_c}}{\boldsymbol{T_h - T_c}} \qquad \textbf{5.7}$$

The thickness is calculated based on the temperature change at each side of the thermocline. For example if Θ = 0.12, the thermocline region will span a temperature difference from 0.12 to 0.88, which contains 76% of the thermocline region.

In the current example study T_c= 20 and T_h= 50, the thermocline thickness is calculated based on 0.5 degree change 19.5° C from the inlet region and 49.5° C at the exit region , therefore Θ = (0.016-0.983), which contains 96% of the entire temperature change.

The thermocline thickness as a measure of efficiency was used in a numerical and experimental study of rectangular tank thermocline system by Baines et al. The study concluded that the thermocline thickness depends on the inlet Froude and, inlet Peclet numbers, and a large Peclet number can lead to a thin thermocline region [64].

Thermal efficiency and inlet relationship (Thermocline Formation)

Oppel et al. [50] performed a numerical and experimental study on stratified thermal storage using a one dimensional implicit, finite difference model with variable flow rates. Mixing inside the tank was calculated using thermal eddy conductivity factors, which was determined from experimental data. The study established that the relation of the inlet's Reynolds's number over Richardson's number determined the mixing inside the tank. In addition, the stability of the thermocline depended mostly on the inlet design. The authors also suggested that the inlet Reynolds's number over Richardson's number relation is dependent on the inlet geometry and that initial mixing is the sole factor for determining the thermocline thickness.

Mixing in the inlet region is influenced by the flow parameters and the inlet shape. Yoo et al. suggests that the inlet configuration and flow relation to the mixing rate have to be determined experimentally for each inlet shape [124]. Several studies

collectively agree that the inlet region is the most influential factor on the thermocline formation and initial thickness, and it has a flow pattern that is difficult to predict and account for numerically but possible to approximate [35, 125-127].

Since the inlet flow is the most influential aspect of thermocline tank formation and volume occupation, an inlet flow characteristic is always within relevant dimensionless numbers. Previous studies describe the flow by using one or two of the following dimensionless numbers and their correlation to the tank efficiency: Richardson, Peclet, Reynolds, Froude, and Grashof numbers [32, 54]. In thermocline tank storage, it is common to see the Froude number as a reciprocal of the Richardson number, and they are used interchangeably throughout the literature. The calculation of Richardson, Froude, Reynolds, and Archimedes numbers uses either the inlet diameter and inlet velocity, the tank diameter and tank relative velocity, or the tank diameter and inlet velocity. Using the inlet velocity and inlet diameter as the characteristic length is most common. The correlation of the Archimedes number in eq. 5.8, which equals the Richardson number, appears in multiple studies and uses the inlet velocity and inlet diameter as the characteristic length [128]:

$$\boldsymbol{Ar = \frac{Gr_{inlet}}{Re^2_{inlet}} = Ri = \frac{gB(\Delta T)d}{v^2} = \frac{1}{Fr}} \qquad \textbf{5.8}$$

Zurigat et al. performed a study relating stratification and the tank Richardson number, where Richardson number is calculated using the tank diameter as the characteristic length and the tank average velocity [62]; they found that for *Ri >10*

thermal stratification remains unaffected by the inlet geometry, while at $Ri < 3.6$ the inlet geometry effect started to become significant.

Spall et al. [128] performed an experiment to determine the relation between the inlet *Ar, Re*, and the tank stratification. The experiment was limited to $Ar = 0.5\text{-}5$ and $Re = 500\text{-}3000$, and concluded that within this experimental range, *Ar* larger than 2 ensures tank stratification regardless of the inlet *Re* number.

An experimental study by Karim on cylindrical tanks [129] shows that using an inlet Froude number of 1 leads to a higher degree of stratification and a more defined thermocline region than Froude numbers larger than or less than one. Shin et al. suggested that the most basic and most used dimensionless parameters in the design of thermal storage tanks are the inlet Reynolds and Froude numbers [130].

In summary, various numerical and experimental studies were conducted to determine Froude, Reynolds, and Richardson numbers, as well as tank aspect ratios, that will ensure thermocline formation and stability for cylindrical and rectangular tanks. No similar correlation or data was found in the previous literature pertaining to spherical thermocline storage tanks.

Thermal efficiency and tank wall relationship (thermocline stability)

Thermocline degradation over time occurs due to thermal diffusion by internal convection, conduction from the tank's walls, and the mixing caused by the inlet flow

[131]. Conduction through the wall has the smallest effect on thermocline degradation in a relatively fast discharge. Nelson et al. concluded that the material of the tank has little influence on the tank stratification during charging or discharging. Nevertheless, when the tank is idle, the wall material has some effect on the tank's stratification [124]. Conductive heat transfer through the wall and convective mixing on each side of the thermocline are responsible for heat loss and thickening of the thermocline layer.

A Numerical and experimental study on thermocline degradation with time was done by Al-Najem in order to investigate the influence of heat loss on thermocline thickness [132]. The study found that thermocline degradation due to heat loss to the ambient is noticeably greater than the heat conduction through the thermocline. The study also showed that convection heat transfer through the side wall initially varies along the tank with location, but this variation decreases with time and becomes uniform due to internal convection effect.

Yee and Lai, performed a study that concluded that heat losses from the tank wall can cause significant degradation to the tank's stratification, and for more robust tank performance *Biot* number $Bi = \frac{hL}{k}$ should be less than 1 [133].

Therefore it can be concluded that the heat loss from the tank wall is the major factor in thermocline thickening after formation, and wall insulation will improve the thermocline stability during the discharge process.

Scaling issues in the thermocline tank system

Previous literatures do not agree on the dimensional numbers that ensure thermocline formation and stability, and they collectively agree that the tank shape and inlet geometry have a significant effect on thermocline formation and movement in a storage tank. Therefore, using a lab scale model became a subject for investigation in a few studies where the real size model is significantly larger than the lab scale model.

Yoo et al.[134] performed an experiment on a scale model of a rectangular tank with side diffuser that runs across the width of the tank with slot opening at the bottom. The study found the inlet Froude number for the diffuser was the most important parameter to optimize performance of a thermocline tank. The lab scale model's volume was 160 gallon and the real tank volume was 16,200 gallons. The full scale tank required a significantly larger flow rate, thus the author stated that the scaling procedure was based on matching the tank's Richardson number, which also led to reproducing the same value of the inlet's Froude number.

An experiment was conducted by Truman et al. in order investigate the effectiveness of using a scale model to replicate thermocline behavior in real rectangular stratified tank [135] The experiment had both a real size model and a scaled size model. The significance of the tank's Richardson number was highlighted in the literature review due to its influence on axial conduction through the wall, which in turn has a direct effect on the thermocline formation, which is similar in both the model and the real tank. The scaling study also mentioned that previous literature collectively agrees on three

dimensionless groups: the inlet's Reynolds's number, the tank's Richardson number, and the inlet's Peclet number. They have also suggested that the Richardson number can be alternatively substituted by the inlet Froude number. The study matched the overall Richardson's number (the tank's length was used as the characteristic length), the inlet Peclet number, and the time scale.

The scaled model was 1/10 of the real size tank and the temperature difference was higher by 10º C. The authors hypothesized at the beginning of the experiment that lowered Re number in the scaled model would reduce mixing that will occur in the real size tank. However, that will be compensated for by increasing the temperature difference between the incoming and the resident fluid. Later on, it was discovered that due to the different tank surface area to volume ratios, which was decreased in the scaled model, vertical conduction through the walls played a major role in distorting the scaled model's ability to match the real size tank's thermocline thickness. The use of insulation produced thermocline shapes closer to those found in the real size tank.

Lavan and Thompson [54] performed an experimental set up on two tanks with diameters of 24.23 cm and 10.41 cm with matching *D/d* ratios (*D* is the tank's diameter and d is the inlet diameter). The scaling parameters considered were the inlet Re number and the tank's Grashof number. The study suggested that matching the Re number and the Grashof number will be sufficient for a large scale model.

An *Electric Power Research Institute* (EPRI) report suggests that a thickening of the thermocline is mainly caused by mixing due to inlet design and inlet temperature.

Hence matching inlet criteria will be the most influential criteria. The standard also states that the tank's depth (height of a cylindrical tank) has a direct effect on the thermocline thickness [118].

Brown and Lai [136] performed a study on a scale model using Richardson numbers. The characteristic length is the tank radius with the inlet velocity. The study produced a tank efficiency model based on the Richardson number and the inverse of Peclet number. The efficiency model was then used to predict the performance of a large scale model. No data were obtained the study for a full size tank.

In the study performed by Nelson et al. [118] on a cylindrical tank thermocline system, the thermocline region thickness was compared at different inlet flow rate (different discharge time) in order to investigate the effect of slower discharge on thermocline thickness. The results obtained from varying the flow rate and consequently the discharge time showed that the thermocline degradation (thickening) proportionally increases with the longer discharge time due to axial conduction through the thermocline region and heat loss from the tank wall. However, the heat loss through the wall is far greater than the axial heat conduction through the thermocline. Therefore, wall insulation has major effect in reducing thermocline degradation at longer discharge cycles. The study showed a relation for time scaling using Peclet number times Fourier number as the dimensionless time:

$$\boldsymbol{Pe \cdot Fo} = \frac{\boldsymbol{v \cdot L}}{\boldsymbol{\alpha}} \cdot \frac{\boldsymbol{\alpha \cdot t}}{\boldsymbol{L^2}} = \frac{\boldsymbol{v \cdot t}}{\boldsymbol{L}} \qquad \textbf{5.9}$$

Where v is the tank bulk velocity and L is the tank's length. For Nelson et al, study, $Pe{\cdot}Fo \leq 0.33$, delivered thermocline that decreases in thickness at the number $Pe{\cdot}Fo$ decreases, and completely destroyed thermocline at $Pe{\cdot}Fo = 0.66$.

It is apparent from the previous literature that even though there is inconsistency in the scaling parameters used in the literature, the majority of the recent scaled models of thermocline tanks relied on matching the inlet's Froude number, the tank's Richardson's number, the d/D ratio, and the use of a dimensionless time scale.

The reason for not matching the Reynolds's number is that it is difficult to replicate a real size tank's large Reynolds's number in a laboratory scale model and keep the same Froude number without a drastic increase in temperature change, fluid viscosity, or unrealistic inlet size. The scale model results produced by Truman et al. [135] showed that not matching Reynolds number did not significantly affect the scale model thermocline behavior and shape, but produced conservative results when axial conduction through the wall is mitigated by using proper insulation.

Table 5.1 Summary of literature on flow parameters' influence on thermocline storage systems

Study	Tank	Diffuser	Scaling parameters	Range	Notes
Lavan and Thompson [54]	Cylindrical	Pipe	Inlet Grashof # Inlet Re#	Re : 2260, 3200, and 4465	Testing on model could be used for a real size tank based on the produced efficiency from the model
Mackie et al [118]	Rectangular	Linear with slots	Inlet Fr number with slot height as L	Q: 20-90 GPM	Correlation between the tank height and thermocline thickness. Same result was obtained from a cylindrical tank with radial diffuser
Yoo et al.[134]	Rectangular	Linear	Inlet Fr		Highest tank efficiencies are obtained at Fr < 1
Brown and Lai [136]	Cylindrical	Porous manifold	Tank Ri number and Peclet number	Ri is calculated with inlet velocity and tank radius	Best tank stratification was obtained at Ri as low as 0.61 Tank efficiency was calculated based on Ri and inverse Peclet number
Truman et al. [135]	Rectangular	Linear	Tank Ri Inlet Re Inlet Peclet	Q : 2-110 liters/min	Inlet Re number has no effect on scaling Using Tank Ri is enough
Shah and Furbo [53]	Cylindrical	Plate, Baffle And pipe	Inlet Ri number	N/A	Center plate delivered the best results
Oppel et al. [50]	Rectangular	Linear	tank Re and tank Ri	Re (946-1000)	Numerical Model can predict tank efficiency using mixing coefficient
Nelson et al. [119]	Rectangular	Linear	tank Re and tank Ri	Re/Ri = 10^{-5} - 10^{-3}	If Z = 1 no mixing occurs
Hooman & Soo [51]	Rectangular	Linear	Inlet Froude	Re= 50	Numerical model based on gravity current.
Spall [128]	Cylindrical	Side inlet	Archimedes Re	Re: 500-3000 Ar: 0.5-5.0	If Ar is held constant Re has low effect on stratification
Bahnfleth and Song	Cylindrical Tank	Octagon with slots	$Fr = \frac{q}{(g\ h^3)^{0.5}}$	Re=10,000	H is the slot height in the diffuser Q is the flow rate per unit length of the diffuser

[120]					Tank volume 2155 m3
Shin et al. [130]	Cylindrical	Radial	Inlet Fr	Flow rate 11.75 liters/min-33000 liter/min	No effect of Fr in large scale tank due to the large body of water
Lever and Lin [137]	Cylindrical	Side inlet pipe	Variable flow rate, *H/D* distances, and location of inlet/outlet	Q: 0.5-1.5 kg/s *H/D:* 2.5-5	Increase in *H/D* results in higher thermal stratification Decrease in flow rate increases thermal stratification Closer placement of inlet/ outlet to the wall leads to better tank efficiency
Baines et al. [64]	Cylindrical	Side pipe	Inlet Froude Inlet Peclet	Large inlet number = thinner TC layer	Stratification is highly dependent on the diffuser shape
Chung et al. [138]	Rectangular	Radial and linear	Inlet Fr Inlet Re	Fr : 0.1, 1, and 2 Re: 400, 800, and 1200	Froude number effect is negligible Re number is most dominate Diffuser shape is very influential on tank stratification
Mussuer and Bahnfleth [139]	Cylindrical	Radial	Inlet Fr Inlet Re, inlet Fr D/d	Re 500-12000 Fr >1	Re # has low effect on the stratification with the proper diffuser length.

Analysis: Thermocline Tank Numerical Modeling

Computational fluid dynamics (CFD) software was utilized to model the fluid flow with thermal transient analysis in three dimensions. CFD limitations and the accuracy of the calculation depend on: *the* mathematica*l* model provided, modeling parameters, time step size, mesh independence, solution residuals, and boundary conditions. Previous studies suggest that current CFD software packages that have been used to simulate active TES systems are capable of producing similar results to the actual storage systems [32].

ANSYS® CFX 14.5 was used in this study to simulate the thermocline formation and movement in tanks. The steps of numerical simulation are: geometry definition, mesh, set up and boundary conditions, result post processing, and iteration and refinement.

Geometry and fluid domain

The geometry constructed for the tank only contained the fluid inside the tank. The walls were not physically modeled in the geometrical model; however the heat transfer coefficient based on the wall material and thickness was calculated and used in the data validation stage where the wall was not adiabatic. Preliminary 2D analyses were performed followed by 3D analysis on one quarter of the tank with symmetry boundary condition on each side of the tank in order to reduce the processing time. Even though 2D simulation was performed in previous literature, in the current study, 2D simulation and

symmetric condition delivered incorrect results in a spherical tank due to the Coanda effect, within the inlet Reynolds number used in the current study. A quarter, half and full model were simulated using the same mesh density and flow conditions in order to compare the thermal efficiency for consistency. A temperature contour for the three models is shown in fig 5.1 at the same time step of the discharge.

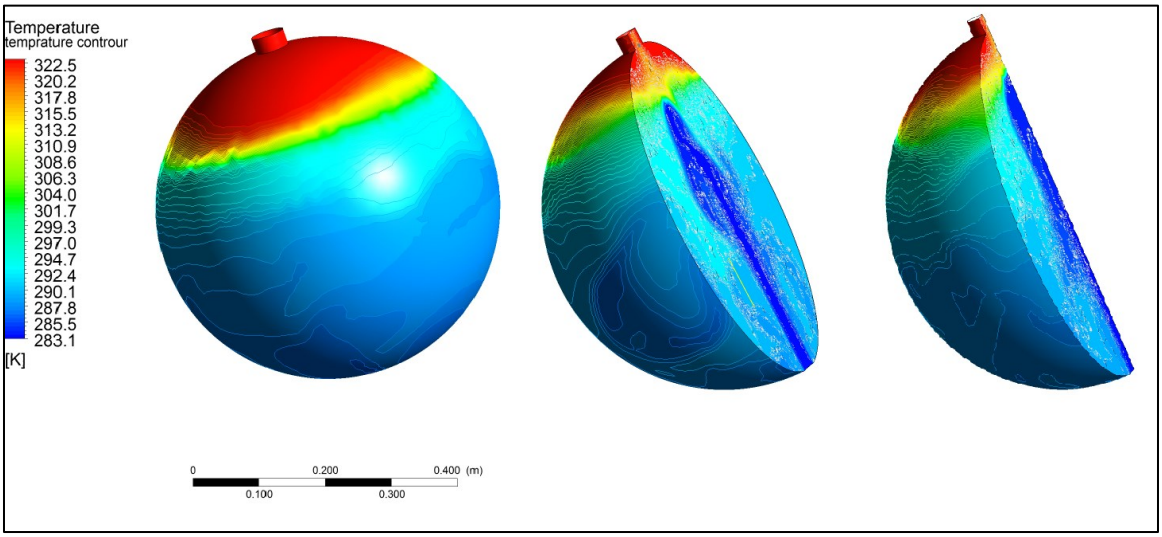

Figure 5.1 Coanda effect in using symmetry for tank simulation

The thermal efficiency calculation for each of the simulation models, quarter, half and full show that the quarter and half model overestimate the thermal efficiency for the same flow and temperature conditions. The thermal efficiency in the full model is 25 % lower than the half and 18% for the quarter model, which produced more mixing and instability in the thermocline region. Full size modeling was used for all the following analyses.

Mesh and mesh refinement

An unstructured tetrahedral mesh was used for the volume of water. Mesh refinement was necessary at the inlet region where most of the mixing is expected to take place. Mesh sensitivity analysis was carried out to ensure mesh independence by reducing the element size for the entire model and increasing the number of elements by 20 % in each simulation. Since the boundary condition at the exit was set as atmospheric pressure, the velocity at the exit was monitored for change until it became stable. Average velocity at the exit was calculated based on the inlet velocity and compared to the model average velocity at the exit. The model was considered mesh independent once increasing the number of elements did not change the exit velocity. For the tank size of 0.065 m^3, 419,000 elements were sufficient to achieve mesh independence.

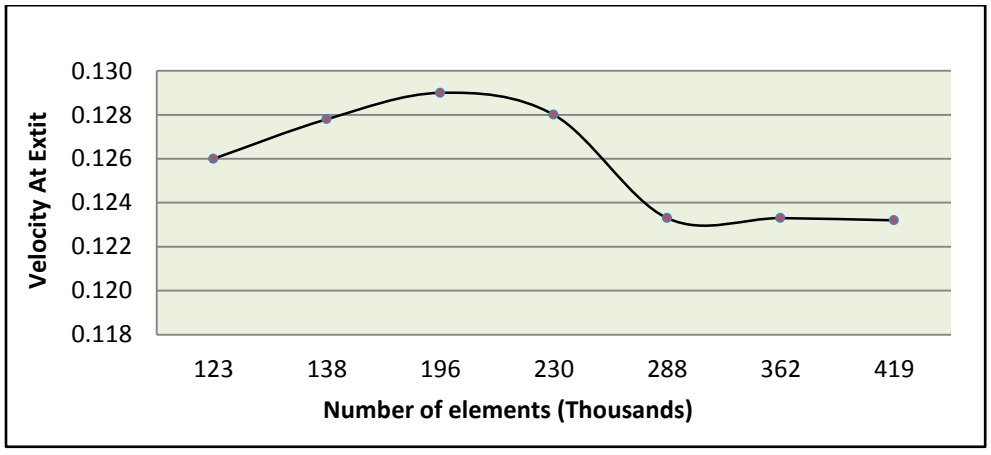

Figure 5.2 Mesh sensitivity study

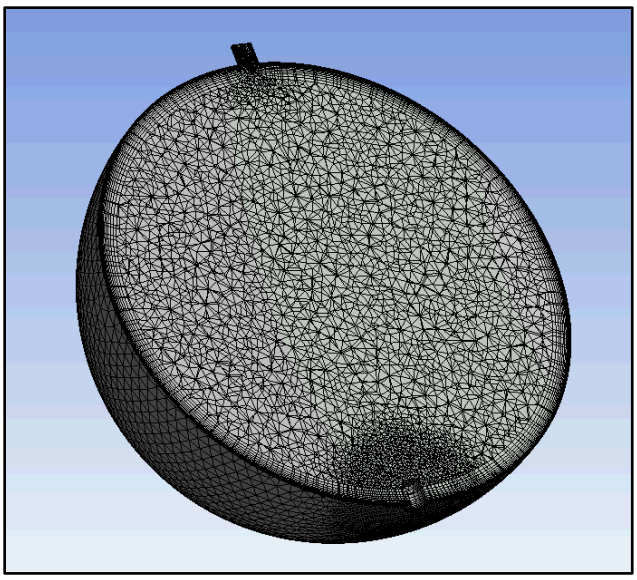

Figure 5.3 Unstructured mesh with wall inflation layers and inlet region refinement

Boundary conditions and solver settings

The model initial boundary conditions were set: inlet velocity, inlet temperature, atmospheric pressure at the outlet, adiabatic no slip wall condition. The default domain was set as water with the buoyancy model with gravity acceleration in the y axis, since the tank is to be used in the upright position, and reference temperature as the inlet temperature.

ANSYS CFX software uses two fluid heat transfer models: total energy equation and thermal energy equation. Thermal energy equation is appropriate for incompressible low velocity flow, which is valid in this study. Viscous dissipation, which is the internal heating caused by the fluid viscosity is ignored in the thermal energy equation. Using the

thermal energy equation saves on processing time when compared to the total energy equation. Thermal energy equation is given as:

$$\frac{\partial(\rho h_{tot})}{\partial t} - \frac{\partial p}{\partial t} + \nabla \cdot (\rho U h_{tot}) = \nabla \cdot (\lambda \nabla T) + \nabla \cdot (U \cdot \tau) \qquad \textbf{5.10}$$

Where the first and second terms from the left are transients, the third term is convection, the fourth term is conduction, and last term is the viscous dissipation term, which was neglected in this study. Heat generation due to viscous dissipation may be significant when using material with at least 10 times the viscosity of water such as Glycol depends on shear rates.

In order to model the thermocline phenomena in a tank, buoyancy has to be activated. Since the buoyancy is driven by a small temperature difference that leads to a density difference, the CFD program assumes the Boussinesq approximation is valid and calculates the incoming fluid density difference in comparison to the reference temperature as [140] :

$$\boldsymbol{\rho - \rho_{ref} = -\rho_{ref} \cdot \beta (T - T_{ref})} \qquad \textbf{5.11}$$

In this model T_{ref} is the initial temperature in the tank, T is the incoming fluid's temperature, and β is the fluid's coefficient of thermal expansion.

The solver used was a high resolution advection scheme. Continuity, energy and Momentum equations were solved using second order backward Euler transient solution, Convergence criteria were based on RMS residual at 1x 10^{-6} residual target.

Material properties for pure water were used. Thermodynamic and transport properties (dynamic viscosity, thermal conductivity, and coefficient of thermal expanstion) were set as functions of temperature.

Turbulence modeling and stability

Previous literature suggests that within the examined Reynolds numbers in this study, the laminar flow model is valid. In a thermocline modeling study performed by Spall et al., the use of k-epsilon (k-ε), k-omega (k-ω), and Reynolds Shear Stress (RSS) models, over predicted the thermocline thickness. The study was performed on an inlet Re range between 500-3000 [128]. A similar study investigated the turbulence mixing in a horizontal cylindrical tank [141] comparing three turbulence models: RNG, k-ε, and k-ω provided the same temperature profile in cylindrical tank thermocline simulation with over prediction of the thermocline thickness [130]. Experimental study on a real size model performed by Musser and Bafleth with Reynolds numbers between 500-12000 suggest that modeling the flow inside a thermocline tank with a laminar flow model is valid and delivers more accurate results than those using turbulence models [139, 142].

In the current study the use of k-ε, k-omega, SST, and BSL Reynolds stress models collectively over predicted the thermocline thickness volume by 30 % compared

to laminar flow model when the thermocline thickness was compared to the thermocline thickness obtained by the experimental result in chapter 6. Therefore, the CFD parametric study was performed using laminar flow model for Reynolds numbers between (500-7500).

In order to ensure model simulation stability, previous studies suggest using a Courant number *(C)* lower than 10 [143]. The Courant number is calculated based on the element size in the CFD mesh, fluid velocity, and the transient time step. If the model is mesh independent, residuals do not decrease with smaller element size, and step size can be reduced to achieve a lower Courant number.

In the optimized time step found by Ismail et al. [144], one second intervals were found adequate to model liquid storage tanks based on the optimized mesh element size used in their study. Nelson et al. found that in order to have a stable model, the time step must be smaller than$(\Delta x^2)/(2\alpha_f)$, where x is the length of each mesh element and α_f is the fluid thermal diffusivity. For the mesh size used by Nelson et al. a time step of 0.01 sec was sufficient. A smaller time step is essential in the simulation of natural convection inside the tank. A numerical simulation of the tank thermocline with ignoring natural convection effect in the tank led to longer thermocline maintenance in the tank than the experimental results [144], which resulted in accurate thermal efficiency. Similar results were found with one dimensional finite volumes where the numerical model over or under estimated the thermocline region thickness later in the discharge due to incorrect simulation of convective mixing [145].

The current study utilized unstructured mesh that contained maximum element size of 0.001 m with inflation layers near the wall region. Grid independence was realized as the residual RMS error values dropped to a value of 10^{-5} were reached as recommended in previous studies [146, 147]. The domain imbalance was monitored and showed an imbalance of less than 1%.

A time step independence study was performed by decreasing the time step value by half and monitoring the exit temperature. The inlet flow rate was used to calculate the time required to completely replace the hot fluid in the tank by the incoming cold fluid. Then exit temperature was taken at the exit after each simulation and plotted against the Courant number resulted from each time step value.

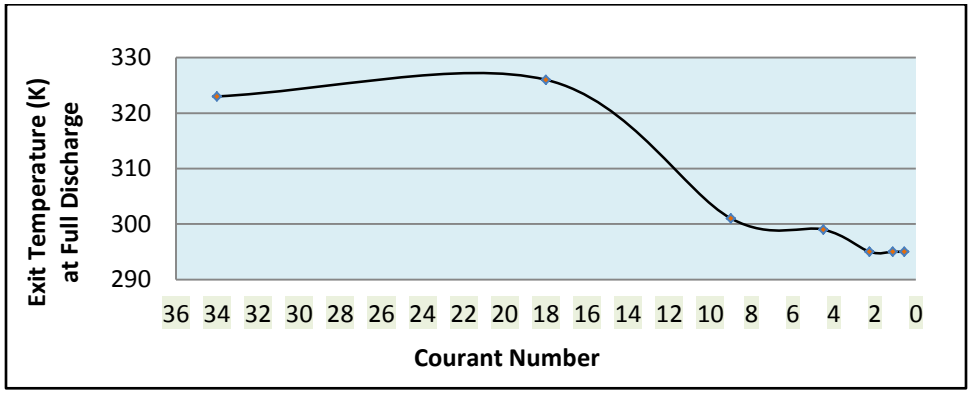

Figure 5.4 Time step independent study

The transient simulation utilized “adaptive time stepping”, which enabled to program to adjust the time step size based on the provided Courant number. The time step monitors shows time steps from (0.01- 0.2) seconds was used in order to maintain Courant numbers between 2 and 5. Second order backward Euler model was used for the

transient scheme, and high resolution advection scheme was utilized in the solver setting. The same advection scheme was used for continuity, energy and momentum equations.

Figure 5.5 show plots of the Momentum imbalance in the x, y, and z directions. An imbalance of less than 1 % during the transient solutions is recommended in the literature for improved solution accuracy. All three momentum imbalance plots show low imbalance, which indicate that the momentum equation is resolved.

Another indicator that the solution is converged is the RMS residuals drop to less than 10^{-6}. Smaller time stepping and a finer mesh were used for the diffuser cases to account for the sharp edges and the fluid impingement on the tank walls or the diffuser.

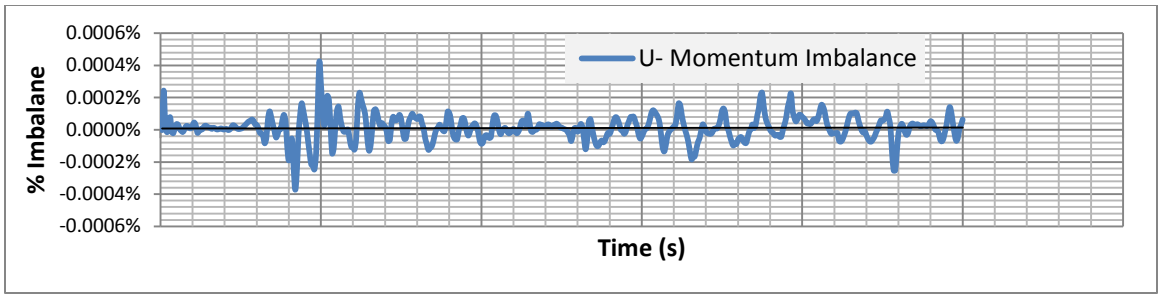

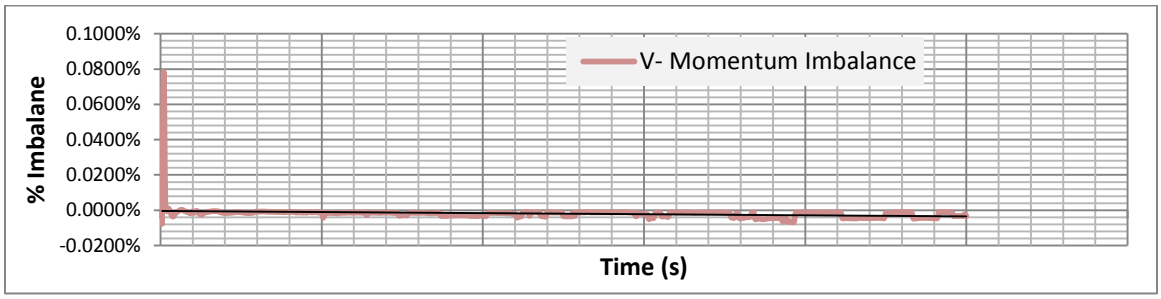

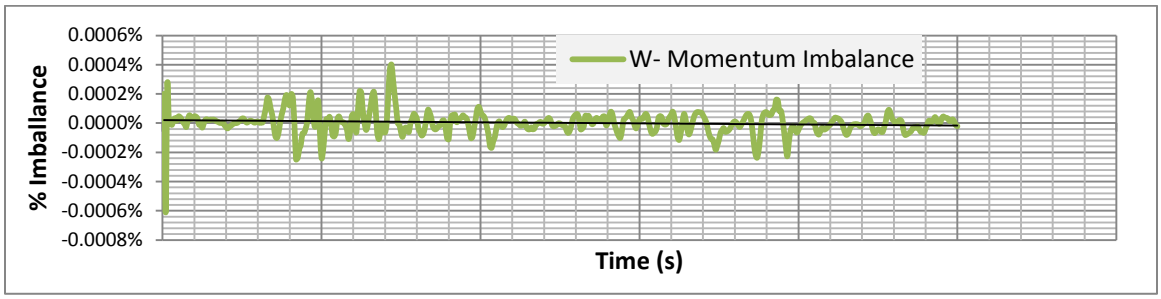

Figure 5.5 Momentum imbalance throughout the solution

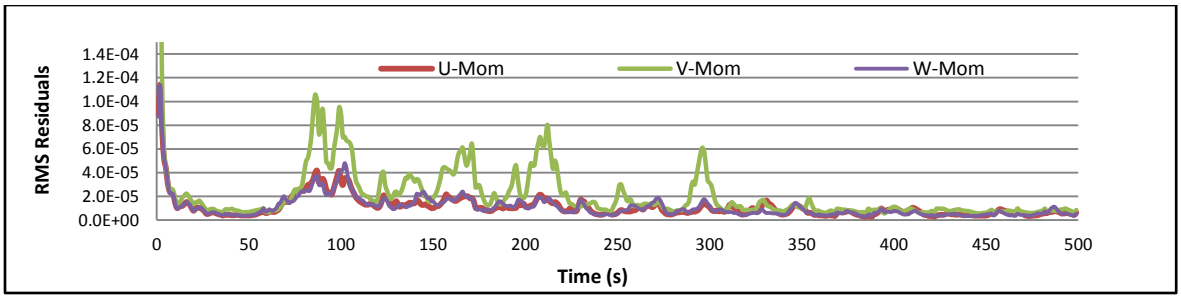

Figure 5.6 Residual RMS Error Values

Comparing Thermocline Thickness and TE in Spherical and Cylindrical Tanks of the Same Volume

The first simulation case compares two tanks of the same volume (0.065 m^3) with the following parameters: inlet diameter ***0.05 m***, inlet velocity of ***0.1 m/s, $\Delta T = 70^{\circ}C$***, inlet temperature ***300K***, spherical tank diameter ***D_{sph} = 0.5 m,*** cylindrical tank diameter ***D_{cyl}= 0.35m***, cylindrical tank height ***H = 0.7m,*** cylindrical tank ***H/D =2***, inlet Froude number = ***1.00***, adiabatic, no slip condition wall, and a pipe diffuser. Thermocline thickness, thermocline vertical movement, and tank TE were compared. The goal of the comparision is to find if a spherical tank will produce similar thermal efficiency and stability to a cylindrical tank with the same volume.

In order to calculate the thermocline thickness for each tank, computed temperatures data points were extracted as follows: mid-plane (Z=0), along the entire Y axis, *X = D/4* (in order to avoid inlet jet distortion at the center of the tank), at 0.01m intervals from the bottom of the tank, and at half the discharge time of 150s. Half

discharge time denotes the thinnest thermocline region in the spherical tank due to the maximum tank diameter at the middle of the tank. Figure 5.8 show the thermocline data along the Y axis at half the discharge. The Y location was normalized by the tank diameter in the spherical tank and the tank height in the cylindrical tank.

Since the temperature in the inlet and outlet region at half discharge was stable, it was possible to measure the thermocline based on temperature change. A temperature increase of $\boldsymbol{0.5^{o}\ C}$ marked the beginning of the thermocline region. The thermocline region ended when the temperature became constant. The thermocline thickness in the cylindrical and spherical tank was 0.07 m and 0.1 m respectively. The volume of the thermocline was calculated in the cylindrical tank as:

$$\boldsymbol{V_{thl} = \pi \frac{D^2}{4} * h_{thl}} \qquad \textbf{5.12}$$

Where the subscript (thl) denotes the thermocline. The thermocline volume for the spherical tank was calculated by using the spherical cap volume (SCV) as:

$$\boldsymbol{SCV = \pi \cdot h_{cap} \cdot \frac{(3\frac{D}{2} - h_{cap})}{3}} \qquad \textbf{5.13}$$

Where h_{cap} the height of the spherical cap and D is the tank diameter. The upper and lower cap volumes were calculated using obtained h_{thl}, and then the thermocline volume was calculated by subtracting both cap volumes from the complete tank volume. Volume comparison based on the volume occupation at the middle of the tank showed that the thermocline in the spherical tank occupied 10 % more volume than the cylindrical tank.

The temperature contour plot shows the thermocline region at 150 s of the tank discharge is shown in Fig. 5.7. Figures 5.8 and 5.9 show the temperature plot along the Y axis for the spherical and cylindrical tank respectively at half of the discharge time. The Y axis was normalized using the tank diameter; hence the larger slope for the spherical tank which has a larger diameter.

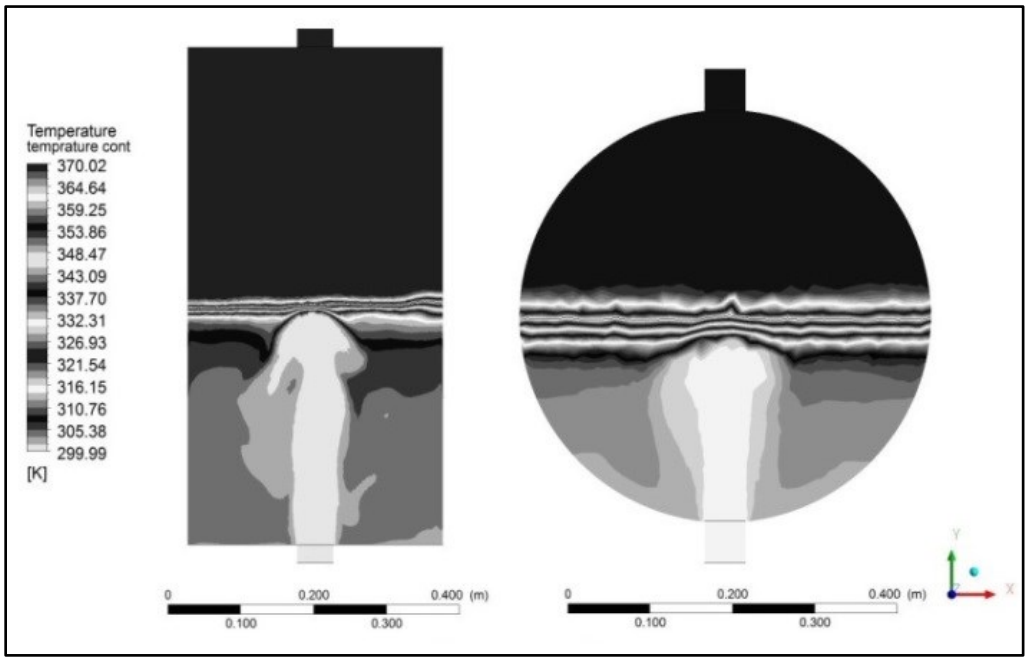

Figure 5.7 Thermocline region in cylindrical and spherical tanks at half the discharge

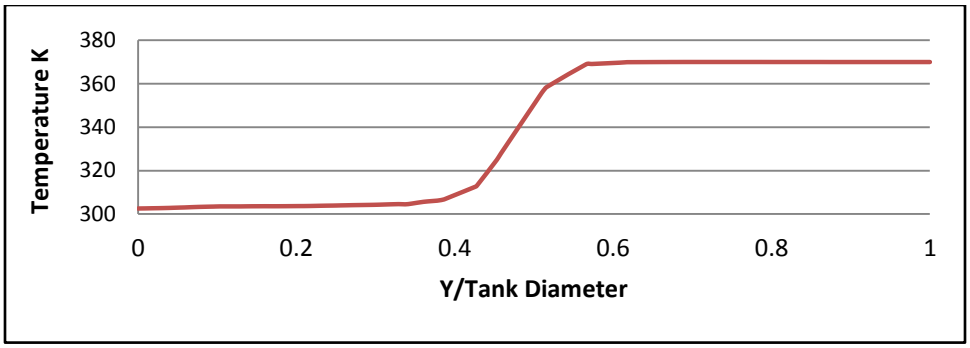

Figure 5.8 Spherical tank thermocline along the Y axis

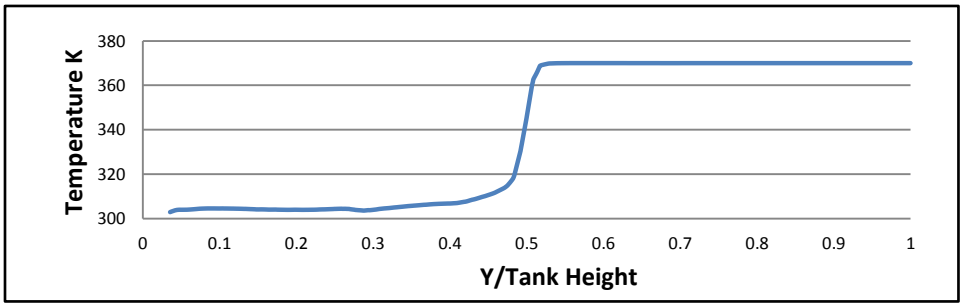

Figure 5.9 Cylindrical tank thermocline along the Y axis

In order to visualize the thermocline stability and movement during the entire discharge process, data points along the Y axis were compared in the cylindrical and spherical tanks at 6 time intervals. Time intervals were taken at every 50 seconds of the discharge process, and data points were extracted in a similar manner to the thermocline thickness data points. Figures 5.10 and 5.11 show the thermocline vertical movement in the spherical and a cylindrical tank respectively at 6 intervals: 50,100, 150, 200,250 and 300 seconds.

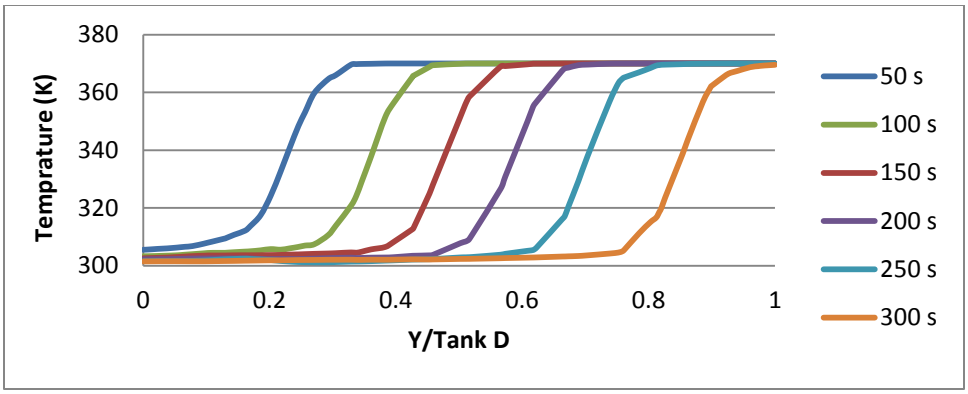

Figure 5.10 Spherical tank thermocline region movement at 50 s time intervals

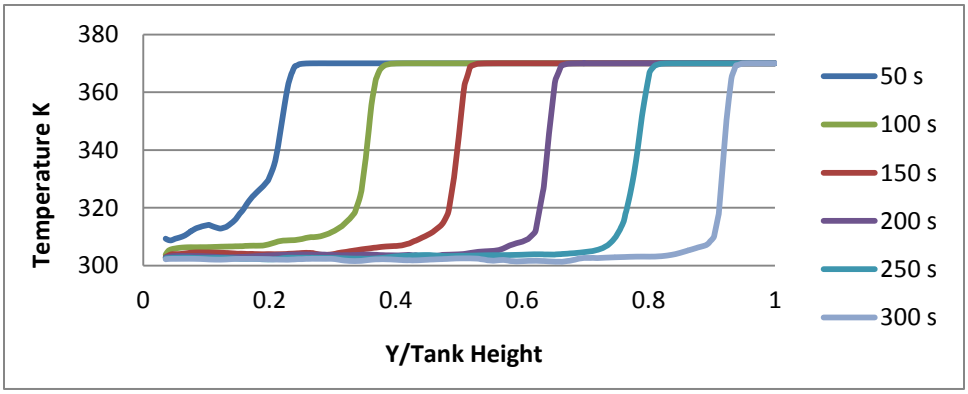

Figure 5.11 Cylindrical tank thermocline region movement at 50 s time intervals

Thermal efficiency was calculated using the time when the exit temperature started to drop below 90% of the storage temperature (363 K). The time of temperature drop was used to calculate the volume extracted based on the inlet volumetric flow rate. Thermal efficiency (TE) was then calculated using Eq. 5.6. The time of temperature drop, based on the CFD time step, is 312 s for the spherical tank and

308s for the cylindrical tank. The drop in cylindrical tank efficiency, in spite of the thinner thermocline region, is attributed to the increased mixing at the exit region at the end of the discharge as shown in fig.5.12.

Results demonstrate that a spherical tank shows the following: (1) thicker thermocline region, (2) steadier inlet region temperature at early discharge stage, (3) less mixing in the inlet region and more tank stratification, and (4) a comparable tank TE.

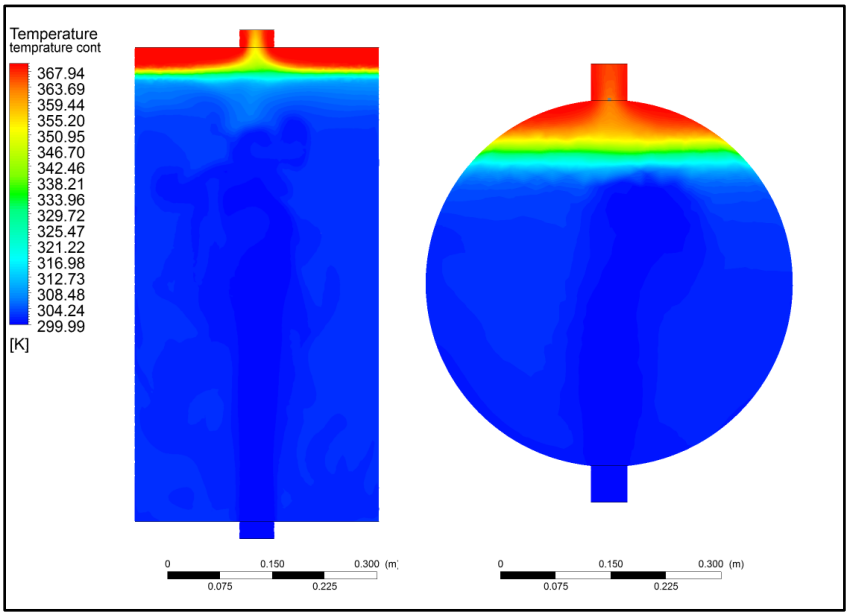

Figure 5.12 End of the dischange processs for cylindrical and spherical tanks

Parametric Study of a Spherical Tank Thermocline System

A parametric study on a spherical tank with variable inlet velocity (0.03-0.15) m/s, and variable ΔT (10-70º C) was performed. The variation covered inlet Reynolds numbers between (1500-7500), inlet Froude numbers between (0.5-3.3), inlet Archimedes numbers between (0.5-10), tank Richardson number between (1-100), and similar tank dimensions to the comparison case involving spherical and cylindrical tanks.

In order to cover the studied range of inlet Reynolds numbers from 1500-7500 with satisfactory data continuity and increased linearity, it was necessary to increase the Re by a magnitude of 500 at variable ΔT (10-70º C) at 10 degrees, which required 70 cases each with different Re, Fr, Ar, and tank Ri numbers.

The first three parameters used inlet velocity and inlet diameter for calculation, whereas the Richardson number used the tank diameter as the characteristic length. In each case, the TE was calculated as η_{90} in Eq. 5.6, and thermocline thickness was measured using extracted temperature values along the tank Y axis.

SSPS statistical software was utilized to compute a Pearson correlation matrix to study the significance of each dimensionless number with TE and thermocline thickness. In addition, a multi variable linear regression analysis and partial correlation was also performed to estimate the tank TE based on dimensionless parameters.

The Pearson correlation analysis showed that all the analyzed dimensionless numbers have correlation with the tank TE. However, Froude number has the foremost correlation. The multi variable linear regression produced a partial correlations for each of the dimensionless numbers as independent variables on the TE (partial correlation is the amount of influence of each independent variable on the dependent variable after all other independent variables have been statistically accounted for) the partial correlation of each of the dimensionless numbers are: Fr = 96%, Re = 16%, Ar = 0.072%, and Ri = 0.08 %. This means that a regression equation can be produced based on Froude number alone with an acceptable accuracy.

A regression equation was then produced based on Froude number and TE with an estimated error of 2% and an adjusted R^2 of 0.98.

$$\boldsymbol{TE = -0.121 \cdot Fr + 1.064} \qquad \textbf{5.14}$$

Figure 8 shows the linear correlation of *TE* and the inlet Froude number. The error percentage predicted from the model is higher at Fr >1.5, but that is also a region of low tank *TE* and unlikely to be used in practice.

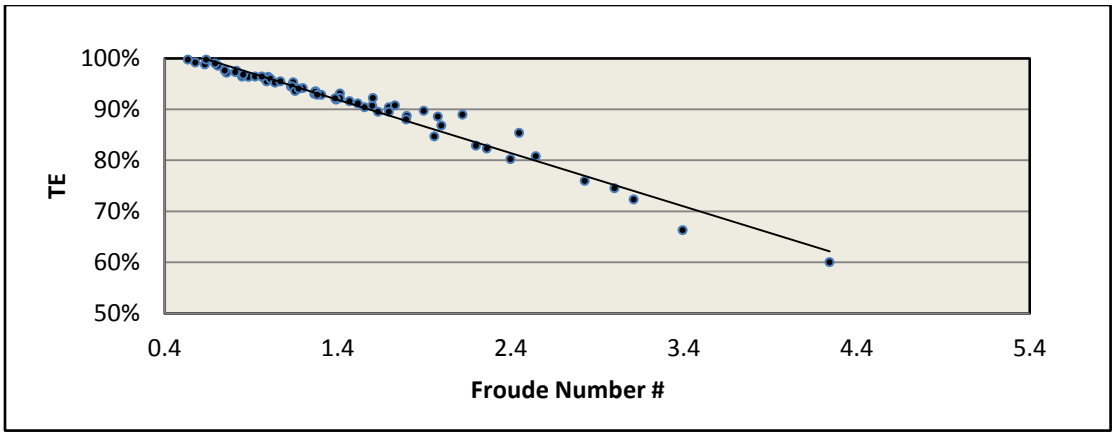

Figure 5.13 TE versus Froude number correlation

The regression analysis and the Pearson correlation showed that there is no significant relation between the thermocline thickness and any of the studied dimensionless numbers.

Numerical Comparison of Three Common Types of Diffusers

Mixing inside the tank is responsible for poor thermocline formation, which leads to a thicker initial thermocline region. The increased mixing at the inlet region also delays the thermocline region formation, which isolates the colder region and the hotter region.

In order to counteract the effect of higher Reynolds number both ASHRAE and EPRI guidelines recommend using a larger area diffuser to mitigate the mixing effect caused by the high Reynolds number [139]. In addition, the increased length of the tank may contribute to improved tank stratification even at Re $\leq$ 12000.

The use of a diffuser in the near inlet region has the potential to reduce the mixing in the inlet region in cases with relatively high Re and Fr numbers. Various studies suggest that the diffuser shape and design can increase the tank stratification. Chung et al. suggest that many diffusers have been evaluated in previous studies and conclude that diffuser performance depends on the tank shape and aspect ratios [138]. Diffuser design in thermocline storage tanks are under-investigated and underutilized due to the incremental cost in solar storage tanks and the installation difficulty in real cases [53].

The parametric study showed that using Fr number ≤ 1 in a pipe diffuser inlet increases the initial mixing in the inlet region and leads to poor tank stratification and consequently a low TE. Therefore, the use of a diffuser was investigated in this section in order to reduce the mixing.

An entropy production plot based on CFD simulation performed by Berkel shows entropy production only in the thermocline region. where the flow is impinging on the thermocline region [148]. Similar correlation was performed using entropy calculation in the current study:

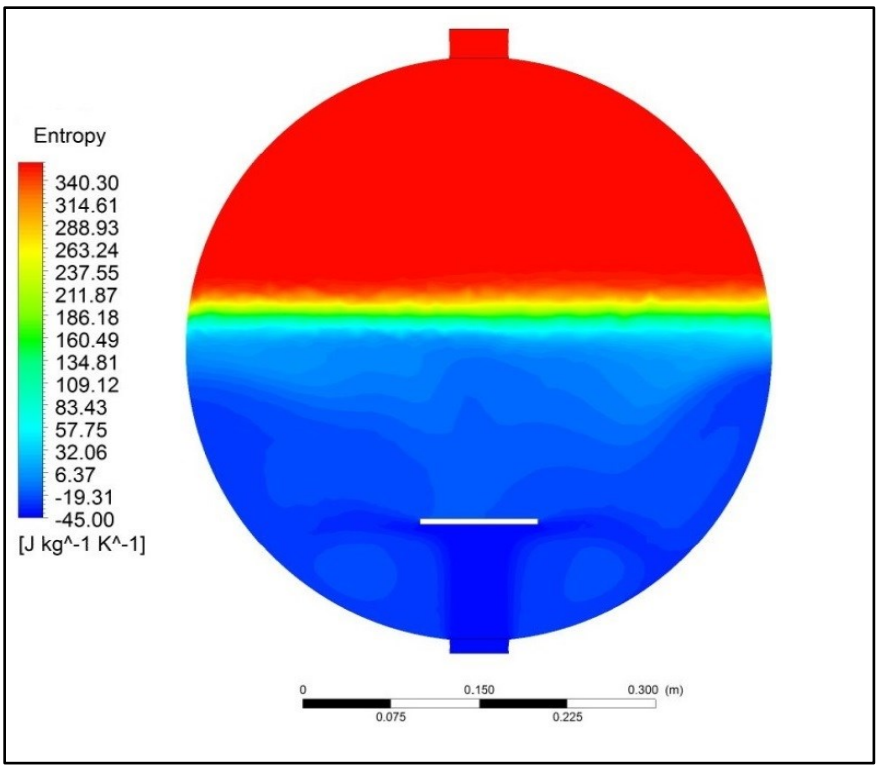

Figure 5.14 entropy production with a plate diffuser

The most common diffusers studied in the literature in rectangular and cylindrical tanks are radial, plate, and circumferential diffusers. In order to find the most effective diffuser for spherical tanks, these diffusers were investigated numerically in a spherical tank at the same flow parameters.

CFD modeling was used to compare these diffusers at inlet velocity = 0.15 m/s, ΔT = 20ºC, leading to inlet Fr number = 3, and low thermal efficiency. Similar spherical tank dimensions to the previous case were used with total discharge time of 350 seconds. The mass flow rate is kept constant throughout the comparison.

Further mesh refinement took place to account for the diffuser geometry at the near inlet region. Figure 5 shows the mesh used for the plate diffuser using inflation layers and regionally reduced mesh size. The mesh consisted of 360,000 tetrahedral elements and was subjected to mesh sensitively analysis and time step stability.

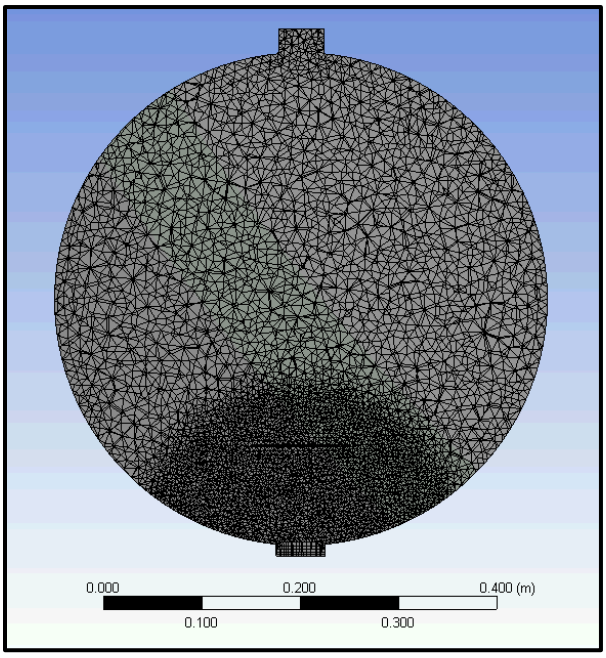

Figure 5.15 Increase mesh element near the diffuser region

The thermocline thickness was investigated for each diffuser at a time of 50s of the discharge process, when the thermocline should have completely formed at a lower Froude number. The thermal efficiency was then calculated for each tank.

The radial diffuser, which has been recommended for cylindrical tanks, showed a reduced mixing in the near inlet region when compared to a pipe diffuser. The circumferential diffuser, which reverses the flow direction to the bottom of the tank,

shows even less mixing. A flat plat diffuser twice the inlet diameter (2d) in size and placed at a distance (2d) from the inlet produced the least mixing in the inlet region.

Using a flat plate diffuser increased the tank stratification to a level where a thermocline started to form at 50 s of the discharge, which means that the tank had the best degree of stratification when compared to the other diffusers. Figure 5.16 show temperature contours for the four diffusers at 50 seconds of the discharge process. The TE was calculated for each diffuser using Eq. 5.6.

No thermocline region was formed for a pipe diffuser due to high inlet flow, which lowered the tank stratification. The radial diffuser caused the tank to start to stratify, however no defined thermocline was noticed at half the discharge time. In the circumferential diffuser, an oscillating thermocline region was formed at half the discharge. The plate diffuser led to a well-defined thermocline region at half the discharge time as shown in fig 5.16. The four diffusers produced the following TE: pipe TE = 69%, circumferential diffuser TE = 77%, radial diffuser TE = 82%, and plate diffuser TE 90%.

Another advantage of using a radial circumferential diffuser, was a decrease in unpumpable volume for spherical tanks compared to cylindrical tanks, as shown in Figure 5.17.

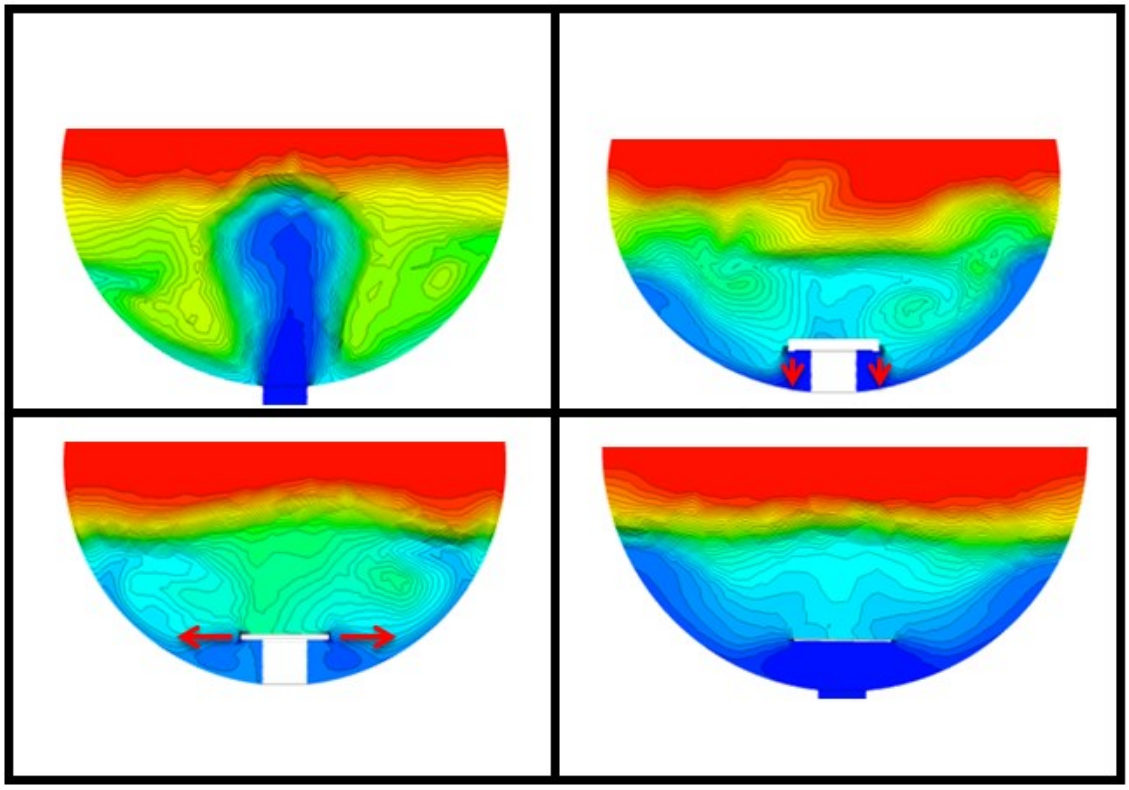

Figure 5.16 Temperature contours for: top left pipe inlet diffuser, top right circumferential diffuser, bottom left, radial diffuser, bottom right, plate diffuser

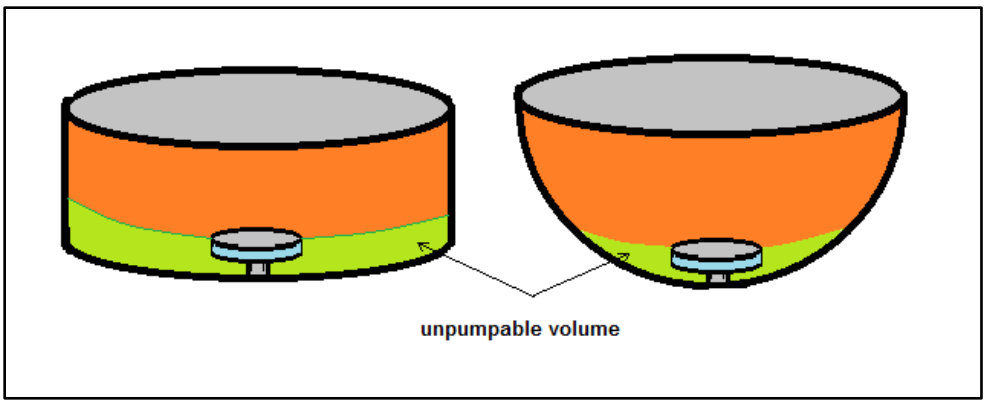

Figure 5.17 Increase of usable volume when using a radial diffuser in a spherical tank

The plate diffuser was optimized for the current flow parameters (Fr = 3, Re= 5500) in terms of plate size and plate distance from the inlet using the inlet diameter ratio. Thermal efficiently was calculated for each case. Distance of 2d from the inlet and plate size 2 d provided the best thermal efficiency.

Plate Distance \ Plate Diameter	1d	2d	3d
1d	77 %	89 %	88 %
2d	69%	90 %	82 %
3d	68 %	74 %	65 %

Figure 5.18 Plate size and distance optimization

Parametric Study Using a Plate Diffuser

The same parametric study that was performed on the pipe diffuser was repeated using a plate diffuser in order to determine the influential flow parameters and produce a tank thermal efficiency equation.

For the plate diffuser, the statistical analysis shows a less linear relation with Froude number as Froude number increases to more than 2. Pearson two tail correlations showed that both Froude number and Reynolds numbers are significant. Although Froude number is more significant, the inlet Reynolds number influence cannot be neglected.

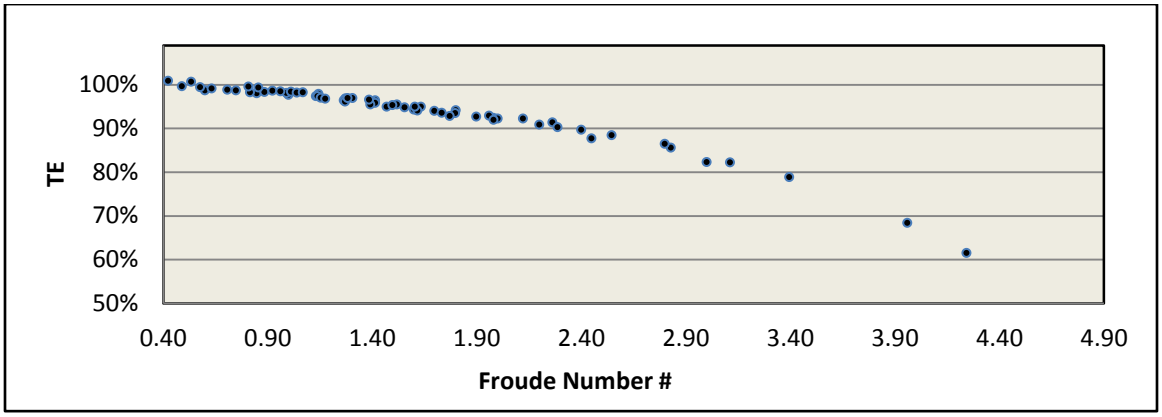

Figure 5.19 Froude number versus TE in a plate diffuser

The multivariate regression analysis showed that the partial correlation of each of the dimensionless number with thermal efficiency as: Fr= 88%, Re = 17%, and both Ri and Ar number = 2.5%.

Using only Froude number for the regression to estimate TE lead to the following equation with $R^2 = 0.90$:

$$TE = -0.0785 \cdot Fr + 1.0616 \qquad 5.15$$

In order to improve the regression equation for linearity, adding Reynolds number in the regression improved the adjusted $R^2 = 0.98$, which means that this equation will produce the same result with 98% confidence for this sample and at a different sample as well:

$$TE = 1.047 - (0.09 \cdot Fr) - (6.6 \times 10^{-7}) \cdot Re \qquad 5.16$$

The regression analysis and the Pearson correlation also showed that there is no significant relation between the thermocline thickness and any of the studied dimensionless numbers.

Summary

This study showed that using a spherical tank in a thermocline storage system delivers comparable results to a cylindrical tank of the same volume. A *TE* equation was developed using a numerical parametric study regression analysis based on 70 cases using a pipe diffuser with variable inlet velocities and temperature differences leading to Reynolds numbers between (500-7500) and Froude numbers between (0.5-3). The regression analysis suggests that within the examined parameters (inlet Reynolds, Froude, and Archimedes, and tank Richardson number), the Froude number is the most influential parameter on tank stratification. The thermal efficiency is the largest for Froude number

0.5 and lower, and there is no relationship between any of the studied dimensionless numbers and thermocline thickness. In addition, when using a pipe diffuser, the TE decreases as Reynolds and Froude numbers increase.

Four types of diffusers (pipe, radial, circumferential, and plate) were numerically compared. The results showed that a plate diffuser will enhance the tank stratification at Froude number = 3 by 20 points (from 69 % to 90 %) when compared to a pipe diffuser. Optimization of a pipe diffuser revealed that within the tested flow parameter, tank diameter, and inlet diameter, a plate with a diameter twice the inlet diameter and a distance from the inlet equals to the twice the inlet diameter provided the best results.

The conclusions of both parametric studies confirm the findings in the literature that the thermal efficiency of a thermocline storage tank is directly related to the tank shape and the inlet geometry along with the flow parameters. The benefits of using a spherical tank with thermocline system become apparent when radial or circumferential diffusers produce more storage volume, allowing the fluid to exit the tank with less mixing when compared to a cylindrical tank.

The next chapter will show data validation for the CFD data for both pipe and plate diffuser using a lab scale model.

CHAPTER 6 : EXPERIMENTAL WORK AND DATA VALIDATION

An experimental set up used to validate the numerical results obtained by the CFD software at the specified Reynolds and Froude numbers with a pipe and a plate diffuser in terms of: (1) the thermocline thickness (2) the exit temperature used for the thermal efficiency calculation, and (3) the gravity current produced at the inlet at the first stage of the discharge during the thermocline formation.

Equipment Specifications

Spherical tank

The tank used for the experiment has a diameter of a 0.5m and made of clear Acrylic. The Acrylic material used in the tank has the following properties: tensile strength of 69 MPa, yield strength of 124 MPa, deflection resistant for up to 99°C, , maximum operating temperature of 82°C, and thermal conductivity of 0.2 W/m·K [149]. The tank wall thickness is 0.003 m.

A circle with 10 cm diameter was cut at the bottom of the tank in order to insert the diffusers assemblies shown in fig. 6.1. The top of the tank was used as an access point for the thermocouple tree and water heater circulating pump. The tank was supported by an enforced plastic cradle.

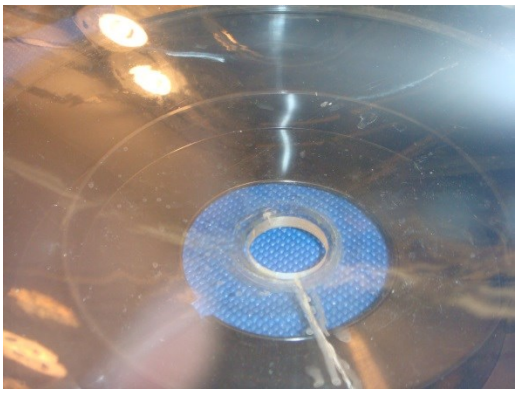

Figure 6.1 Tank bottom hole cut for inlet diffusers

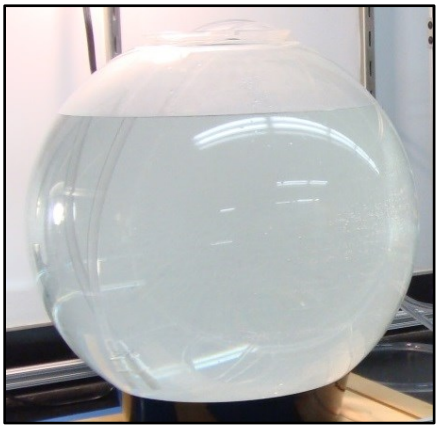

Figure 6.2 Acrylic tank 0.5 m Diameter

Circulating water bath

A water bath with a heater and a pump system was used in order to bring the water inside the tank to the desired temperature. A gradual increase in temperature is necessary in order to avoid sudden thermal expansion that could lead to cracking.

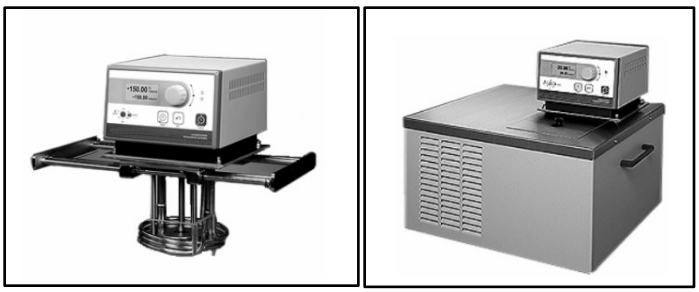

Figure 6.3 Circulation pump / heater (left), circulation bath (right)

The circulating bath pump has a maximum flow rate of 22 LPM and has an operating temprature range of 5-200°C. The circulating water bath pump was also used after the tank was completedly heated, to maintain the cold fluid tempurature in order to reduce the upstream temperature fluctuation.

Inlet pump

A self-priming centrifugal pump with motor speed controller was used at the tank inlet. The pump used was a Cole-Parmer *Masterflex*® centrifugal pump with a maximum flow rate of 10 GPH (0.8LPM at 600 RPM). The pump has a maximum pressure of 1.4 bars, and operating temperature between 0-40°C.

Thermocouples

For temperature measurement, 24 gauge thermocouples, T type, and Teflon insulation with no sheathing were selected based on the operating conditions (Temperatures between 0-70° C, and required response time of 0.5 second). In order to measure the thermocline thickness during the discharge, a group of thermocouples was

distributed vertically. Alternatively, the thermocouple could have been placed on the outside of the tank and the thermocline detected using the temperature change from the outside wall. However, the placement of the thermocouple on the outside wall proved inaccurate due to the wall thermal resistance, the thermocline response time, and the thermocline vertical movement.

Drilling holes on the wall of tank was not a suitable option because of possible tank fracture due to acrylic brittleness. Temperature sensitive film was another option to measure the thermocline thickness from the outside of the tank wall. However, the temperature ranges for the available thermos-film (usually between 10 degrees) do not cover the temperature range needed in the experiment. In addition, film has a short shelf life, is highly sensitive to incandescent light, has a slow response time, and can degrade with usage. Figure 6.4 shows the reaction of two thermos-films to the thermocline temperature at one region only.

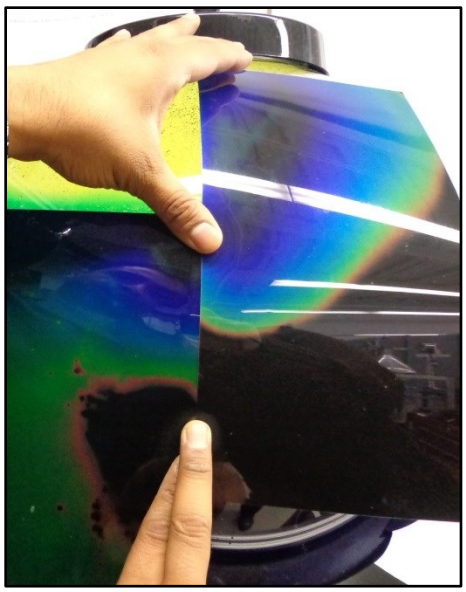

Figure 6.4 Thermocline thickness via thermal film using two different sheets with different temperature ranges.

The preliminary CFD data showed a thermocline thickness of between 6-8 cm for Froude of 1 and Reynolds of 500 for the pipe diffuser and Froude number of 2.5 and Reynolds number of 1000 for the plate diffuser. Therefore, 14 thermocouples placed 1 cm apart should be sufficient to completely capture the thermocline thickness as it travels vertically inside the tank.

In order to satisfy the measuring requirement and to have more flexibility in measuring the thermocline thickness during the discharge, a thermocouple tree shown in fig 6.4 was constructed containing 15 thermocouples. The first thermocouple is placed 2 cm from the edge of the tree, fourteen thermocouples were equally spaced 1 cm apart and 12 cm from the bottom end, and the last thermocouple was placed 45 cm from the bottom

of the tree to measure the exit temperature. The tree was mounted vertically from the top of the tank on rigid holder to ensure vertical placement, shown in fig 6.6, after the tank was completely heated and before the cold fluid was pumped into the tank.

Figure 6.5 Thermocouple tree consisting of 15 J type thermocouples

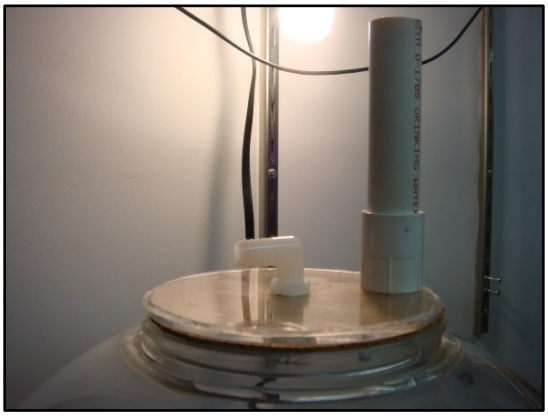

Figure 6.6 Top cover of the tank with water outlet and thermocouple tree mount

The thermocouples were made using thermocouple wires and spot welding to join the wire tips instead of iron soldering, this improved reading accuracy and reduced measurement noise. After the thermocouples were made, they were tested, calibrated for reading. Response time was determined to be within 0.5s in water. All thermocouples were calibrated based on the maximum, minimum and middle temperature (70°, 23°, 0° C) using digital and analog thermometers, boiling water, ice water, and water at room temperature. The calibration was repeated after each experiment and data were stored in the LabVIEW program and the DAQ system. The repeatability of the calibration and the offset show an accuracy of +/- 0.5°C based on the actual cold junction temperature. Furthermore, to ensure less fluctuation in temperature a cold junction channel (CJC) temperature was maintained at 0° C by using an insulated mug full of crushed ice that is continuously monitored.

Inlet, diffusers and outlet

The tank was cut at the bottom center in order to allow the inlet diffuser assembly to be installed. The inlet diffuser assembly was placed in the bottom of the tank and tightened from the outside. Rubber gaskets were place on each side of the tank wall to prevent leakage. Figure 6.6 show a brass inlet pipe diffuser with 0.022m diameters and 0.015m connection. Figure 6.6 shows a plate diffuser with diameter (d) = 0.011m and a 2d diameter center plate placed 2d away from the pipe outlet. Both diffusers were made of brass, fitted into acrylic base, and connected to the pump through vinyl tubing with a check valve.

Figure 6.7 Inlet pipe diffuser of 0.022 m diameter

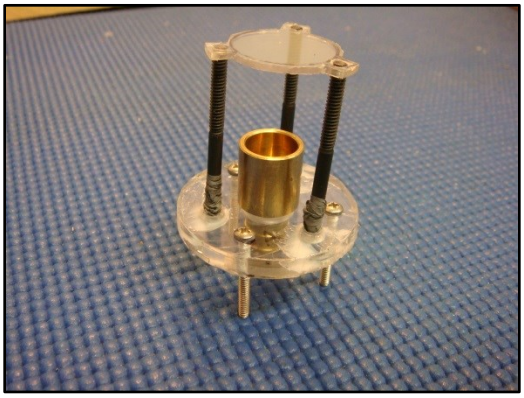

Figure 6.8 Optimized plate diffuser

The top of the tank was used as the access port for the heater, thermocouple tree, and the water drain. Therefore it had to be easily removed, securely fastened, and water tight. The top was made of 0.004 m thick acrylic sheet with a grooved edge to enable the

use of clamps. To ensure a water tight condition, a cork sheet was placed between the tank top and the removable cover. The outlet of the tank was located at the middle of the top plate as an L shaped elbow pipe. A side PVC pipe with 4 cm diameter was placed on the top cover to allow the insertion of the thermocouple tree after the tank was heated and the top cover was secured to the tank. Figure 6.9 shows a view of the top cover from the bottom of the tank after it has been clamped with the thermocouple tree in place and the drain hose is connected.

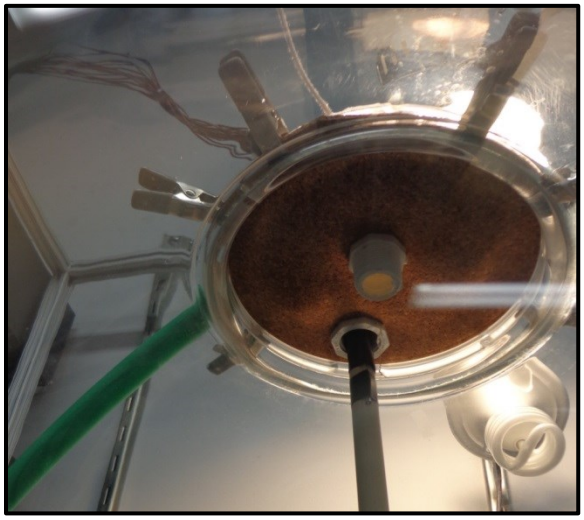

Figure 6.9 Tank top cover with thermocouple mount

Data acquisition (DAQ) and LabVIEW program

The data acquisition system used in this experiment is NI-USB-6229. The DAQ has 16 analog input channels, and can be programmed to directly read temperature after setting up thermocouple type, gauge and calibration data. One channel was set to act as

cold junction channel (CJC) where the temperature will be constant in order to adjust the reading for the other input channels.

The labVIEW virtual instrument input (VI) was written to record temperatures from each of the thermocouples every second with 100 data readings per second. The data were averaged over 1 second in order to reduce noise. An active data recording was transferred atone second intervals to a spread sheet file based on a stacked array for 15 channels, which continuously stored the data during the entire run of the experiment.

A snap shot of the LabVIEW front panel shows the program during the experiment. Input flow rate, time elapsed and individual thermocouple location and temperature were monitored during the entire discharge process. After the program has stopped, the results for the entire run were stored on a spreadsheet for further analysis.

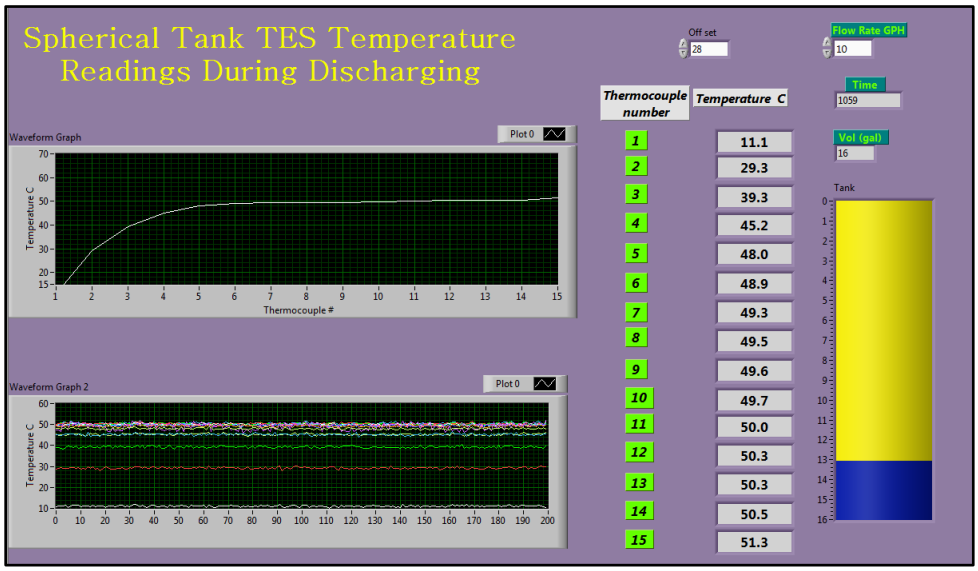

Figure 6.10 LabVIEW front panel screenshot

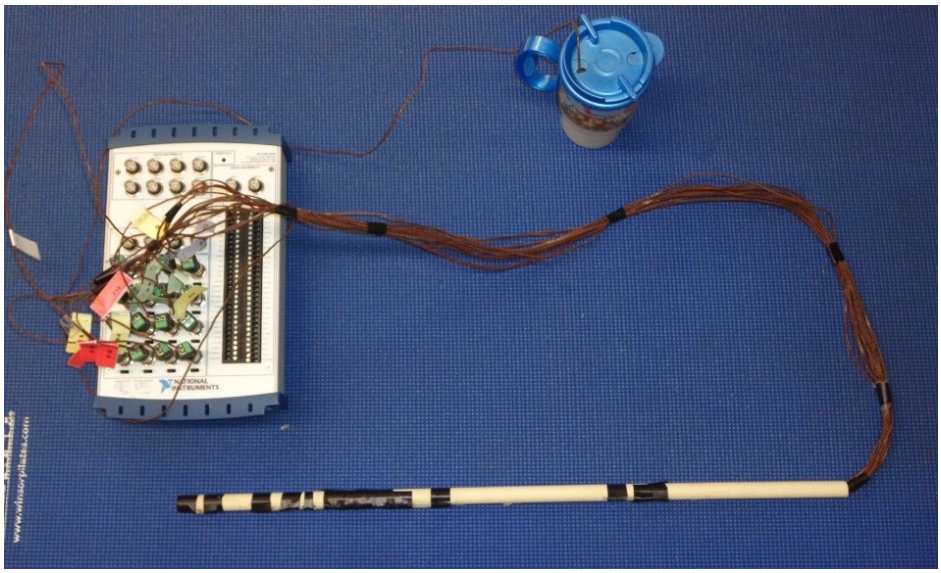

Figure 6.11 Thermocouple tree, CJC and DAQ

Experiment Considerations

Due to the curvature of the tank, it is difficult to view the gravity current in the first few seconds of the discharge. Therefore, it was essential to place a camera at a 45° angle on the tank surface to take a picture of the inlet flow, and use to an underwater camera to video capture the gravity current of the cold water being pumped into the tank.

Working with acrylic is very challenging due to its brittleness; tightening of the inlet diffuser bolts had to be done simultaneously in five intervals in order to avoid cracking. All material used inside the tank such as gaskets, tubes and dye had to be checked for compatibility since acrylic is chemically reactive to other hydrocarbon materials. Because of the temperature difference between the inside of the tank and the

outside surface (20-30° C), bubble formation took place on the inner wall making it difficult to visualize the flow inside the tank. Therefore clearing the bubbles prior to the discharge process was necessary.

The tank surface was not insulated, and the experiment duration is relatively long (2.5 hours); external monitoring of the surface temperature was important in order to improve the accurate estimation of heat loss coefficient in the CFD data.

In order to reduce noise in the thermocouple reading, it was essential to avoid placing any electrical wire, instrument, or the pump assembly near the thermocouple wire.

Monitoring of flow rate during the discharge is essential since the level of cold water decreased, leading to a different pump head and higher flow rate. Since the pump has a fixed tube diameter (0.003m) and the inlet diffuser diameter is (0.022 m) the flow was kept at an angle below 10° to order avoid flow separation and reduce any possible pump head loss [150]. This was achieved by gradually increasing the diameter through a set of tubes to allow for flow reattachment. Figure 6.12 show a schematic of the all the equipment integrated together during the discharge process. The circulation water bath, which was used as a water heater, doubles as a water chiller after the tank is completely heated in order to maintain the incoming cold water temperature.

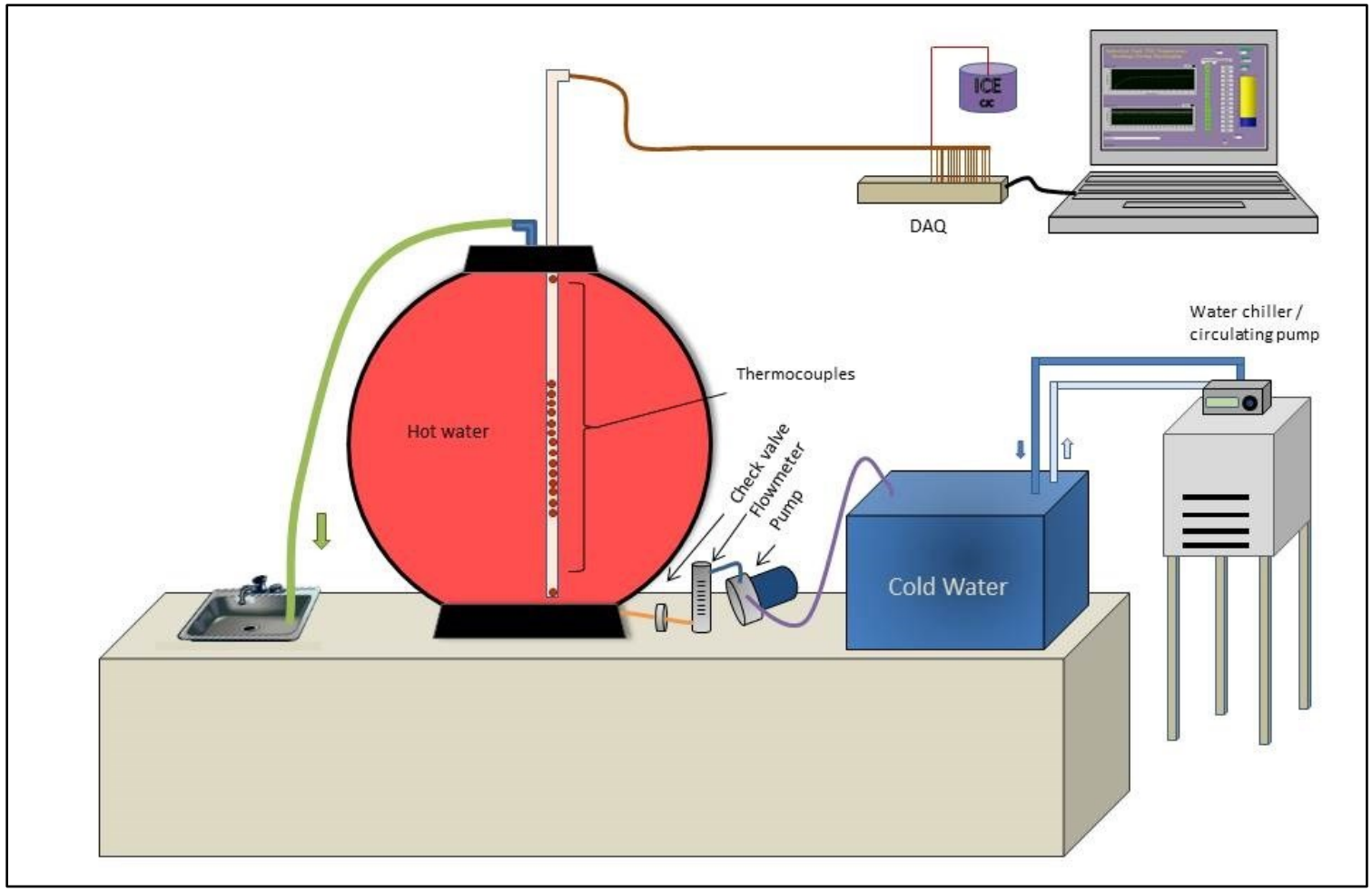

Figure 6.12 Schematics for the experimental set up during the discharge

Procedure of the Experiment

The experiment consisted of two cases. The first case involved a raw pipe diffuser with diameter of 0.022 m, inlet velocity 0.022 m/s (Q = 8 GPH), inlet temperature of 23° C and tank temperature equal to 55°C. This corresponded to Reynolds number = 600, Froude number = 0.5 and complete discharge time of 8000s (2.5 hrs.).

The second run was targeted to test thermocline formation at a higher Froude number (Fr = 2.5) using a plate diffuser with a diameter of 0.011 m, plate to inlet pipe distance equal to twice the diameter (0.022 m), and plate diameter = 0.022 m. The tank temperature and inlet temperature were 55°C and 15°C , and inlet velocity of 0.1 m/s which corresponds to Reynolds number = 1000.

The experiment started by filling the tank with water at room temperature (22°-23°C). The water circulation bath temperature was set to 55°C. Both inlet and outlet tubes of the circulation baths were inserted into the tank from the top cover. Yellow food coloring was added to the water. Increasing the tank water temperature from room temperature to 55°C took around 1.5 hours.

The cold water tank was filled with room temperature water and dyed blue. In cases where the inlet temperature was below room temperature, the circulation bath was used after heating the resident water to stabilize the cold water temperature.

Once the temperature inside the tank reached 55°C, circulation bath tubes were taken out, bubbles were cleared, the cover was replace and secured, the exit hose was connected, and the thermocouple tree was inserted. After the LabVIEW program was started and the CJC set, all the thermocouples showed a constant temperature that corresponded to the temperature inside the tank.

The inlet pump had to be pre-primed with hot water in order to reduce the interface temperature that could disturb the gravity current visualization using the colored cold water. Because of the tube diameters expansion in three steps sizing, bubbles were cleared from the inlet tubes; bubbles in the incoming water could cause increased mixing in the tank and diminish the thermocline region.

Cameras are placed in location (inside the tank affront of the diffuser, and at 45° angle on the top half of the tank. Once the pump is started, the inlet gravity current is recorded for the first 200 seconds. The underwater camera was removed immediately after 200s to allow the thermocline to form without interference.

The variation of temperature in the thermocouple tree was monitored along with the green colored region, which contains the thermocline region. Thermocline thickness was measured based on the thermocouple tree temperatures taken at 2000s. This is the time when the thermocline region was expected to be within the range of the 14 thermocouples. Once the thermocouple passed this region, the program showed the temperature at the exit thermocouple; while the remaining thermocouples recorded the inlet temperature.

The tank external surface temperature was recorded every 5 minutes at the top, bottom and the middle of the tank using an infrared thermometer.

The thermocouple recorded the temperature at one second interval. The readings showed a fluctuation of 0.05 degree between each measurement, indicating 0.05 degree margin of error in each reading. With 1cm spacing between the thermocouple, thermocline thickness measurement is within 12.5 % accuracy.

Experimental and CFD Data Comparison

The CFD model was modified to account for the heat loss from the tank wall since the tank is not insulated. A heat loss coefficient was calculated based on acrylic thermal conductivity (k = 0.2 W/m·K) and tank thickness of 0.003m. Internal and external convection were calculated using the spherical tank internal and external Nusselt number correlations discussed in chapter 3. The calculated overall heat loss coefficient of 5 W/m^2 K. was applied to the external wall. Meridian conduction and heat loss from the cold part of the tank were neglected.

CFD boundary layer thickness was calculated in order to determine the inflation layers thickness required for the model. Estimation of the boundary layer thickness using flow over a flat plate was used by the given relation [151]:

$$\delta = \frac{4.91 \cdot x}{\sqrt{Re}} \qquad 6.1$$

With *x* being the distance from the inlet along the tank inside wall taken as 0.2m. This distance was calculated using the arc distance along the spherical tank wall at a 45° angle from the inlet and tank radius of 0.25m. For a Reynolds number of 600 a boundary layer thickness δ was estimated as 0.04 m. The thermal boundary layer along the wall is given by the relation [152]:

$$\frac{\delta_{th}}{\delta} = \frac{1}{1.026} \cdot Pr^{-1/3} \qquad 6.2$$

The Prandtl number of 4.9 was averaged between the cold and hot temperature as 4.9 resulting in a thermal boundary layer thickness of 0.02m.

In the CFD model, a total of seven inflation layers were constructed in the mesh at the near wall region with a grown rate of 1.2 and total thickness of 0.022 m in order improve the heat loss calculation from the tank wall in the numerical model.

Comparing Gravity Current

The first comparison made from the experiment is the inlet gravity current. The blue dye water entering the tank was video captured in slow motion at 120 frames per second. A similar video was produced by the CFD program for comparison using a 0.002 second time step. The video comparison showed the following: (1) the experiment showed taller plumes and more irregular plume formation in the first 20 seconds of the discharge compared to the CFD results, (2) the plumes are less defined in the CFD than

the experiment, (3) the spread of the incoming water along the bottom of the tank is less uniform compared to the CFD.

Photo capturing of the dyed water was done on a 45° angle tripod from the top half of the tank in order to reduce picture distortion. In order to capture the plumes at the inlet region, an underwater camera reduced distortion due to tank wall curvature. Camera placement is shown in fig. 6.13.

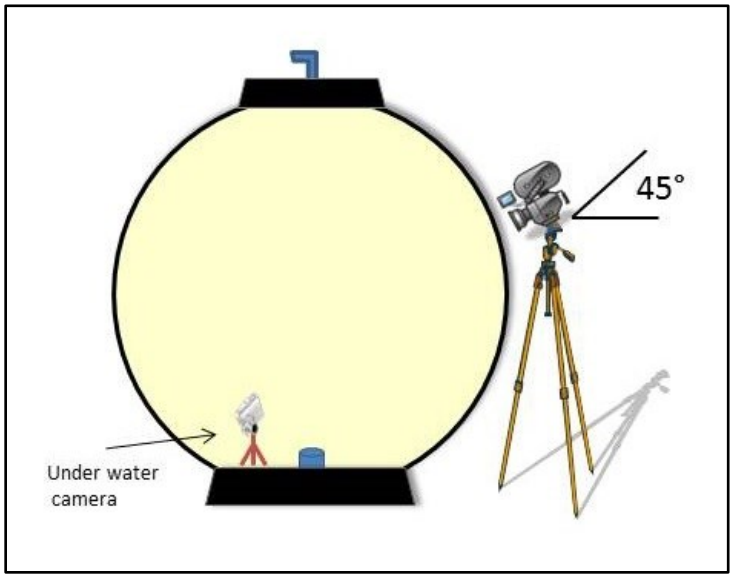

Figure 6.13 Two camera placement for gravity current capture

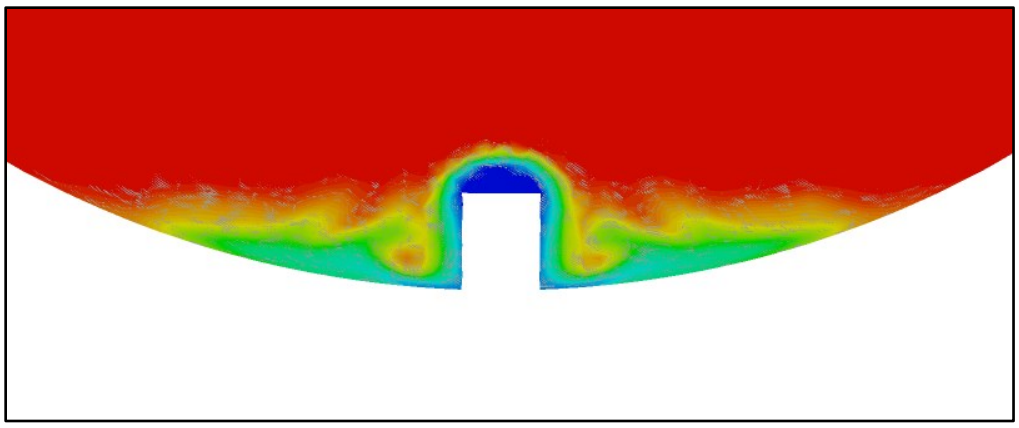

Figure 6.14 Gravity current side view using CFD

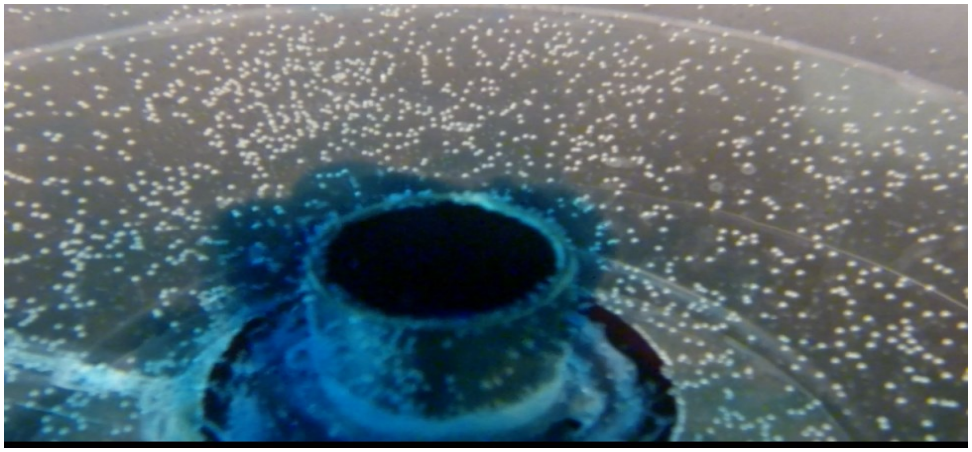

Figure 6.15 Photo of the gravity current taken by underwater camera

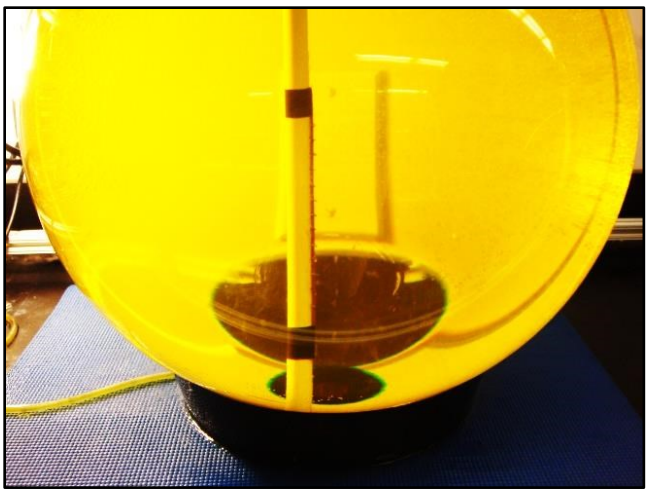

Figure 6.16 Picture distortion due to tank curvature

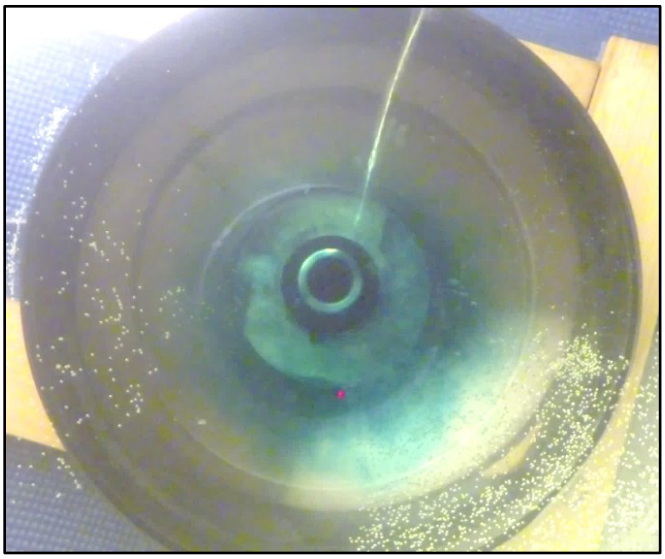

Figure 6.17 Irregular spread of gravity current

Comparing thermocline thickness

The second comparison was performed to compare the thermocline thickness in the pipe and plate diffuser at 2000s of the discharge. The complete discharge is expected at around 8000s depending on the inlet flow rate. At 2000s of the discharge, the CFD indicated that the thermocline region is completely formed and the inlet flow has no effect on its stability.

Thermocouples were distributed according to the anticipated location of the thermocline for comparison. Corresponding data points for temperature along the y axis were extracted from the CFD result for comparison. Figure 6.18 show the thermocline in green color at a time of 2000 second of the discharge. Even though the thermocline region shows a 3 cm thickness, measured by taking visually reading along a vertically straight edge, the actual thermocline region was measured to be 2 cm thicker than what is visually shown.

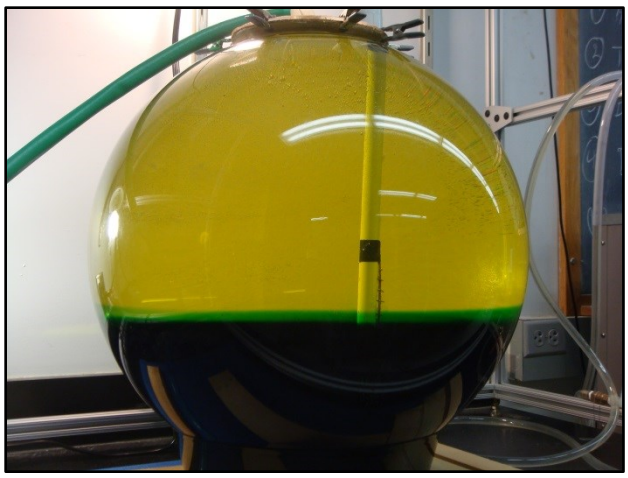

Figure 6.18 Measuring thermocline thickness using thermocouple tree at 2000s

The literature review indicated that the thermocline formation stage is the most critical to produce a thin and stable thermocline region. Once the thermocline is formed, it is carried upward without change although conduction through the walls might widen the thermocline. In addition, the effect of conduction through the thermocline region is very small compared to the heat loss from the wall or the mixing effect. The following results agree with the findings in the literature review.

The snap shots of four intervals during the discharge process show that the volume of the thermocline region remains the same while the thickness slightly changes according to the tank diameter at the thermocline level. Figure 6.19 shows snapshots of the tank thermocline region in green during 4 intervals of discharge: at 20%, 40%, 60%, and 80% of the total tank volume discharged.

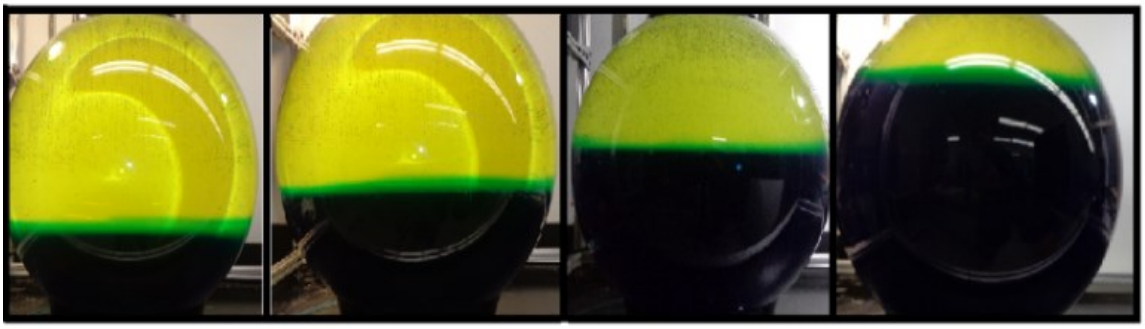

Figure 6.19. Visualization of thermocline thickness and entrainment at 20, 40, 60, & 80 percent of the discharge

The dye visualization is in agreement with the CFD results; the volume occupied by the thermocline region is constant during the discharge. The thermocline stretches out as the diameter of the tank level increases, to be the thinnest at the tank's equator, and then shrinks as the diameter decreases again, to its original thickness.

Figure 6.20 and 6.21 show the thermocline thicknesses obtained for the pipe diffuser and the pipe diffuser comparison with the CFD results:

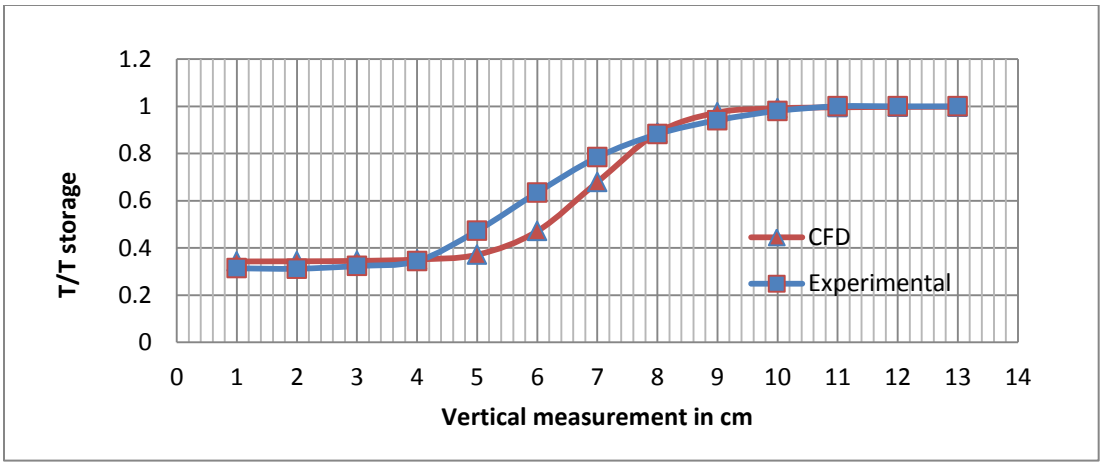

Figure 6.20 Thickness of Thermocline at 2000s in the pipe diffuser case

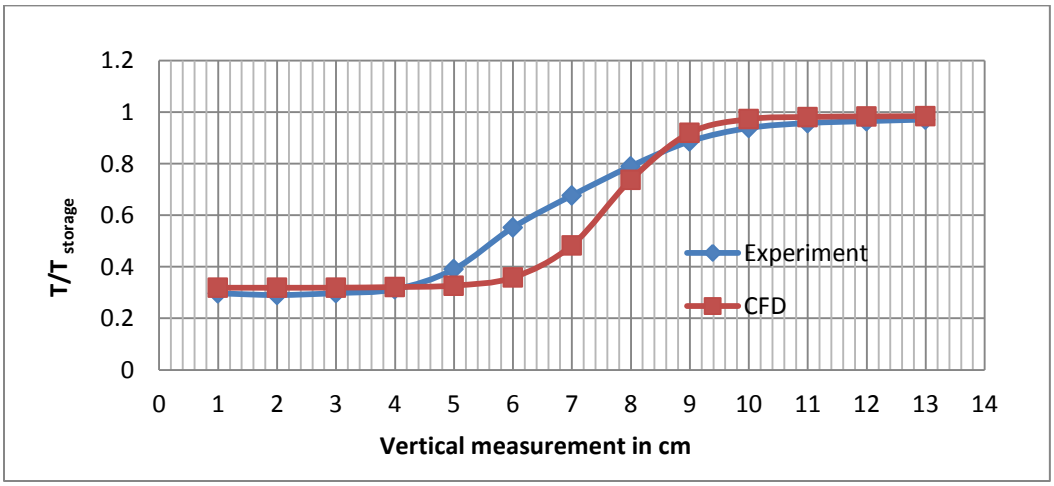

Figure 6.21 Thickness of Thermocline at 2000s in the plate diffuser case

The temperature based measurement of the thermocline region shows a thicker thermocline than the green region formed by the mixing of yellow and blue dyed water, which indicates thickening of the thermocline region due to internal convection and heat loss through the wall, and not mixing at the inlet region.

Comparing exit temperature

In order to compare the tank performance and thermocline stability during the entire discharging process, temperatures from thermocouples located at 0.02, 0.22, and 0.45m were recorded for the entire discharge process and plotted against the corresponding temperature plots obtained from the CFD for the pipe diffuser case. A similar process was performed for the plate diffuser.

The data appear to agree in the first stages of the discharge with a similar heat loss trend for all three thermocouples. However, an increase in the thermocline thickness was seen after one third of the tank has been discharged at 2500s.

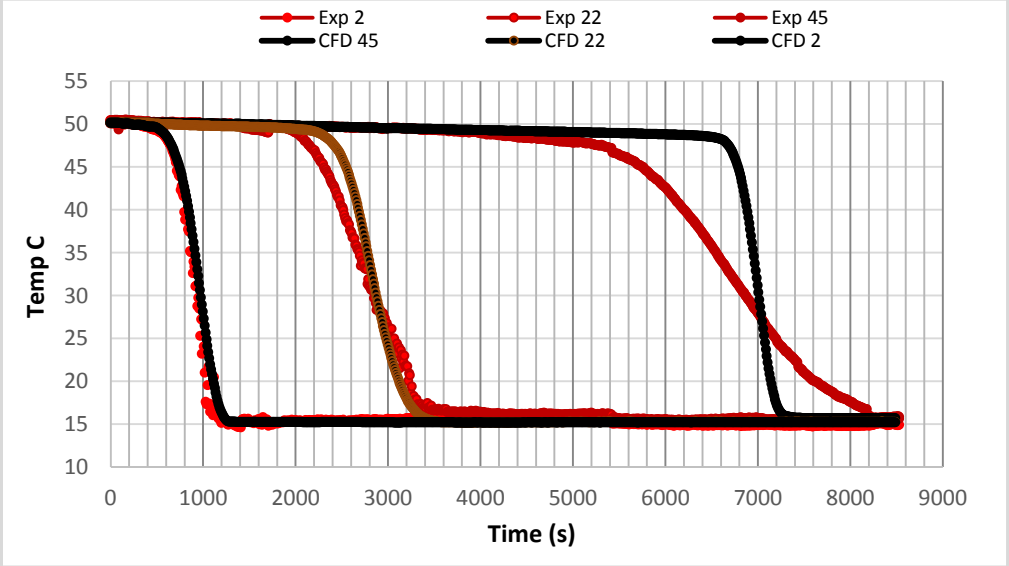

Figure 6.22 Overlay of CFD and experimental data

Data discrepancy discussion

The literature review performed earlier indicated that once the thermocline region was established, it should maintain the same volume throughout the discharge, and only heat loss from the wall can lead to thickening of the thermocline region [134]. Numerical estimation of the heat loss coefficient due to conduction through the wall, internal and external convection, led to a similar heat loss trend throughout the discharge, which indicates appropriate modeling of the heat loss function from the walls. Turbulent mixing in the top of the tank flow caused deviation from the CFD results, and was attributed to the different thermal efficiencies produced by the experimental set up [141].

In the current study, the practice of using a positive displacement pump to empty the tank was replaced by a vacuum draw of hot water from the top of the tank, for two reasons: to further reduce the mixing in the exit region in the experimental set up, and to investigate the influence of turbulence on the experimental results with the CFD data. This practice produced a slightly improved agreement with the CFD results, which indicated that the previous data disagreement was due to turbulence modeling. Figure 6.23 shows the increased mixing at the end of the discharge due to exit geometry.

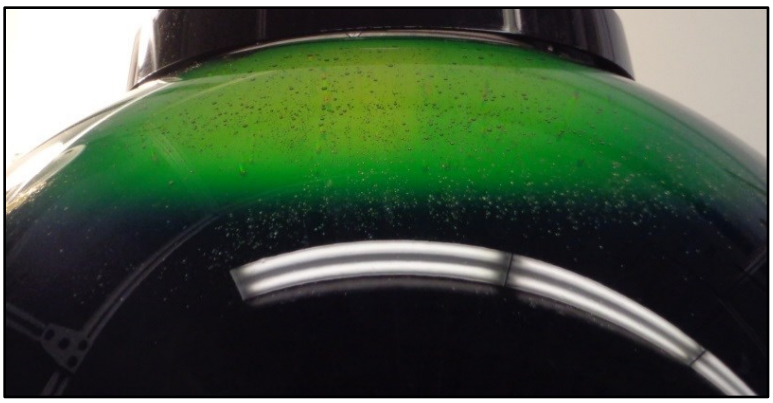

Figure 6.23 Increased mixing due to exit geometry

The experimental data obtained using siphoning instead of positive displacement with same flow parameters was compared against the CFD data and show improved results from the previously obtained results. Figure 6.24 compares CFD and experimental data for the dimensionless exit temperature versus time. The temperature is normalized with the initial storage temperature while time is scaled with the total time to empty the tank. $T_{exit}/T_{initial}$ is the temperature of at the exit of tank over the initial stored temperature, and $t/t_{empty.}$ The time the measurement was taken over the total time required to empty the tank.

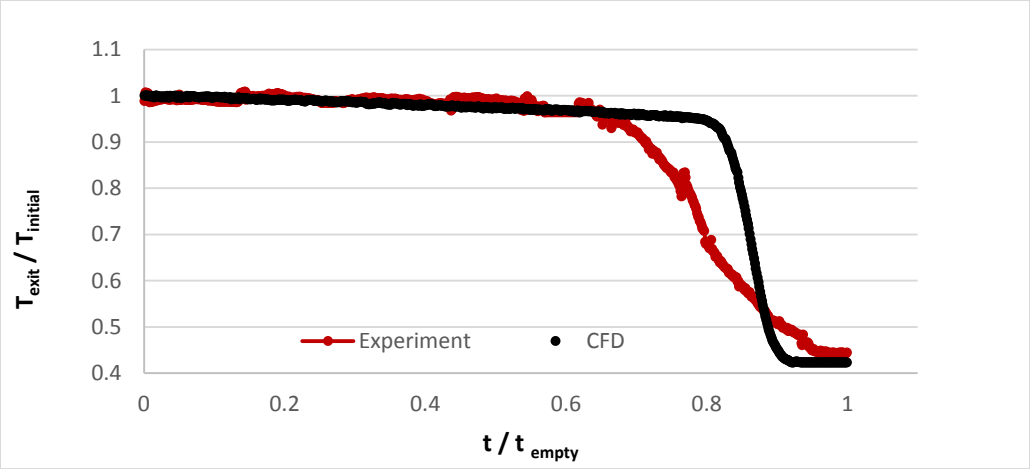

Figure 6.24 Comparison of exit temperature after using syphoning

Even though there is significant improvement of the exit temperature agreement with the CFD results, other experimental factors could lead to discrepancies such as: (1) internal convection modeling and the size of the time step, fluctuations in velocity, temperature, and oscillation, (3) outside temperature variability due to room conditions. The heat loss coefficient was calculated based on natural convection on the outside of the tank, while the room air conditioning system might have caused an air current that increased the heat loss for short periods of time.

The current CFD package is capable of internal natural convection at a low flow rate. Previous CFD studies showed that natural convection effect is realized in the CFD model using buoyancy effect with different heat transfer coefficients and variable Ra and Nu number after mesh independence has been achieved with 7.5% discrepancies between the CFD and experimental results and uncertainty of ±5 % [153-155]. Therefore, there is

little possiblity that the data discrepencies between the current expermetnal set up and the CFD model are due to natural convection inside the tank.

In a simulation study conducted by Bayon and Rojas, a mismatch similar to the current study in the temperature profile at the outlet region was deemed reasonable because the CFD model does not account for the turbulence that occurs at both the inlet and outlet, and is responsible for thickening of the thermocline region [103].

Applying a turbulence model to the CFD calculation

In order to investigate the data discrepancy between the CFD and the experimental results, the following subjects were examined: (1) exit geometry effect on the flow in the CFD model, (2) overall heat loss coefficient from the tank wall and top cover, (3) boundary layer thickness in the inside wall for free convection effect due to water cooling in the near wall area, (3) the tank in the experiment was boxed and covered to mitigate the effect of forced convection on the tank wall since the CFD model assumed free convection to the outside, (4) instruments were checked for noise and thermocouple response times, (5) finally, the experimental results were checked for repeatability.

The previous findings along with the findings in the literature suggest that the data discrepancy in the outlet region is caused by the turbulence at the exit region mainly due to the outlet shape.

The current results assume completely laminar flow; however the experimental results show notable turbulence in the outlet region, while the rest of the tank follows a laminar flow behavior. In order to get a better match for the CFD results, a suitable turbulence model for the current study should be applied. The literature suggests that the laminar flow assumption is the most appropriate for thermocline modeling for up to inlet Reynolds of 7500. However the results will deviate from the experimental results [156].

The experimental results show that the fluid follows a turbulent behavior in the inlet and outlet region, and laminar behavior in the midsection of the tank. Simulation of three regions is necessary to capture the three flow regimes. A turbulence model with variable intensity can capture the mixing that takes place in the inlet and outlet region.

Turbulence models such as: k-ε and k-ω k, and SST were investigated for the current application. Since the flow is not turbulent in the entire domain, these models are not valid [157]. These models were applied and the results showed tank thermal efficiencies that are different from the experimental data by 30 % different, and the models predict an unstable thermocline region. The v^2-f (V2F), which was recommended to resolve flow separation from curved surfaces delivered similar results to those from the SST model.

Eddy viscosity model assumes that turbulence consist of small eddies that continuously form and dissipate. The Reynolds stresses are assumed to be proportional to the mean velocity gradient [140]. Eddy viscosity turbulence model:

$$-\rho\overline{u_\iota u_j} = \mu_t\left(\frac{\partial U_i}{\partial x_j} + \frac{\partial U_j}{\partial x_i}\right) - \frac{2}{3}\delta_{ij}\left(\rho k + \mu_t\frac{\partial U_k}{\partial x_k}\right) \quad \textbf{6.3}$$

The turbulence viscosity μ_t is calculated as:

$$\mu_t = 1000\, I\, \mu \quad \textbf{6.4}$$

Where *I* is turbulence intensity is calculated based on the velocity as:

$$I = \frac{u'}{U} \quad \textbf{6.5}$$

Where the u' is the root mean square of the turbulence velocity fluctuation and U is the average Reynolds mean velocity

$$u' = \sqrt{\frac{1}{3}(u'^2_x + u'^2_y + u'^2_z)} \quad \textbf{6.6}$$

$$U = \sqrt{(U_i^2 + V_j^2 + W_k^2)} \quad \textbf{6.7}$$

The auto compute length scale uses a value calculated based on the velocity, time step and the mesh size between the nodes. Therefore, the model has a variable intensity scale based on the mesh element size and velocity. This approach is appropriate for the current study.

An eddy viscosity turbulence model with the following specification was used: (1) domain initial condition of low intensity, (2) inlet turbulence at low intensity and auto compute length scale, (3) and exit at medium intensity and ambient condition, (4) second

order equation solution, (4) high resolution advection scheme, (5) double precision, and upper limit Courant number of 2.

After the solution converged, temperature data were taken at two locations, (Y= 0.35m and Y= 0.5, which correspond to the region where the temperature starts to diverge after half the discharge and the exit location respectively. The temperature data were extracted for the entire discharge for each time step and plotted against the results obtained from the experimental set up. Thermocline thickness was calculated at 2000s and compared to experimental data. The CFD data showed the following: (1) similar thermocline thickness at 2000s, (2) similar thermocline thickening behavior to the experimental results at Y=035 m, (3) similar temperature drop profile for both locations.

However, during the last quarter of the discharge region, the water in the exit region of the tank started to stratify into three different sections as shown in fig.6.25. This stratification indicated that the mixing at the exit region was accounted during this simulation. In order to approximate the temperature profile of the exit region, temperatures values were linearly fit by: (1) using linear regression equation for data after the temperature stared to drop and the start of the stratification, (2) re-calculating the temperature at each point using the regression equation, (3) re-plotting the section with the three stratification sections. Fitting the stratified region with a linear fit resulted in similar results to the experimental data in terms of temperature drop with time and tank thermal efficiency.

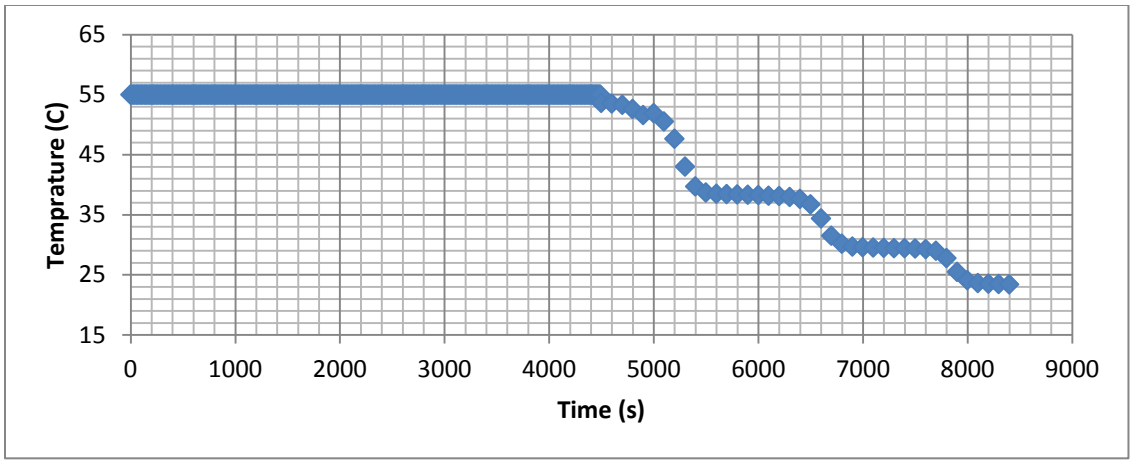

Figure 6.25 Exit temperature profile with eddy viscosity model

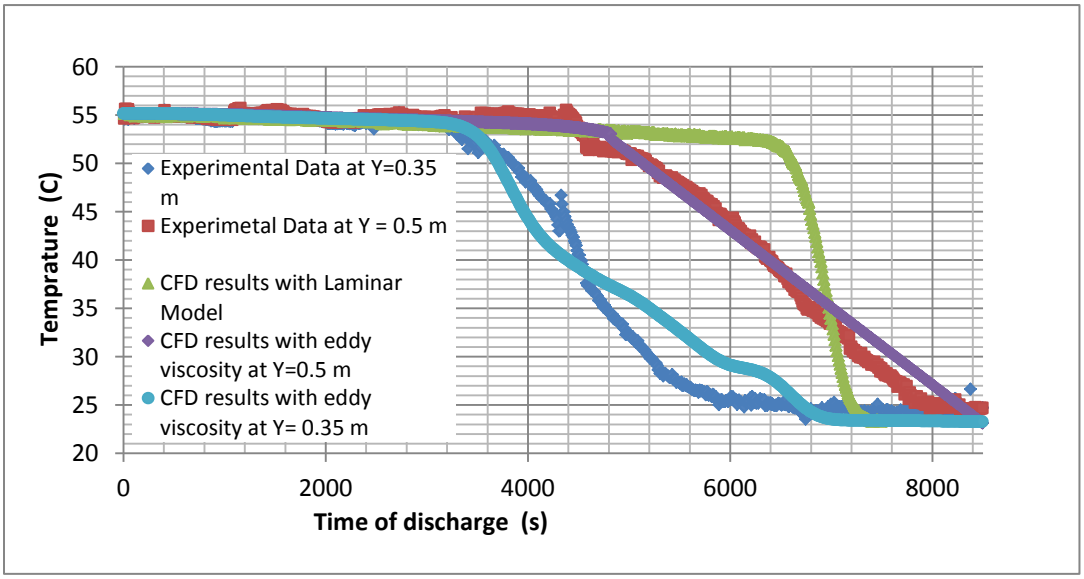

Figure 6.26 Comparison of experimental data, linearized CFD eddy viscosity model at the exit, and CFD Laminar model

The following conclusions can be drawn from these last results: the data discrepancy between the CFD data and the experimental results is due to turbulence modeling in the CFD, Eddy viscosity is the most suitable turbulence model at Reynolds number = 600, the thickening of the thermocline region at the second half of the discharge in the experimental results is due to the mismatch between the inlet and outlet shape, mixing inside the tank in the inlet and outlet region is the most influential flow aspects on the tank thermal efficiency.

Summary

The experimental data show good agreement with the CFD results in terms of predicting thermocline thickness and vertical movement inside the spherical tank. Experimental data deviation from CFD occurred only at the second half of the discharge due to the exit shape geometry and the presence of turbulence in the exit region, which causes increased mixing and results in thickening of the thermocline region. These findings are in agreement to the findings obtained in similar study by Bayon and Rajas [156], where collective experimental data from previous studies were compared to various CFD results trend. The use of a full turbulence model instead of a laminar model will lead to significantly incorrect fluid behavior in a thermocline tank. Therefore, the results obtained in the current study are sufficient to validate the CFD results within the tested flow parameters.

The gravity current produced by the experimental set up is more irregular and less uniform when compared to the CFD gravity current. The rising plumes of incoming water

have direct effect in increasing the mixing inside the tank and eventually lead to a thicker thermocline region, which could also explain the steeper thermocline temperature slope increase in the CFD results when compared to the experimental results.

Further refinement of the CFD model such as: defining different flow criteria (turbulence at the inlet and exit region, and laminar at middle of the tank) could produce better agreement. Improving the experimental exit geometry along with using two pumps of the same flow rate instead of one pump could potentially reduce the mixing in the exit region.

The prediction of the thermocline thickness and consequently the volume of the thermocline region are acceptable. The experiment showed thickening to the thermocline due to heat loss from the tank wall. Proper insulation of the tank wall has the potential of reducing the thermocline region during the discharge.

The spherical tank thermocline storage tank efficiency equations in (chapter 5) are valid with over estimation of tank's thermal efficiency by 10% due to inlet and outlet turbulence, which were neglected in the CFD model. Heat loss has to be accounted for in the thermal efficiency calculation for actual tank model since the parametric study assumed adiabatic walls.

CHAPTER 7 : APPLICATION OF SPHERICAL TANK STORAGE IN DESALINATION

This chapter will provide an overview of thermal desalination technologies and their possible coupling with renewable energy resources. Furthermore, the application of using a spherical tank as a thermal storage system for a multi-effect desalination unit will be evaluated in terms of performance and efficiency using the thermal efficient function obtained in chapter 5, along with a heat exchanger cost function.

Fresh Water Scarcity and the Need for Desalination Capacity Increase

One fifth of the human population suffers from fresh water scarcity. Water scarcity is apparent in every single continent. Moreover, twenty five percent of humans suffer from water shortages, which affect their economic growth [158]. The United Nations predicts that by 2025, 1.8 billion people will suffer from water scarcity [159] that is an increase of world water scarcity by 30%. In particular, countries located within the latitude 15-35° N face a severe shortage of fresh water [160]. Following the current climate change trend, by 2030, half of the human population will be under the threat of water shortage.

The average human need of fresh drinking water is estimated to be between 2-8 liters per person [161]. The minimum requirement of overall human needs of water, which includes drinking, hygiene, cooking, and washing is 50 liter/day [162]. Fresh

water is also directly related to agriculture and livestock, which in turn governs the food supply and regional economy. Thereby, the type of grain, vegetable and meat consumed by a region contributes to its water demand. For example it requires 1800 gallons of water to raise one pound of beef versus 10 gallons of water to raise one pound of chicken. For grain production, 60-100 gallons of water is required to grow one pound of wheat and 200 gallons to grow one pound of rice [163, 164].

Fresh water is found in lakes, rivers and some underground natural reservoirs. Rain water is collected in ponds, lakes, underground, and natural or man-made reservoirs. Alternatively fresh water can be produced from desalinating seawater and brackish (medium salinity) water, or purifying waste water. Many organizations advocate harnessing rain (natural purification of water), reducing consumption by conservation, and waste water treatment instead of increasing the manufacturing of fresh water [165]. The reasoning behind this approach is the high energy consumption associated with water desalination and the current inefficiency of water consumption and amount of wasted water in household leaks (10,000 gallon of water a year in the U.S.) of in city piping systems (36 million gallon a day in New York City alone) [166, 167]. However, this is not possible in all areas of the world. Many regions have shortages of fresh water resources to start with, due to the lack of rain, lengthy droughts, geographical location, or political conditions.

Seawater desalination is the most suitable solution for the water shortage problem in areas with no access to fresh water resources. Most of the areas with fresh water

shortages, Middle East and North Africa (MENA), are near the shoreline, which provides easy access to seawater. Additionally, the MENA area has an abundance of sunlight and wind for most of the year, which facilitate the use of alternative energy resources in water desalination.

Desalination dates back to 1684 as reported by Jim Birkett on the British Navy trials to desalinate water on board of ships [168]. The first multistage flash desalination unit was developed in the 1950s by Aqua-Chem in Wisconsin. In 1958, the office of saline water (OSW) research and development was established. The development of water desalination technology continued throughout the 1960s and the 1970s to improve the reliability, efficiency, and engineering for large scale desalination plants. Reverse osmosis (RO) was introduced in the early 1960s by Dupont with the development of a proper membrane that can filter out salt from water in moderate salinity water. The research on RO membrane continued to improve for brackish water desalination and extended to sea water capturing 70% market share by the mid-1980s.

Water desalination technologies developed significantly since then. In 2003, over 25 million m^3/day of drinkable water in the world was produced by water desalination technologies with 12,500 desalinations plants in 120 countries [169]. As of 2009, the desalination capacity has increased to 59.9 million m^3/day, with 14,451 active desalination plants in 130 countries, in addition to 244 desalination plants under construction with a capacity of 9.1 million m^3/day [170].

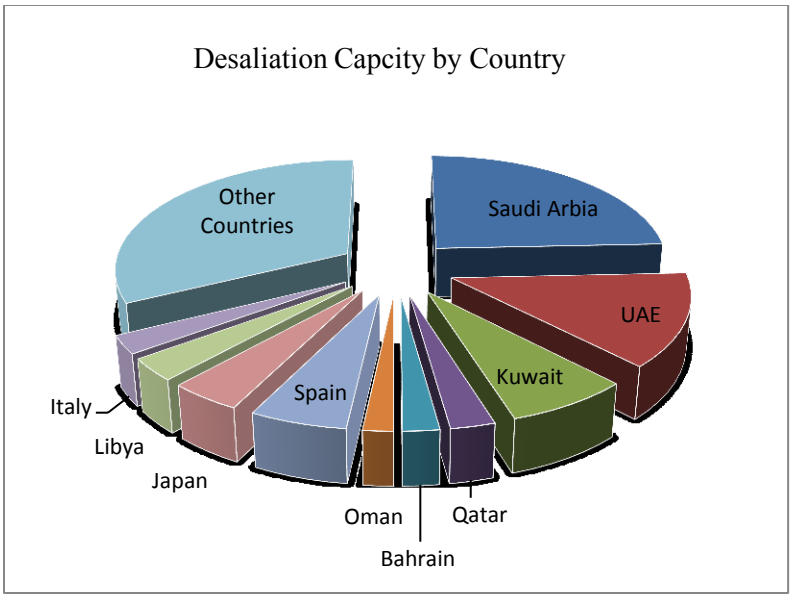

Figure 7.1 World Desalination Capacities by Country

Figure 7.1 shows the world desalination capacity by country. Saudi Arabia has the highest global desalination capacity of 18 % [171]. The United States has the second largest water desalination capacity of 17 % of the total global desalination capacity. It can be seen from Figure 7.1 that 43 % of the world water desalination production is concentrated in the Persian Gulf countries: Saudi Arabia, United Arab Emirates, Kuwait, Qatar, Bahrain, and Oman [158]. The Gulf countries have abundant solar irradiation almost all year round, which makes the use of solar thermal water desalination an attractive alternative to the current practice of burning fossil fuel for water desalination energy requirements. In Europe, Spain and Italy, which also have adequate solar irradiation for most of the year, are the main countries with seawater desalination projects.

In the United States, the demand of fresh water has increased due to industrial growth, lengthy droughts, and increased populations. As a result, the U.S. is investing more in desalination technology development in order to meet the demand. In 2003, the municipal water agencies from California, Arizona, New Mexico, Texas, and Florida gathered resources to form the "U.S. Desalination Coalition" in order to lobby for new desalinations projects [172]. New desalination plants project are funded and the research and development for water conservation and production were procured, but the demand keep growing and drought seasons are getting longer.

Currently, most of seawater desalination is achieved by burning fossil fuel e.g. fuel oil, natural gas, or coal. It requires 203 million tons of oil a year (2.36×10^{12} *kW h/year*) to produce 22 million m^3/day of fresh water (23 kg of fuel oil to produce 1 m^3 of fresh water) [173]. This large consumption of fossil fuel has significant impact on the cost of water produced and the greenhouse gas emission. Given current increasing demand and the alarming greenhouse gas level, using fossil fuel for desalination power requirement is not sustainable. Thereby, the coupling of desalination technologies with the appropriate renewable energy became an active area of research to make it more feasible and economical to use renewable energies as a mean for water desalination.

Because all water desalination technology requires either or both electrical and thermal energy, alternative energy resources such as wind or solar can be directly coupled with water desalination cycles. Seawater desalination using concentrated solar power (CSP) dates back to 1862 when the French scientist Pasteur used concentrators to direct solar rays to copper container that contained saline water. The solar irradiation caused the

water to boil and vaporize. The vapor was then guided through naturally cooled tubes, condensed, and collected as desalinated water. Small scale solar desalination units were revamped during WWI for use on board of ships or in temporary locations, which led to a variety of systems that use direct solar thermal power as solar stills or concentrated solar power (CSP). However, most of those systems were not put into practice on an industrial scale after the war due to low efficiency and small amount of fresh water produced [174].

Solar thermal desalination could be an effective solution for the southern area of the U.S. and the MENA region. Other alternative energy such as wind power and solar photovoltaics might be more practical than solar thermal power in the Northeastern region of the U.S. or northern Europe where solar irradiation is not regular and where the water salinity is not very high due to ability of PV cells to work even at moderate sunlight.

Large scale water desalination units depend largely on thermal energy, which makes coupling large scale water desalination units with CSP more viable than wind energy or solar PV. Power generation using solar thermal energy as CSP has the potential to cover 25% of the world energy demand by 2050 [175]. The use of solar thermal energy has been proven to be practical for various applications including: electricity generation, direct heating of buildings, and water desalination.

A large investment has been placed on concentrated solar power (CSP) collector to replace fossil fuel operated desalination plants in Saudi Arabia, the world largest desalination capacity [176]. Currently, 1.5 million barrel of crude oil are consumed a day

to cover the country's water demand of 3.5 million m³ of potable water. The plan is to have the largest solar power desalination plant in 2013 in the north eastern region of the country with a production capacity of 300,000 m^3 a day as a part of a series of solar desalination plants that will open as projected between the years 2016-2018.

Figure 7.2 shows the current desalination technology coupled with renewable energy sources [177]. While the share of renewable energy desalination plants of the total world desalination capacity is still small, the rapid advancement of renewable energy power generation is expediting its spread and popularity especially in the Gulf countries where desalination is taking a big toll on the local oil consumption, atmosphere and marine life.

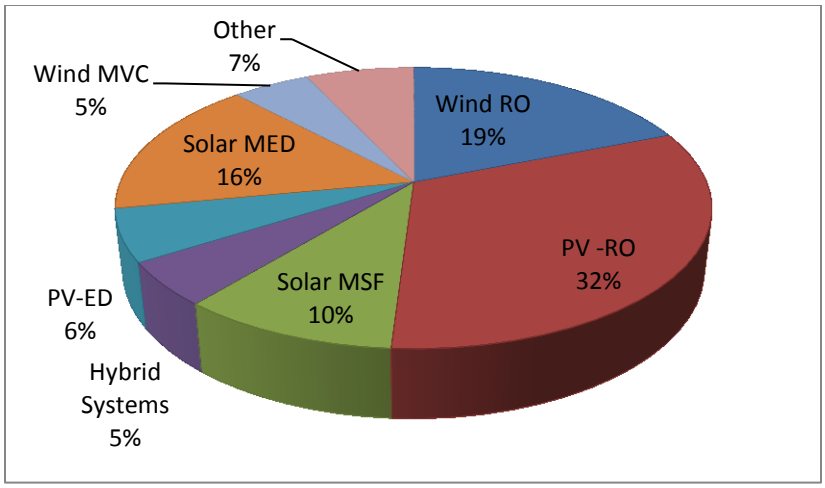

Figure 7.2 Desalination with renewable energy resources. Reverse osmosis (RO), mulistage flas (MSF), photovoltic (PV) eletrodyalsis (ED), multi-effect flash desalination(MED), mulistage vapor compression (MVC)

Types of Water Desalination Technologies

Water desalination technologies are divided into two main types: thermal water desalination and membrane water desalination. The most common thermal water desalination technologies are: Solar sills, humidification and dehumidification, multi - stage desalination, multi-effect evaporation, and vapor compression. The most common membrane desalination methods are: reverse osmosis, nano-filtration and Electrodialysis. Figure 7.3 shows a chart of the most common desalination technology and their market share of the world desalination capacity [178].

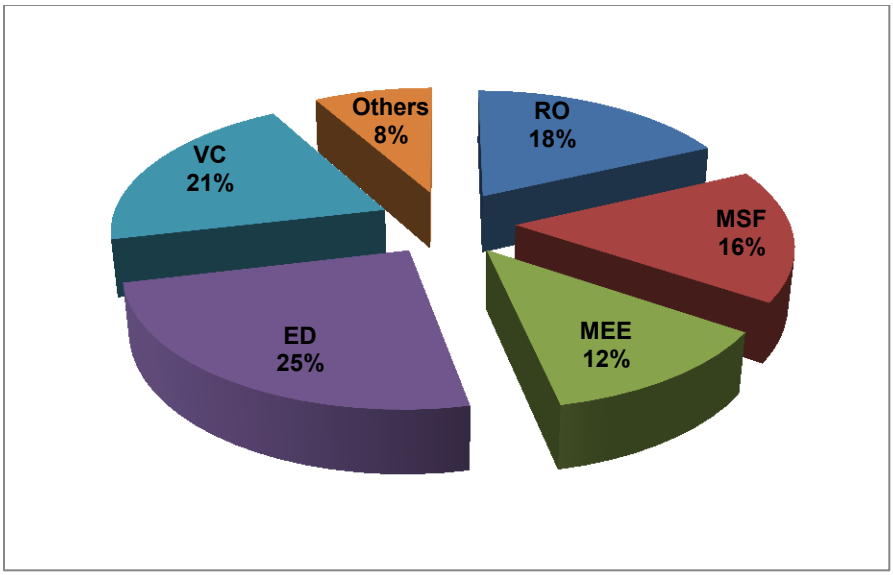

Figure 7.3 Desalination capacities by technology

In water desalination technologies, performance is evaluated by one or more of the following: (1) Thermal efficiency η, (2) gain output ration (GOR), or (3) performance ratio (PR). The thermal efficiency is calculated as [179] :

$$\eta = \frac{Q_{in} - Q_{out}}{Q_{in}} = 1 - \frac{Q_{out}}{Q_{in}} \qquad 7.1$$

Another measure of efficiency in desalination technology that is based on water evaporation and condensation is the gain output ratio (GOR), which is the total energy required to evaporate water over the heat input to the system. GOR is also a measure of the steam economy and is calculated as the amount of desalinated water to the heating steam used in the evaporator [180]. GOR is calculated as:

$$GOR = \frac{\dot{m}_p \, h_{fg}}{\dot{Q}_{in}} \qquad 7.2$$

Where $\dot{m}_p$ is the flow of condensate steam and h_{fg} is the vaporization energy evaluated at the water inlet. The GOR has a different definition, which is usually provided by the desalination unit manufacture as: the ratio of mass of desalination water produced to the mass of steam put into the system [181]. With more sophisticated heat exchangers systems GOR, up to 7.5 has been achieved [24].

The performance ratio (PR) is the third mean to evaluate the desalination technology efficiency. While the GOR is a dimensionless ratio, the performance ratio has dimensions of mass per energy. The calculation of PR varies from one study to another, and based on the unit system or the input energy calculation considered in the calculation, but mostly commonly it is the amount of fresh water produced divided by the total energy consumption of the desalination unit in kg of water per mega Joule [181].

Direct solar water desalination (Solar Stills)

In direct solar water desalination, the solar energy is used directly to evaporate water. The water vapor is then collected by a cooled pane and drained as desalinated water. This type of desalination is known as a solar still. An example of a single stage solar still without heat recovery system is shown in Figure 7.4.

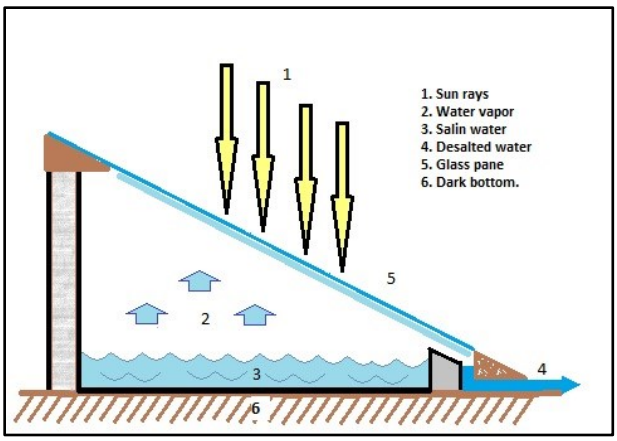

Figure 7.4 Example of solar still

The fresh water production rate of solar stills depends on the solar irradiation, which depends on the geographical location and time of the day. Daily production rate is calculated based on the area exposed to the sun irradiation, and ranges from 1-15 liters/m^2 a day without deploying a heat recovery system [182]. When a heat recovery system is used, the production rate can increase to 23 liters/m^2 a day [183]. More complex direct solar water desalination can increase the water production rate to up to 25 liters/ m^2 [a] day and solar irradiation of 4.8kWh/m^2. This is accomplished by using multi-effect solar stills, which recycle the latent heat from water evaporation and condensation to be used in the a following stage [184].

Although solar stills are simpler and more economical to construct and operate than other desalination technologies, their production rate is not appropriate for large scale production. They are more suitable for single home drinking water requirements or for use in portable systems in remote locations. Solar still technologies also have the potential of being used as a water recovery system in green houses by collecting

evaporated water in order to improve the green houses water consumption efficiency. Solar stills are characterized by a low thermal efficiency of 45 % or below.

Humidification and dehumidification (HD) desalination

Thermal water desalination by humidification and dehumidification uses air as the desalination medium to carry water vapor from one stage to another. This is performed using three main stages: (1) humidifier (evaporator), where air humidity is increased to saturation, (2) condenser, where the saturated air is then run through cooled pipes and condensate is collected, (3) heater, where the air is heated before it goes back to the humidifier again. These equipment can be arranged in various configuration based on the flow of sea water and air inside the cycle such as closed air open water (CAOW) where the air circulates inside the cycle and the water is open to salty water, and open air open water (OAOW) were air is open to the atmosphere and the water is open to salty water. In a most recent study of optimization of three configurations of HD, a GOR for up to 5.3 was achieved [180]. Other developments to HD methods can include the use of mechanical compression, heated air cycle, or membrane air drying for water recovery [185].

HD desalination is considered to be a lower energy consumption desalination technology and can be used with moderate sources of heat such as direct sunlight. Like solar stills, the most basic form of desalination, there is no need for electrical power since the cycle simulates the water cycle in nature. HD process can also be achieved using a

heat source, usually a boiler powered by fossil fuel, electricity, or solar thermal energy. It requires 2200 kJ to evaporate one liter of water [186].

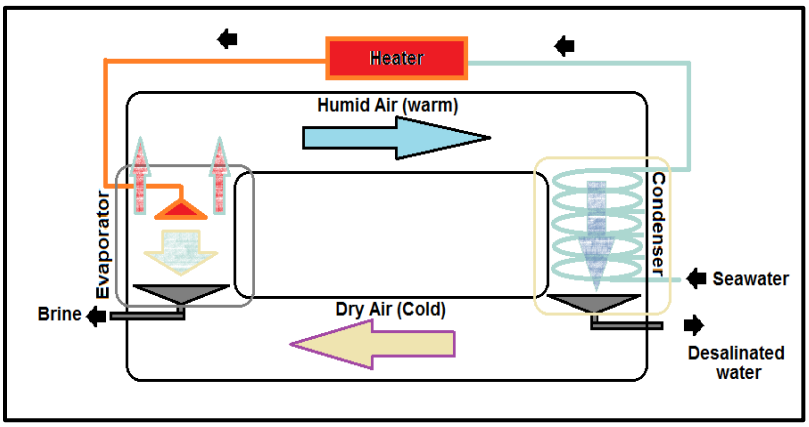

Figure 7.5 Basic CAOW HD cycle

Multi stage flash (MSF)

Multi stage flash operates on the principle of passing the heated seawater through different chambers with different pressures and different temperatures. The pressure in each chamber is set to correspond to the boiling temperature of the heated seawater at that chamber. Incoming cold seawater is used for cooling in the condensation section of the chamber where the distillate is collected and the brine water is discarded from the last stage.

For example, taking the Red sea saline water at a temperature of 20° C and salinity of 40 g/Kg, if the water was to be heated to 80° C the vapor pressure will be 46.3 kPa; therefore the first chamber should be maintained at 46.3 kPa pressure and the second

chamber should be kept at 19.5 kPa. This assumes that 20° C is the design water temperature difference between chambers. The brine water will keep evaporating throughout the stages and a condenser at each room will collect the fresh water. Figure 7.6 shows an example of a two stage flash desalination unit with 20° C cold seawater intake and boiler heating the seawater to 80° C.

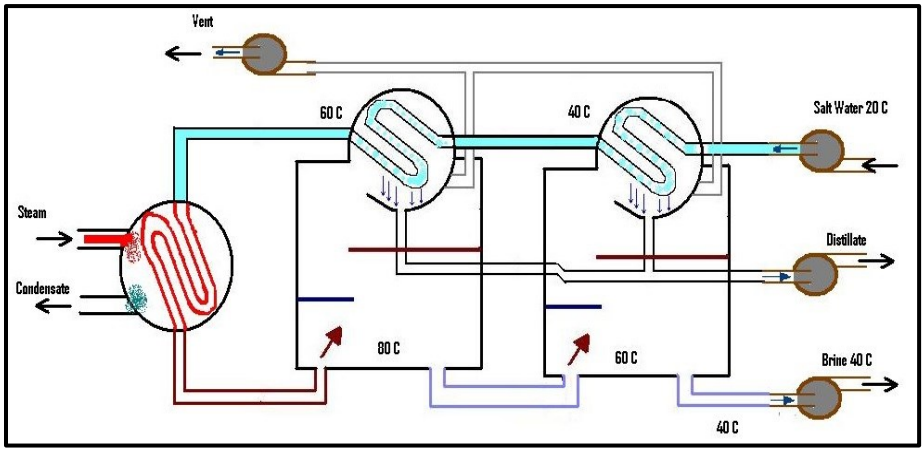

Figure 7.6 Example of two stages MSE desalination

Clearly, increasing the seawater initial temperature will increase the efficiency of the MSF. In addition, increasing the number of stages increases the GOR. However, increasing the temperature will increase the corrosion rate, which is why it is preferred to keep the incoming sea water at a relatively low temperature, 70-85° C [187]. Increasing the number of stages is dependent on the cost of construction and the required rate of production. Multi stage flash dominates the water desalination market with 70 % of the current market share in seawater desalination due to its high capacity production per unit of up to 10,000 m^3/d [158]. The suitability of MSF technology to be used for high

salinity water made it the most growing water desalination technology throughout the world for high capacity water production.

Multi-effect evaporation (MEE)

Multiple effect evaporation MEE, also known as Multi Effect Desalination MED, uses different chambers (effects) to boil water similarly to MSF desalination unit. However, the steam heat that is generated from the first boiling chamber is utilized to boil more water and generate more steam in the next effect. In this system, the heat from one effect's outlet is used to evaporate water in the next effect contrary to MSF unit where the heated sea water passes through different chambers with different pressures. An illustration of a four chambers MED unit is shown in Figure 7.7.

In an MED unit, a boiler produces steam that runs through a loop of pipes inside the first effect. Sea water is continuously sprayed on heated pipes causing the majority of sea water to evaporate. The vapor is collected from the top of the effect and directed into the second effect where it is used to heat the loop of pipes similarly to what happened in the first effect only this time it is recycling the hot vapor produced from the first effect instead of steam from the boiler. Sea water is sprayed again on the vapor pipes to be evaporated and the cycle is repeated through all the effects. The unevaporated sea water (brine) collects at the bottom of each effect and dispose of along with the cooling seawater running through the condenser in order to reduce the salinity of the MED unit discharged brine.

The efficiency of the MED unit is measured using the GOR and thermal efficiency. The thermal efficiency increases proportionally to the number of effects in the MED unit [188]. The optimum number of effects is obtained by solving the following equation for the water desalination requirement:

$$\frac{W}{A} = \left(\frac{U}{h_{fg}}\right)\left[\frac{n}{(n+1)^2}\right](\Delta T - n \cdot BPE) \qquad 7.3$$

Where: $\frac{W}{A}$ is the rate of distillate produced to the heat surface area, n is the number of effects, U is the overall heat-transfer coefficient of the piping system inside the unit, h_{fg} is the latent heat of the distillate, ΔT is the temperature drop between the first and last effect, BPE is the boiling point elevation. The temperature difference (ΔT) between effects should be more than at 0.7° C in order to have an adequate heat transfer rate.

Most multiple effect plants production is within medium capacity production of around 1000 m^3 /d [158]. In MED the more effects the plant has the more water it will produce, however increasing the number of effects results in more initial and maintenance cost. The total cost of an MED unit per unit of effect is calculated using the following equation:

$$C = An + \frac{S}{n} \qquad 7.4$$

where n is the number of effects, A is the cost of equipment, S is the cost of steam of the amount of water produced, and C is the cost per unit of effect [161]. The optimum

number of effect is provided by differentiating equation 2.4 with respect to n and setting the derivative to zero, then solving for $n_{optimum.}$

$$\boldsymbol{n_{optimum} = \sqrt{S/A}.} \qquad \textbf{7.5}$$

For a typical large desalination plant the number of effects ranges from 4-21 with performance ratio between 8-10 [189]. For more accurate cost feasibility, other component of the system such as condensers and piping should be taken into consideration as well to get more accurate economical calculation.

Even though MED is the most thermodynamically efficient desalination technology, MED lost its commercial attractiveness from the 1960s-1980s to MSF due to increased problems with scaling on the heat transfer surfaces, which limits their operating temperature and consequently leads to lower production rate [186].

Recently, MED gained more popularity over MSF due to lower operating temperature (70° C vs. 90° C), higher GOR (15 vs. 10) and lower power consumption (1.8 to 4 k W.hr /m^3) [190]. These advantages of MED made them very suitable to be coupled with renewable energy sources or to be used for waste heat reclamation systems. Current research on MED involves finding materials that will resist corrosion at higher inlet temperatures and prevent scale formation.

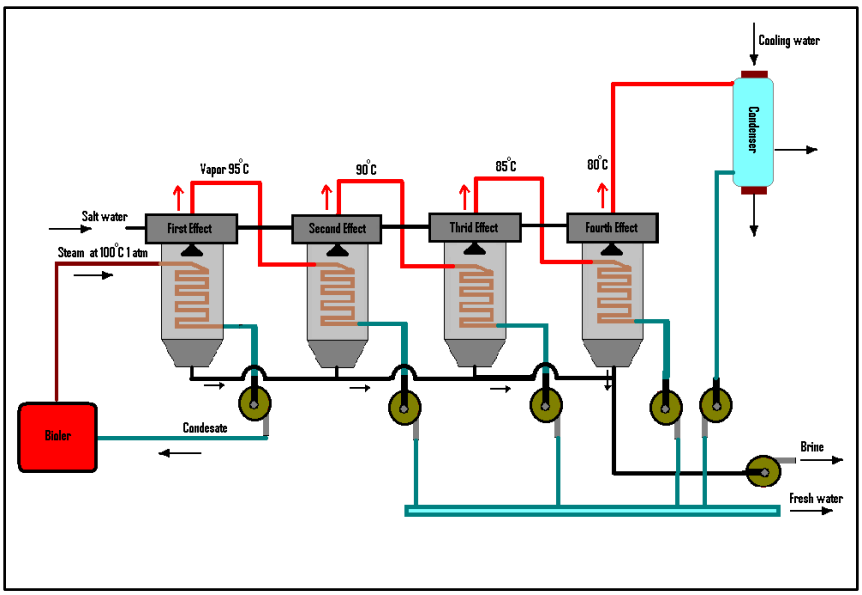

Figure 7.7 Four chamber MED unit

The theoretical minimum energy for desalination of saline water is 3 kJ/liter. This minimum amount of energy is the energy change related to salt disbanding and can be arrived at by all desalination means such as boiling point elevation, freezing point, and osmotic pressure [186]. Based on the evaporation energy required to evaporate 1 m^3 of water at 100° C, it will require 51 kg of fuel oil, 123 kg of wood, or 625 *kW.hr* of electricity [161]. The minimum power required to produce fresh water varies accordingly with the seawater salinity and the method of desalination.

Since the economics is currently the main driver for water desalination projects until carbon tax takes effect on fossil fuel operated plants, most plants rely on fossil fuel for the desalination process. Currently, coal fired desalination plants are the most pollutant and also the cheapest. However, major companies such as : eSolar, Brightsource

and Abengoa have already beaten the price of solar photovoltaic and natural gas power by using solar thermal technology and they have plans in the near future to beat the price of coal as a source of energy [12].

Solar thermal energy plants operate with similar theory to traditional fuel oil or diesel power plants, but the fuel is free. The environmental impact of solar thermal plants operation is almost negligible [191]. The theoretical values produced by the studies in [192, 193], which compete in the long run with traditional power plants, were produced at a time before the oil prices spiked to 148 $ a barrel and stabilized to around $85 as of 2012.

Even though it has been apparent from previous literature and theoretical studies that solar thermal water desalination is a feasible technology for water desalination in arid region, it has not been put into practice in an industrial scale until recently. There are several desalination plants that are actively running on solar thermal energy. Abu Dhabi solar desalination plant was established in 1984. The plant uses MED desalination technology coupled with solar thermal power [194]. The plant has maximum production capacity of 120 m^3/day and using 18 stages MED units. This plant utilizes a heat accumulator and an evaporator that enables it to run 24 hours during sunny days and process water with salinity level of 55,000 ppm. The plant was criticized for it is high maintenance cost. However, the desalination technology and solar thermal power collectors have improved significantly since the plant commission.

Another coupling of solar thermal power and MSF desalination, one of the most referenced sites of solar thermal energy, is the MSF using parabolic toughs in Kuwait plant with a production rate of 100 m^3 per day [195]. It has also been reported that in 1997 an experimental plant in Kuwait using solar powered MED did not prove to be practical in the absence of adequate solar radiation [196].

Thermo-compressors and absorption heat pumps were studied in the solar de Almeria to improve the performance of the solar water desalination, and it was reported to increase the performance ratio up to 20. However the economical aspect of the system is still under study [197]. AQUASOL has started a new initiative in 2002 to deploy the following innovations: Static CPC (Compound Parabolic Concentrator), double effect absorption heat pump, and passive solar dryer technique that are aimed to eliminate the discharged brine [197].

Computer simulation programs are utilized for performance optimization, and to estimate the desalination systems performance with new components and different possible combination. For example, the number of flash stages, solar ponds, heat storage source, etc. can be simulated now for optimization using computer software or mathematical modeling. The objective of optimizing the solar thermal desalination plant is to drive down the cost of the water produced and make it competitive to conventional plants. Since the performance of the desalination place depend on the location these optimization process has to be evaluated on a case to case basis.

Some of the obstacles that have been highlighted in the literature when using solar thermal water desalination (STWD) on a large scale are the: the low thermal efficiency, low production rate, large land requirement for heat collection [160]. Based on a review done by Fiorenza et al. the most economical alternative energy for water desalination in high capacity is high temperature solar technology using solar troughs or solar towers [158]. STWD has also been applauded for its low environmental impact, simple operation and lower maintenance. In order to maximize the use of solar thermal energy it is very essential optimize the use of two major solar energy components: (1) solar thermal collectors due to its large capital (almost half of the plant capital cost), and (2) thermal storages since the use of solar energy is always coupled with either a passive or active solar energy storage systems [5].

The next section will describe the AQUASOL MED solar desalination proposed plan in 2008, and provide possible tank sizing, and storage performance estimate using a spherical thermocline storage system.

Analysis: Spherical Tank Sizing for MED Powered by CSP

For an MED unit to perform completely on solar power, a thermal storage unit for heating the incoming sea water and a separate thermal storage unit for power generation to supply the required electrical power to run the unit (pumps, vacuum, solenoid valves, and control system) are needed.

In the most recent experimental four stages unit proposed by AQUASOL, the unit was completely run by concentrated solar power during the day. The unit was not designed to run during the night. The plant proposed adding a solar dryer for the MED discharged brine in order to reduce the impact of sea water salinity increase on marine life, and also for the purpose of economical usage of the dried sea salt [198].

The AQUASOL desalination plant is to be powered by a hybrid solar and gas power generation system that operates an MED unit with 14 effects, which produces 3 m^3/h of fresh water. Compound parabolic concentrators with an area of 500 m^2 were used for the solar field. A cylindrical tank with volume of 24 m^3 was used for the TES. A Solar dryer was used for the discharged brine evaporation.

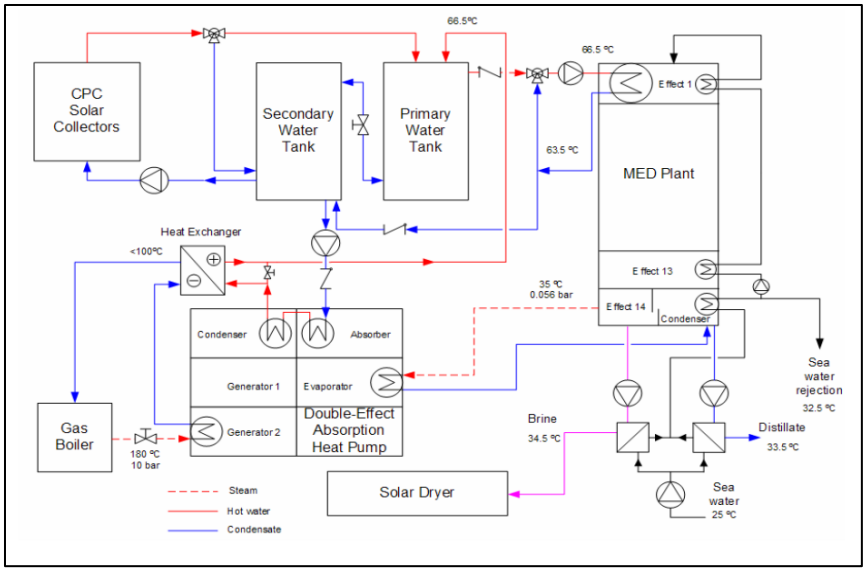

Figure 7.8 Schematic of Aquasol proposed plan [198]

The plant can run on solar only or on gas only modes. The thermal energy storage tank consisted of two tanks. The first tank was directly connected to the solar collector. Due to variable solar irradiation during the day, having the heat transfer fluid circulate in the first tank until it reach the required operating temperature is necessary before transferring the fluid to the second tank, which supplies water at constant temperature to the MED unit.

The MED unit requires hot water inflow with 66.5° C at 12 kg/s mass flow rate. The water is discharged at 62.5° C. The current thermal storage tanks are used for during day time operation not for overnight operation.

TES requirement and tank sizing

If the MED unit at AQUASOL project were to run 24 hours a day, a thermal storage tank supplying the required temperature increase of 4° C for the duration of 12 hours at mass flow rate of 12 kg/s second is needed. Additional solar collector has to be placed to provide the thermal energy required for the thermal storage.

Based on the previous findings on thermocline storage flow parameter, a higher ΔT and a lower mass flow rate are desired. The use of a thermocline storage tank will not be feasible at 4° C and mass flow rate of 12 kg/s without complete mixing of the storage fluid inside the tank and loss of thermal capacity. Therefore, the use of a heat exchanger is necessary in order to store temperature at a higher ΔT, lower flow rate to maintain a high thermal efficiency for the storage tank. Using the same time scaling criteria provided in chapter 5:

$$\boldsymbol{Pe \cdot Fo = \frac{v \cdot t}{D}} \qquad \textbf{7.6}$$

Where *v* in this case in the inlet velocity, t is the total time of discharge and *D* is the is the spherical tank diameter. The parametric study for the plate diffuser showed a *Pe·Fo* of 66. The same time scaling factor was utilized for sizing the MED storage tank in order to ensure the lowest thermocline degradation of the complete storage period.

The following section provides the sizing steps that were taken to provide the required spherical tank diameter, shell thickness, weight, heat exchanger specifications needed for the 14 stage MED desalination unit.

Tank storage size and cost function

The tank volume was calculated based on the energy storage requirement for 12 hours at a mass flow rate of 12 kg/s with a temperature difference of 4° C in order to raise the incoming sea water in the first effect of MED by the number of degrees. Therefore, the thermal storage system is responsible for increasing the temperature in the first effect from 60° C to 64° C. The storage medium selected for the application is water due to its low cost and high thermal capacity, and because the storage temperature is below the boiling point. The energy storage requirement is calculated to be $200 kW_{th}$. To account for heat exchanger losses and losses due to unpumpable volume due to thermocline occupation, and additional, 20 % increase in energy storage has to be accounted for. This results in a storage requirement of 240 kW_{th}. Based on the water thermal capacity and the temperature difference, the volume required to store this amount of energy will vary based on the ΔT for the storage as the volume was calculated based on the mass required to store the energy with variable density as given by the function:

$$\boldsymbol{\rho = 1000 \times \left[1 - \frac{(T+288.9)}{508929.2\times(T+86.1)\times(T-3.986)^2}\right]} \qquad \textbf{7.7}$$

The volume was calculated using density as a function of temperature (averaged over the inlet and outlet). The tank volume is plotted against the storage ΔT in fig 7.9.

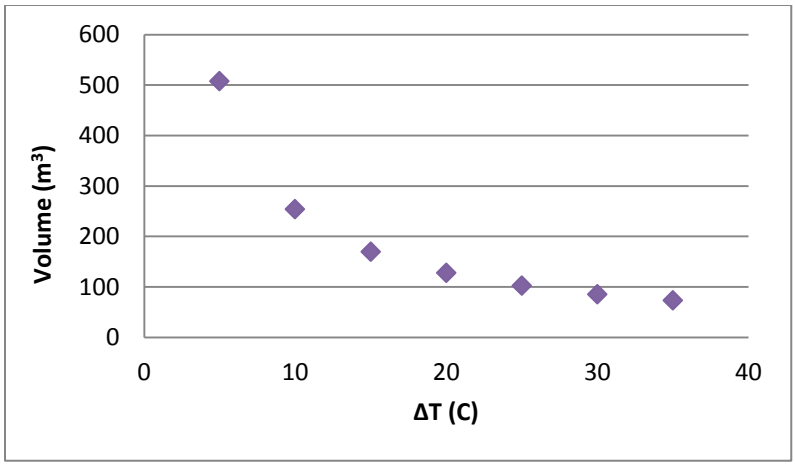

Figure 7.9 Required water volume versus ΔT

The tank volume decrease as the ΔT decreases following the equation:

$$\boldsymbol{Volume} = \mathbf{2525.7} \times (\Delta \boldsymbol{T})^{\mathbf{-0.995}} \qquad \mathbf{7.8}$$

Increasing the temperature difference (ΔT) leads to better tank stratification since it lowers the Froude number. In addition, increasing the ΔT leads to lower mass flow rate at the storage tank side, according to the application ΔT and mass flow rate. The mass flow rate at the storage tank will be lowered according to the relation:

$$\dot{\boldsymbol{m}}_{\boldsymbol{storage}} = \frac{(\Delta \boldsymbol{T} * \dot{\boldsymbol{m}})_{\boldsymbol{Application}}}{\Delta \boldsymbol{T}_{\boldsymbol{storage}}} \qquad \mathbf{7.9}$$

The lower mass flow rate results in a lower Reynolds number at the tank inlet, which along with the Froude number, are the main contributors to better tank efficiency. Therefore, using ΔT of 35 will keep the water below the boiling temperature and will deliver the best storage tank stratification.

Based on the lowest tank volume possible 73 m^3, a tank diameter of 2.6m was obtained. Nominal shell thickness of 5 mm was calculated based on hydrostatic pressure using the following equation [199]:

$$h_i = \frac{D \cdot P}{4 \cdot \frac{\sigma_c}{s_i} \cdot N + P} + C1 + C2 \qquad 7.10$$

where h_i is the minimal thickness on the vessel bottom, s_i is the safety factor, D is the tank diameter, P is the total internal hydrostatic pressure, σc is the characteristic stress value (maximum allowable stress), N is the coefficient of weld joint, $C1$ is addition due to sheet thickness tolerance, $C2$ is addition due to corrosion. Using a hydrostatic pressure of 30 kPa, maximum allowable stress of steel of 510 MPa, N = 0.85, C1= 3 x 10^{-4} mm, and C2 = 0.001mm, the minimum thickness of the vessel bottom of 0.002 m and total shell weight of 90 kg without the base and 200 kg including the braces and pillars.

Based on the shell thickness, the average wind speed at Almeria of 5m/s, and the average atmospheric temperature of 20° C, external tank isolation is necessary to counteract heat loss due to external forced convection. Conduction heat loss to the ground is higher in a cylindrical tank case than forced convection forces with respect to ground average temperature and tank storage temperature. Therefore having a suspended spherical tank will result in a lower heat loss in comparison to a cylindrical tank with ground foundation.

Heat exchanger sizing

In this section, a heat exchanger (HEX) is sized and optimized to function alongside the storage tank in order to provide the MED unit with the required flow rate and temperature difference. A cost function is obtained for both the tank and the heat exchanger to determine if using a one tank spherical thermocline system is more economical than using a separate tank system to provide the required storage energy. The TES tank and HEX are evaluated with pumping power requirement and installation costs. The cost of control system, tank installation, and piping were not accounted for in in this study.

Based on the MED unit requirement and the spherical tank thermocline TES the HEX design has the following constraints:

Table 7.1 HEX constraints with TES and MED

$\dot{m}_{tu}$ (kg/s)	**12**	T_{ish} (C°)	**80**	T_{itu} (C°)	**60**
$\dot{m}_{sh}$ (kg/s)	1.4	T_{osh} (C°)	62	T_{otu} (C°)	64
ρsh (kg/m^3)	972	ksh (W/mK)	0.62	Rf (m^{2}K/W)	0.00017
ρtu (kg/m^3)	980	Cp (kJ/kg)	4.18	μ (Pa.s)	0.0009

The surface area required for the heat transfer between the tube and shell is calculated as [152]:

$$S = \frac{Q}{U\Delta T_{LMTD}F} \quad (7.11)$$

$$\Delta T_{LMTD} = \frac{(T_{ish}-T_{otu})-(T_{osh}-T_{itu})}{ln((T_{ish}-T_{otu})/(T_{osh}-T_{itu}))} \quad (7.12)$$

$$Q = \dot{m}_{sh}C_{psh}(\Delta T_{sh}) = \dot{m}_{tu}Cp\ (\Delta T_{tu}) \quad (7.13)$$

with *F* as the correction factor and U is calculated based on the total thermal resistance as:

$$R_{tot} = R_{conv(s)} + R_{fs} + R_{cond(t)} + R_{ft} + R_{conv(t)} \quad (7.14)$$

The thermal resistance was calculated based on the convection heat loss coefficients using h_s and h_t as follows

$$h_s = 0.36 \cdot \frac{k_s}{D_e} \cdot Re_s^{0.55} \cdot Pr_s^{0.3} \quad (7.15)$$

$$D_e = \frac{4(Pt^2-(0.25\cdot\pi D_t^2)}{\pi D_t} \quad (7.16)$$

$$h_t = 0.027\frac{k_t}{D_i} \cdot Re_t^{0.8} \cdot Pr_t^{0.3} \quad (7.17)$$

The conduction heat resistance was calculated using cylindrical wall conduction resistance using:

$$R_{cond} = \frac{ln\left(\frac{ro}{ri}\right)}{2\pi kL} \quad (7.18)$$

The number of tubes was calculated by using the ratio of mass flow rates and the tube velocity that corresponds to the mass flow rate of the tube of 12 kg/s. The total length of the tube was calculated based on the tube diameter.

$$n = \frac{\dot{m}_{sh}}{\dot{m}_{tu}} \quad (7.19)$$

$$L_{tu} = \frac{S}{\pi D_o n} \quad (7.20)$$

Pressure drop in the tube side and the pressure drop in the shell side were calculated based on the water density, velocity and diameter of the tubes and the friction factor:

$$\Delta P_{tu} = \frac{\rho_{tu} {v_{tu}}^2}{2} \cdot \left(\frac{L_{tu}}{D_i} f_{tu}\right) \cdot n \quad (7.21)$$

$$\Delta P_{sh} = f_{sh} \cdot \frac{\rho_{sh} {v_{sh}}^2}{2} \cdot \left(\frac{L_{tu}}{B}\right) \cdot \left(\frac{D_{sh}}{D_e}\right) \quad (7.22)$$

$$f_{sh} = 1.44 \cdot Re_{sh}^{-0.15} \quad (7.23)$$

$$f_{tu} = (.82 \cdot log_{10} \cdot Re_{tu} - 1.64)^{-2} \quad (7.24)$$

The total power consumption was calculated using the following equation with pump efficiency of 75 percent

$$P = \frac{1}{\eta}\left(\frac{m_{tu}}{\rho_{tu}}\Delta P_{tu} + \frac{m_{sh}}{\rho_{sh}}\Delta P_{sh}\right) \quad 7.25$$

The objective function used for the optimization study considered the cost of installation of heat exchanger, pumping power consumption per year adjusted for present value based on annuity at an interest rate of 6% over the period of 10 years.

$$C_{total} = Cost_{installation} + Cost_{operation} \quad 7.26$$

$$Cost_{\ installation} = 8000 + 259.2 \cdot S^{0.91} \quad 7.27$$

$$Cost_{operation/year} = P \cdot C_{el} \cdot H \cdot D \quad 7.28$$

$$\Sigma\ Total\ Cost_{operation/year} = \frac{(1+i)^n - 1}{i(1+i)^n} \quad 7.29$$

The heat exchanger dimension were optimized in terms of the objective function, tube diameter, and tube length using Lagrange multiplier with pipe diameter between 0.01 and 0.1 m, shell velocity between (0.5-2) m/s. Figure 7.10 shows the heat exchanger cost plotted versus the inlet diameter.

The capital cost of the heat exchanger was calculated based on the cost of the inside tubes. The cost of the tubes increases with diameter, however the increasing the cost of diameter will increase the operating cost.

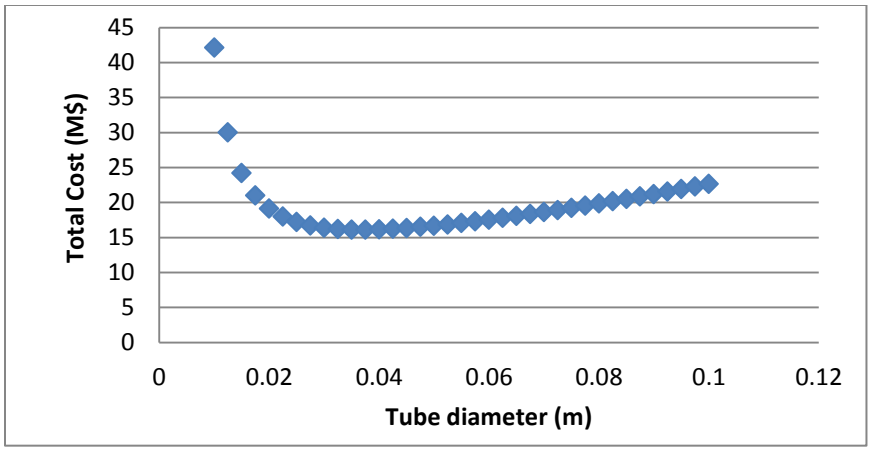

Figure 7.10 HEX cost versus tube diameter

Table 7.2 HEX optimization parameters

D_s (m)	0.195	n	17	Pr_t	3	ΔP_t (kPa)	45.6
L (m)	17.4	v_t (m/s)	0.75	h_t (W/m^2 K)	3443	ΔP_s (Pa)	945
B (m)	2	v_s (m/s)	0.77	h_s (W/m^2 K)	1141	P (*kW*)	0.75
D_o (m)	0.035	Re_t	58400	f_t	0.0167	D_e (m)	0.172
Pitch (m)	0.07	Re_s	140000	f_s	0.2776	D_s (m)	0.195
U (W/m^2 K)	702	S (m)	39	V_{TES} (m^3)	73	ΔT_{TES}	35
C_i ($)	14,125	C_o ($/yr)	350	C_{tot} ($)	17,700	C_{TES} ($)	32,300

Table 7.2 show the results of the optimized HEX design along with the cost of the TES tank. Optimization of the TES spherical tank was performed by optimizing the storage temperature, which resulted in tank size reduction, and maintaining Froude

number of 0.5. The cost of tank shell and installation was obtained based on the tank volume from tank shell manufacturing guidelines from the state of Michigan tank information section UIP 11 [87] for water tanks with the added 25% cost for spherical tank sectional welding as:

$$C_{tank} = 1.25 \times (2968 \times V^{0.5036}) \qquad 7.30$$

Using shell volume of 73 m3 and the previous HEX optimization parameters the cost of the tank is $32,000 and the total cost of the HEX is $16,198. This cost estimation showed a 50% cost saving when using a thermocline storage tank compared to constructing an additional tank in a two tank system configuration.

Summary

Using a spherical tank thermocline system for actual application in solar MED desalination results in lower TES cost than using a two tank system even with the added cost of a heat exchanger to meet the operation requirement. Utilizing a thermocline system instead of a using a one tank mixed tank result in tank size reduction by a factor of 7 based on the operation hours and the temperature difference requirement, which lead to significant saving TES in term of tank construction.

In addition, for the AQUASOL location, and based annual ambient temperature, heat loss from the tank wall and the tank base is significantly reduced by using a suspended spherical tank instead of cylindrical tank for TES.

Conclusions

This study, which focused on sensible heat storage systems in tanks, investigated the use of spherical tanks as an alternative to traditional cylindrical tanks. This is a novel practice in both two tank systems and one tank (thermocline) systems. The utilization of spherical tanks has the potential for cost savings and performance improvement of sensible TES in liquids, in both types of systems.

In two tank systems maintained at a high storage temperature (above 200° C) , the use of spherical tanks with molten salt as the storage medium resulted in possible cost savings due to a reduction in tank shell volume and insulation cost. Comparing the heat loss from spherical tanks and cylindrical tanks in molten salt storage resulted in a 30% reduction in heat loss for spherical tanks, in addition to mitigating conduction heat loss from the bottom of the tank. The practice of using a spherical tank with columns for support eliminates the need for a multilayer foundation necessary for cylindrical tanks, which is costly and requires additional construction time.

The use of spherical tanks in a two tank system results in fewer limitations that are found in the existing cylindrical tank system, including: (1) side pumping, which limits tank size and consequently the storage capacity, (2) required additional safety measures for sudden pressure increases in the system, and (3) the inability to pressurize the system and store products with a high vapor pressure.

In a one tank system at low to medium storage temperatures (between 40-100°C), spherical tanks offer alternative options to the traditional rectangular or cylindrical tanks, and they provide increased rigidity, lower heat loss, and possible improvement for tank thermal efficiency. Additional benefits can be found for underground seasonal storage. In the studied application of an MED storage requirement, the substitution of one fully mixed tank with a thermocline system resulted in a reduction in the tank size by a factor of 7. This size reduction could reflect largely on the TES cost and space allocation.

The current study identified the thermal efficiency correlation to four flow dimensionless numbers (inlet Reynolds, tank Richardson, inlet Froude, and inlet Archimedes). A CFD parametric study was performed, along with statistical tests, in order to identify the significance of the correlation between each these dimensionless parameters to the tank thermal efficiency, and to thermocline thickness. The study revealed that the inlet Froude number is the most influential dimensionless number on spherical tank thermal efficiency when using a raw pipe diffuser. In addition, when using a pipe diffuser, the maximum TE is achieved at Froude number ≤ 0.5.

The parametric CFD study led to investigating the proper diffuser for spherical tank thermocline systems, in order to produce and maintain a thermocline region at a higher Froude number (Fr >3). The investigation showed that a plate diffuser will produce the largest thermal efficiency when compared to raw pipe, radial, and circumferential diffusers. Further optimization on a plate diffuser showed that a plate diffuser with a plate size twice the inlet diameter (2d) and placed at a distance (2d) will

produce the best thermal efficiency. One additional benefit realized during the diffuser selection when using circumferential, radial or plate diffusers in a spherical tank, was the reduction of unpumpable volume when compared to cylindrical tanks.

A second parametric study using the plate diffuser was performed on thermocline thickness and thermal efficiency, and it led to producing a thermal efficiency equation based on Froude and Reynolds numbers. The plate diffuser parametric study was used to determine the standard deviation of the thermocline thickness, in order to predict the total volume occupation by the thermocline region. The prediction of the thermocline volume enabled the utilization of ramp up flow rate into the tank after the thermocline region has completely formed. This procedure reduces the mixing inside the tank, resulting in the ability of using an inlet Froude number up to 9 while maintaining the thermocline region. This practice can be useful in applications that require high flow rate into a TES system.

The computational fluid dynamic (CFD) study performed on a spherical tank was validated by an experimental set up. The result showed that the current CFD package is capable of capturing the thermocline phenomena in a spherical tank using the tested parameters, within an acceptable margin of error. The use of an eddy viscosity turbulence model with a variable turbulence intensity provided closer agreement to the experimental setup, compared to the results from a laminar flow model.

In order to test system practicality in a real case scenario, investigation into potential applications for a spherical tank thermocline system included tank sizing for TES in a solar thermal desalination MED unit. The use of a spherical one tank system

with a shell and tube heat exchanger proved to be more economical than using two tank systems or a fully mixed one tank system within the studied parameters.

In Summary, the current study investigated the use of spherical tanks in TES systems for potential cost saving and performance enhancement. Experimental and numerical considerations were provided for thermocline storage system in spherical tanks along with thermal efficiency and sizing aspects for full scale spherical thermocline system using water as the storage medium.

The role of TES continues to grow and has become essential in lowering the levelized cost of energy for solar thermal energy, as well as making solar thermal energy more viable. Future research studies on cost reduction and performance improvement in TES systems can help improve the technology and enable it to become more practical and cost effective.

REFERENCES

[1] Leone, S., 2012, "Renewable Rankings Galore: How G20 Nations Measure Up," http://www.renewableenergyworld.com/rea/news/article/2012/06/renewable-rankings-galore-how-g20-nations-measure-up.

[2] 2012, "Renewable Energy," http://www.utc.wa.gov/regulatedIndustries/utilities/energy/Pages/renewalEnergy.aspx.

[3] Hoeven, M. 2011, "Solar Energy Prospective."Renewable Energy, http://www.iea.org/about/copyright.asp

[4] Pierce, E. R., 2012, "Top 6 Things You Didnt Know About Solar Energy," http://www.energy.gov/articles/top-6-things-you-didnt-know-about-solar-energy.

[5] Tester, J. W., Drake, E. M., Driscoll, M. J., Golay, M. W., and Peters, W. A., 2005, Sustainable Energy, MIT Press, Cambridge, Chap 2-7.

[6] Wagner, S. J., 2011, "Environmental and Economic Implications of Thermal Energy Storage for Concentrated Solar Power Plants," Ph.D. Thesis, Carnegie Mellon University.

[7] 2014, "Ivanpah Project Facts," http://ivanpahsolar.com/about.

[8] Rodriguez, L. G., Marrero, A. I., and Camacho, C. G., 2001, "Comparison of Solar Thermal Technologies for Applications in Seawater Desalination," Desalination, 142, pp. 132-142.

[9] Kalogirou, S., 1998, "Use of Parabolic Trough Solar Energy Collectors," Applied Energy, 60, pp. 65-88.

[10] 2009, "Technology Overview," BrightSourceEnergy, Junba.org. http://www.junba.org/docs/junba2009/techfair/A-1-3BrighSourceEnergy.pdf

[11] Khalifa, A. N., and Al-Mutawalli, S. S., 1996, "Effect of Two-Axis Sun Tracking on the Performance of Compound Parabolic Concentrators,"Energy Converservation Management, 39(10), pp. 1073-1079.

[12] 2008, "An Industry Report on Solar Thermal Energy." http://www.solar-thermal.com/solar-thermal.pdf

[13] Qiblawey, H. M., and Banat, F., 2008, "Solar Thermal Desalination Technologies," Desalination, 220(1-3), pp. 633-644.

[14] Mancini, T. H., Peter; Butler, Barry; Osborn, Bruce; Wolfgang, Schiel; Goldberg, Vernon; Buck, Riener; Driver, Richard; Andarka, Charles; Moreno, James, 2003, "Dish-Stirling Systems: An Overview of Development and Status," Journal of Solar Energy Engineering, 125(2), p. 135.

[15] LaMonica, M., 2010, "Solar-Driven Stirling Engine Get to Work," http://www.cnet.com/news/solar-driven-stirling-engines-get-to-work/.

[16] Frazer, P. R., 2008, "Stirling Dish System Performance Prediction Model," University of Wisconsin-Madison, National Renewable Energy Laboratory.

[17] MacCracken, M. M., 2009, "Thermal Energy Storage Myths," Energy Engineering, 101(4), pp. 69-80.

[18] Gil, A., Medrano, M., Martorell, I., Lazaro, A., Dolado, P., Zalba, B., and Cabeza, L., 2010, "State of The Art on High Temperature Thermal Energy Storage for Power Generation. Part 1-Concepts, Materials and Modellization," Renewable & sustainable energy reviews, 14(1), pp. 31-55.

[19] Liu, M., Saman, W., and Bruno, F., 2012, "Review on Storage Materials and Thermal Performance Enhancement Techniques for High Temperature Phase Change Thermal Storage Systems," Renewable and Sustainable Energy Reviews, 16(4), pp. 2118-2132.

[20] Stekli, J., 2011, "Thermal Energy Storage Research," U.S. Department of Energy, http://www1.eere.energy.gov/solar/pdfs/storage_award_progress_seia.pdf

[21] Dincer, I. R., Marc, 2011, Thermal Energy Storage : Systems and Appliations, Wiley, Hoboken, N.J.

[22] Sheremet, M. A., 2011, "Mathematical Simulation of Unsteady Natural Convection Inside a Sphere," Computational Thermal Sciences, 3.

[23] Mathioulakis, E., Belessiotis, V., and Delyannis, E., 2007, "Desalination by Using Altenative Energy : Review And State-of-the-Art," Desalination, 203, pp. 346-365.

[24] Parekh, S., Farid, M. M., Selman, J. R., and Al-Hallaj, S., 2004, "Solar Desalination with a Humidification-Dehumidification Technique a Comprehinsive Technical Review," Desalination, 160, pp. 167-186.

[25] Kearney , D., Kelly, B., and Hermann , U., 2004, "Engineering Aspects of A Molten Salt Heat Transfer Fluid in a Trough Solar Field," Energy, 29 (5-6),pp. 861-70.

[26] Steinmann, W. B., J., 2005, "Analysis of Thermal Storage Systems Using Modelica," Proc. 4th International Modelica Conference,, G. Schmitz, ed., Hamburg University of Technology,, Hamburg, pp. 331-337.

[27] Bacha, H., Dammak, T., Abdualah, A., Maalej, A. Y., and Ben Dhia, H., 2003, "Desalination Unit Coupled with Solar Collectors and a Storage Tank : Modelling and Simulation," Desalination, 206, pp. 341-352.

[28] Xu, C., Wang, Z., He, Y., Li, X., and Bai, F., 2012, "Sensitivity Analysis of The Numerical Study on The Thermal Performance of a Packed-Bed Molten Salt Thermocline Thermal Storage System," Applied Energy, 92, pp. 65-75.

[29] Gabbrielli, R., and Zamparelli, C., 2009, "Optimal Design of a Molten Salt Thermal Storage Tank for Parabolic Trough Solar Power Plants," Journal of Solar Energy Engineering, 131(4), pp. 041001-041010.

[30] Moens, L., and Blake, D., 2005, Advanced heat transfer and thermal storage fluids, United States. Department of Energy.

[31] Goswami, Y. N., Sudhakar; Muley, Arun; Roe, George, 2013, "Canned Heat," Mechanical Engineering, ASME, New York, NY, pp. 36-41.

[32] Han, Y. M., Wang, R. Z., and Dai, Y. J., 2009, "Thermal Stratification within the Water Tank," Renewable and Sustainable Energy Reviews, 13(5), pp. 1014-1026.

[33] Novo, A. V., Bayon, J. R., Castro-Fresno, D., and Rodriguez-Hernandez, J., 2010, "Review of Seasonal Heat Storage in Large Basins: Water Tanks and Gravel–Water Pits," Applied Energy, 87(2), pp. 390-397.

[34] Wang, X., Liu, J., Zhang, Y., Di, H., and Jiang, Y., 2006, "Experimental Research on a Kind of Novel High Temperature Phase Change Storage Heater," Energy Conversion and Management, 47(15-16), pp. 2211-2222.

[35] Duffie, J. A., and Beckman, A. W., 2006, Solar Engineering of Thermal Processes, John Wiley & Sons. Inc., New Jersey.

[36] Farid, M. M., Khudhair, A. M., Razack, S. A. K., and Al-Hallaj, S., 2004, "A Review on Phase Change Energy Storage: Materials and Applications," Energy Conversion and Management, 45(9-10), pp. 1597-1615.

[37] Tyagi, V. V., and Buddhi, D., 2007, "PCM Thermal Storage in Buildings: a State of Art," Renewable and Sustainable Energy Reviews, 11(6), pp. 1146-1166.

[38] Zalba, B., Marín, J. M., Cabeza, L. F., and Mehling, H., 2003, "Review on Thermal Energy Storage with Phase Change: Materials, Heat Transfer Analysis and Applications," Applied Thermal Engineering, 23(3), pp. 251-283.

[39] Gabriela, L., 2012, "Thermal Energy Storage with Phase Change Material," Leonardo Electronic Journal of Practices and Technologies(20), pp. 75-98.

[40] Felix Regin, A., Solanki, S., and Saini, J., 2009, "An Analysis of a Packed Bed Latent Heat Thermal Energy Storage System Using PCM Capsules: Numerical Investigation," Renewable Energy, 34(7), pp. 1765-1773.

[41] Erek, A., and Dincer, I., 2009, "Numerical Heat Transfer Analysis of Encapsulated Ice Thermal Energy Storage System with Variable Heat Transfer Coefficient in Downstream," International Journal of Heat and Mass Transfer, 52(3-4), pp. 3-4.

[42] Michels, H., and Pitz-Paal, R., 2007, "Cascaded Latent Heat Storage for Parabolic Trough Solar Power Plants," Solar Energy, 81(6), pp. 829-837.

[43] Kikuchi, H., Watanabe, T., and Kanzawa, A., 1993, "Enhancement of Charging and Discharging Rates in a Latent-Heat Storage-System by Use of PCM with Different Melting Temperatures," Heat Recovery Systems & CHP, 13(1), pp. 57-66.

[44] Gong, Z.-X., and Mujumdar, A. S., 1996, "Cyclic Heat Transfer in a Novel Storage Unit of Multiple Phase Change Materials," Applied Thermal Engineering, 16(10), pp. 807-815.

[45] Fernandes, D., Pitié, F., Cáceres, G., and Baeyens, J., 2012, "Thermal Energy Storage: “How Previous Findings Determine Current Research Priorities”," Energy, 39(1), pp. 246-257.

[46] Hasnain, S. M., 1998, "Review on Sustainable Thermal Energy Storage Technologies, Part I: Heat Storage Materials and Techniques," Energy Conversion and Management, 39(11), pp. 1127-1138.

[47] 2014, "Solar Ponds," http://www.energyeducation.tx.gov/renewables/section_3/topics/solar_ponds/index.html.

[48] Ha, B., 1984, Sunworld, 8(1) p. 18. http://www.sunworld.com

[49] Singh, R., Tundee, S., and Akbarzadeh, A., 2011, "Electric Power Generation From Solar Pond Using Combined Thermosyphon and Thermoelectric Modules," Solar Energy, 85(2), pp. 371-378.

[50] Oppel, F., Ghajar, A., and Moretti, P., 1986, "A Numerical and Experimental Study of Stratified Thermal Storage," ASHRAE Trans.;(United States), 92(CONF-8606125-).

[51] Homan, K. O., and Soo, S. L., 1997, "Model of the Transient Stratified Flow Into a Chilled-Water Storage Tank," International Journal of Heat and Mass Transfer, 40(18), pp. 4367-4377.

[52] Yumrutaş, R., and Ünsal, M., 2012, "Energy Analysis and Modeling of a Solar Assisted House Heating System with a Heat Pump and an Underground Energy Storage Tank," Solar Energy, 86(3), pp. 983-993.

[53] Shah, L. J., and Furbo, S., 2003, "Entrance Effects in Solar Storage Tanks," Solar Energy, 74(4), pp. 337-348.

[54] Lavan, Z., and Thompson, J., 1977, "Experimental Study of Thermally Stratified Hot Water Storage Tanks," Solar Energy, 19(5), pp. 519-524.

[55] Dahghan , A., and Barzegar, A., 2011, "Thermal Performance Behavior of a Domestic Hot Water Solar Storage Tank During Consumption Operation," Energy Conversion and Management, 52(1), pp. 468-476.

[56] Haller, M. Y., Cruickshank, C. A., Streicher, W., Harrison, S. J., Andersen, E., and Furbo, S., 2009, "Methods to Determine Stratification Efficiency of Thermal Energy Storage Processes Review and Theoretical Comparison," Solar Energy, 83(10), pp. 1847-1860.

[57] Yang, Z., and Garimella, S. V., 2010, "Thermal Analysis of Solar Thermal Energy Storage in a Molten-Salt Thermocline," Solar Energy, 84(6), pp. 974-985.

[58] Van Lew, J. T., Stephens, J., Li, P., Chan, C. L., and Karaki, W., 2011, "Analysis of Heat Storage and Delivery of a Thermocline Tank Having Solid Filler Material," Journal of Solar Energy Engineering, 133(2), p. 021003.

[59] Medrano, M., Gil, A., Martorell, I., Potau, X., and Cabeza, L. F., 2010, "State of The Art on High-Temperature Thermal Energy Storage For Power Generation," Elsevier, 14, p. 56.

[60] Brosseau, D., Kelton, J. W., Ray, D., Edgar, M., Chisman, K., and Emms, B., 2005, "Testing of Thermocline Filler Materials and Molten-Salt Heat Transfer Fluids for Thermal Energy Storage Systems in Parabolic Trough Power Plants," Journal of Energy Resources Technology, 127(1), pp. 109-116.

[61] Herrmann, U., and Kearney, D. W., 2002, "Survey of Thermal Energy Storage For Parabolic Trough Power Plants," Journal of Solar Energy Engineering, 124, pp. 145-152.

[62] Zurigat, Y. H., Liche, P. R., and Ghajar, A. J., 1991, "Influence of Inlet Geometry on Mixing in Thermocline Thermal Energy Storage," International Journal of Heat and Mass Transfer, 34(1), pp. 115-125.

[63] Taylor, M., Krane, R., and Parsons, J., 1991, "Second Law Optimization of a Sensible Heat Thermal Energy Storage System With a Distributed Storage Element—Part 1: Development of the Analytical Model," Journal of Energy Resources Technology, 113, p. 20.

[64] Baines, W., Martin, W., and Sinclair, L., 1982, "On the Design of Stratified Thermal Storage Tanks," ASHRAE Trans.;(United States), 88(2).

[65] Brosseau, D., Kelton , J., Ray, D., M., E., Chisman, K., and Emms, B., 2005, "Testing of Thermocline Filler Materials and Molten-Salt Heat Transfer Fluids for Thermal Energy Storage Systems in Parabolic Trough Power Plants.," 127(109-16).

[66] Wagner, S. J., and Rubin, E. S., 2010, "Economic implications of thermal energy storage for concentrated solar thermal power," Renewable Energy(0).

[67] 2011, FE supplied-reference handbook, NCEES, Clemson, SC.

[68] Do Couto Aktay, K., Tamme, R., and Müller-Steinhagen, H., 2008, "Thermal Conductivity of High-Temperature Multicomponent Materials with Phase Change," International Journal of Thermophysics, 29(2), pp. 678-692.

[69] Laing, D., Steinmann, W.-D., Tamme, R., and Richter, C., 2006, "Solid Media Thermal Storage for Parabolic Trough Power Plants," Solar Energy, 80(10), pp. 1283-1289.

[70] Tamme, R., Laing, D., and Steinmann, W. D., 2004, "Advanced Thermal Energy Storage Technology for Parabolic Trough," Journal of Solar Energy Engineering, 126, p. 794.

[71] Nithyanandam, K., and Pitchumani, R., 2011, "Analysis and Optimization of a Latent Thermal Energy Storage System with Embedded Heat Pipes," International Journal of Heat and Mass Transfer, 54(21), pp. 4596-4610.

[72] Shabgard, H., Bergman, T. L., Sharifi, N., and Faghri, A., 2010, "High Temperature Latent Heat Thermal Energy Storage Using Heat Pipes," International Journal of Heat and Mass Transfer, 53(15), pp. 2979-2988.

[73] Laing, D., Bahl, C., Bauer, T., Lehmann, D., and Steinmann, W.-D., 2011, "Thermal Energy Storage for Direct Steam Generation," Solar Energy, 85(4), pp. 627-633.

[74] 2012, "Water Tank Guide," http://www.caldwellwatertanks.com/tank-multicolumn-overview.html.

[75] Andracchio, C. R. A., K. L., 1968, "An Experimental Study of Liquid Flow Into a Baffled Spherical Tank During Weightlessness," NASA TM X-1526, Springfield, Virginia.

[76] Dodge, F. T., 2000, "The New “Dynamic Behavior Of Liquids In Moving Containers”," NASA SP-106, Southwest Research Institute, San Antonio, Texas.

[77] 2010, "Company History," http://www.cnipvc.com/about/2/company-history.html.

[78] Yuan, S., Fengzhi, W., and Wang, Z. R., 1997, "Safety Analysis of 200 m3 LPG Spherical Tank Manufactured by The Dieless Hydro-Bulging Technology," Journal of Materials Processing Technology, 70(1-3), pp. 215-219.

[79] Hoggan, S. J., 1982, "Spherical Concrete Water Tank Design," Master of Science, Brigham Young University.

[80] Gedion, S., 2003, "Spherical Water Tanks," Leisa Magazine, p. 17.

[81] 2010, "Undergound Water Storage," http://www.thermal-storage-tanks.com/thermal-storage.html

[82] Pacheco, J. E., Showalter, S. K., and Kolb, W. J., 2002, "Development of a Molten-Salt Thermocline Thermal Storage System for Parabolic Trough Plants," ASME Journal of Solar Energy Engineering, 124(2), pp. 153-159.

[83] Aly, S., and El-Sharkawy, A., 1990, "Transient Thermal Analysis of a Spherical Liquid Storage Tank During Charging," Heat Recovery Systems and CHP, 10(5), pp. 519-526.

[84] Annaratone, D., 2007, "Pressure Vessel Design," Springer, New York.

[85] Yukio, N., 2010, "Design Recommendation for Storage Tanks And Their Supports with Emphasis on Seismic Design," Architectural Institute of Japan, Academia.edu, p. 176.

[86] Wieschollek, M. K., Maik; Hoffmeister, Benno; and Feldmann, Markus "Seismic Design of Spherical Liquid Storage Tanks," Proc. Thematic Conference on Computational Methods in Structural Dynamics and Earthquake Engineering, III ECCOMAS.

[87] 2003, "Tanks," SECTION UIP 11www.michigan.gov, pp. 1-9.

[88] 2011, "Design Recommendation for Storage Tanks and Their Supports with Emphasis on Seismic Design," Architectural Institute of Japan, Tokyo, Japan.

[89] Anttila, J., Gustafsson, J., Heinakari, M., Linja, J., and Vaihinen, M., 1996, "Spherical LNG-Tank and a Production Method for Such a Tank," Google Patents.

[90] Arne, C., 1954, "Spherical Segment Tank and Method," Google Patents.

[91] Baysinger, F. R., 1980, "Liquefied Natural Gas Tank Construction," Google Patents.

[92] Lindahl, J. R., 1993, "Tank Construction and Method of Manufacture," Google Patents.

[93] Suzuki, T., and Takenaka, N., 1975, "Method of Constructing a Spherical Tank or the Like," US Patent 3,921,555.

[94] Cengel, Y. A., 2003, Heat Transfer a Practicle Approach, McGraw-Hill, New York. Chap 2-4.

[95] Whitaker, S., 1972, "Forced Convection Heat Transfer Correlations for Flow in Pipes, Past Flat Plates, Single Cylinders, Single Spheres, and For Flow in Packed Beds and Tube Bundles," AIChE Journal, 18(2), pp. 361-371.

[96] Jafarpur, K., and Yovanovich, M., 1992, "Laminar Free Convective Heat Transfer From Isothermal Spheres: A New Analytical Method," International Journal of Heat and Mass Transfer, 35(9), pp. 2195-2201.

[97] Churchill, S. W., 1983, Heat Exchanger Design, Hemisphere Publishing, New York, NY.

[98] Sheremet, M. A., 2011, "Mathematical Simulation of Unsteady Natural Convection Inside a Sphere," Computational Thermal Sciences, 3(4), pp. 277-287.

[99] Hutchins, J., and Marschall, E., 1989, "Pseudosteady-State Natural Convection Heat Transfer Inside Spheres," International Journal of Heat and Mass Transfer, 32(11), pp. 2047-2053.

[100] Tan, F. L., 2008, "Constrained and Unconstrained Melting Inside a Sphere," International Communications in Heat and Mass Transfer, 35(4), pp. 466-475.

[101] Saitoh, T., 1983, "On the Optimum Design for Latent Heat Thermal Energy Storage Reservoir," Refregeration, 58(670), pp. 749-756.

[102] Roy, S., and Sengupta, S., 1987, "The Melting Process within Spherical Enclosures," Journal of Heat Transfer, 109(2), pp. 460-462.

[103] Bayón, R., and Rojas, E., 2013, "Simulation of Thermocline Storage for Solar Thermal Power Plants: From Dimensionless Results to Prototypes and Real-Size Tanks," International Journal of Heat and Mass Transfer, 60, pp. 713-721.

[104] Coppola, G., "Above Ground Storage Tank Design, Inspection, and Compliance Management," Proc. 14th California Unified Program Annual Training Conference, California Cupa Forum.

[105] Herrmann, U., and Kearney, D. W., 2002, "Survey of Thermal Energy Storage for Parabolic Trough Power Plants," Journal of Solar Energy Engineering, 124(2), pp. 145-152.

[106] Pacheco, J. E., 2002, "Final Test and Evaluation Results From the Solar Two Project," SAND2002-0120, January.

[107] 2014, "Factor of Safety," http://www.engineeringtoolbox.com/factors-safety-fos-d_1624.html.

[108] Barth, D. L., Pacheco, J. E., Kolb, W. J., and Rush, E. E., 2002, "Development of A High-Temperature, Long-Shafted, Molten-Salt Pump for Power Tower Applications," Journal of solar energy engineering, 124(2), pp. 170-175.

[109] Gilbert, R., and Pacheco, J., 1999, "Overview of Recent Results of the Solar Two Test and Evaluations Program," Sandia National Labs., Albuquerque, NM (US); Sandia National Labs., Livermore, CA (US).

[110] Moore, R., Vernon, M., Ho, C. K., Siegel, N. P., and Kolb, G. J., 2010, "Design Considerations for Concentrating Solar Power Tower Systems Employing Molten Salt," SANDIA, Albuquerque, NM.

[111] Herrmann, U., Kelly, B., and Price, H., 2004, "Two-Tank Molten Salt Storage for Parabolic Trough Solar Power Plants," Energy, 29(5), pp. 883-893.

[112] Institute, A. P., 2007, "Welded Tanks for Oil Storage," API Standard 650.

[113] Lin, Y., and Akins, R., 1986, "Pseudo-Steady-State Natural Convection Heat Transfer Inside a Vertical Cylinder," Journal of Heat Transfer, 108(2), pp. 310-316.

[114] McWilliams, J. C., 2006, Fundamentals of Geophysical Fluid Dynamics, Cambridge University Press.

[115] Niemela, J., Skrbek, L., Sreenivasan, K., and Donnelly, R., 2001, "Comments nn High Rayleigh Number Convection," Fluid Mechanics and its Applications, 59, pp. 269-278.

[116] Milligan, D. A., 2007, "Pressure Vessel Cost," http://matche.com/EquipCost/Vessel.htm.

[117] Cristofari, C., Notton, G., Poggi, P., and Louche, A., 2003, "Influence of The Flow Rate and the Tank Stratification Degree on the performances of a Solar Flat-Plate Collector," International Journal of Thermal Sciences, 42(5), pp. 455-469.

[118] Reeves, E. I. M. G., 1988, "Stratified Chilled-Water Storage Design Guide," Technical Report, Electric Power Reserach Institute.

[119] Nelson, J. E. B., Balakrishnan, A. R., and Srinivasa Murthy, S., 1999, "Parametric Studies on Thermally Stratified Chilled Water Storage Systems," Applied Thermal Engineering, 19(1), pp. 89-115.

[120] Bahnfleth, W. P., and Song, J., 2005, "Constant Flow Rate Charging Characteristics of a Full-Scale Stratified Chilled Water Storage Tank with Double-Ring Slotted Pipe Diffusers," Applied thermal engineering, 25(17), pp. 3067-3082.

[121] Krane, R., and Krane, M., 1992, "The Optimum Design of Stratified Thermal Energy Storage Systems—Part II: Completion of the Analytical Model, Presentation and Interpretation of the Results," Journal of Energy Resources Technology, 114, p. 204.

[122] Krane, R., and Krane, M., 1992, "The Optimum Design of Stratified Thermal Energy Storage Systems—Part I: Development of the Basic Analytical Model," Journal of Energy Resources Technology, 114, p. 197.

[123] Berkel, J. v., 1997, Thermocline Entrainment in Stratified Energy Stores, Eindhoven : Technische Universiteit Eindhoven.

[124] Yoo, H., Kim, C.-J., and Kim, C. W., 1999, "Approximate Analytical Solutions for Stratified Thermal Storage Under Variable Inlet Temperature," Solar Energy, 66(1), pp. 47-56.

[125] Osman, K., Al Khaireed, S. M. N., Ariffin, M. K., and Senawi, M. Y., 2008, "Dynamic Modeling of Stratification for Chilled Water Storage Tank," Energy Conversion and Management, 49(11), pp. 3270-3273.

[126] Zurigat, Y., Maloney, K., and Ghajar, A., 1989, "A Comparison Study of One-Dimensional Models for Stratified Thermal Storage Tanks," Journal of Solar Energy Engineering, 111(3), pp. 204-210.

[127] Jordan, U., and Furbo, S., 2005, "Thermal Stratification in Small Solar Domestic Storage Tanks Caused by Draw-Offs," Solar Energy, 78(2), pp. 291-300.

[128] Spall, R. E., 1998, "A Numerical Study of Transient Mixed Convection in Cylindrical Thermal Storage Tanks," International Journal of Heat and Mass Transfer, 41(13), pp. 2003-2011.

[129] Karim, M. A., 2011, "Experimental Investigation of a Stratified Chilled-Water Thermal Storage System," Applied Thermal Engineering, 31(11-12), pp. 1853-1860.

[130] Shin, M.-S., Kim, H.-S., Jang, D.-S., Lee, S.-N., Lee, Y.-S., and Yoon, H.-G., 2004, "Numerical and Experimental Study on The Design of a Stratified Thermal Storage System," Applied Thermal Engineering, 24(1), pp. 17-27.

[131] Walmsley, M. R., Atkins, M. J., and Riley, J., 2009, "Thermocline Management of Stratified Tanks for Heat Storage."

[132] Al-Najem, N., 1993, "Degradation of a Stratified Thermocline in a Solar Storage Tank," International Journal of Energy Research, 17(3), pp. 183-191.

[133] Yee, C. K., and Lai, F. C., 2001, "Effects of a Porous Manifold on Thermal Stratification in a Liquid Storage Tank," Solar Energy, 71(4), pp. 241-254.

[134] J. Yoo, M. W. W., C. R. Truman, 1986, "Initial Formation of a Thermocline in Simplified Storage Tanks," ASHRAE Transactions., 92(2), p. 12.

[135] Yoo, C. R. T. M. W. M. J., 1985, "Scale Modeling of Stratified Water Thermal Storage Tanks," International Symposium on Modeling Environmental Flows, The Joint ASCE/ASME Mchanics ConferenceAlbuquerque, NM.

[136] Brown, N. M., and Lai, F. C., 2011, "Enhanced Thermal Stratification in a Liquid Storage Tank With a Porous Manifold," Solar Energy, 85(7), pp. 1409-1417.

[137] Ievers, S., and Lin, W., 2009, "Numerical Simulation of Three-Dimensional Flow Dynamics in a Hot Water Storage Tank," Applied Energy, 86(12), pp. 2604-2614.

[138] Chung, J. D., Cho, S. H., Tae, C. S., and Yoo, H., 2008, "The Effect of Diffuser Configuration on Thermal Stratification in a Rectangular Storage Tank," Renewable Energy, 33(10), pp. 2236-2245.

[139] Musser, A., and Bahnfleth, W., 2001, "Parametric Study of Charging Inlet Diffuser Performance in Stratified Chilled Water Storage Tanks with Radial Diffusers: Part 2–Dimensional Analysis, Parametric Simulations and Simplified Model Development," HVAC&R Research, 7(1), pp. 51-65.

[140] ANSYS, I., 2011, "ANSYS CFX-Solver Theory Guide," ANSYS Manuel, ANSYS, Inc, http://www.ansys.com.

[141] Alizadeh, S., 1999, "An Experimental and Numerical Study of Thermal Stratification in a Horizontal Cylindrical Solar Storage Tank," Solar Energy, 66(6), pp. 409-421.

[142] Musser, A., and Bahnfleth, W., 2001, "Parametric Study of Charging Inlet Diffuser Performance in Stratified Chilled Water Storage Tanks with Radial Diffusers: Part 1–Model Development and Validation," HVAC&R Research, 7(1), pp. 31-49.

[143] 2009, "Introduction to CFX," Transient Simulations, ANSYS, Inc. https://intranet.birmingham.ac.uk/as/libraryservices/library/skills/digitaltechnologyskills/documents/public/cfxpre.pdf

[144] Ismail, K., 1997, "Models of Liquid Storage Tanks," Energy, 22(8), pp. 805-815.

[145] Eames, P. C., and Norton, B., 1998, "The Effect of Tank Geometry on Thermally Stratified Sensible Heat Storage Subject to Low Reynolds Number Flows," International Journal of Heat and Mass Transfer, 41(14), pp. 2131-2142.

[146] Fernández-Seara, J., Uhı´a, F. J., and Sieres, J., 2007, "Experimental Analysis of a Domestic Electric Hot Water Storage Tank. Part II: Dynamic Mode of Operation," Applied Thermal Engineering, 27(1), pp. 137-144.

[147] Fernández-Seara, J., Uhía, F. J., and Sieres, J., 2007, "Experimental Analysis of A Domestic Electric Hot Water Storage Tank. Part I: Static Mode of Operation," Applied Thermal Engineering, 27(1), pp. 129-136.

[148] Van Berkel, J., Rindt, C., and Van Steenhoven, A., 2002, "Thermocline Dynamics in a Thermally Stratified Store," International Journal of Heat and Mass Transfer, 45(2), pp. 343-356.

[149] 2014, "Physical Properties of Acrylic," B. i. solar, ed., Kaysons.

[150] Çengel, Y. A., 2010, Fluid Mechanics, Tata McGraw Hill Education Private.

[151] Schetz, J. A., 1984, Foundations of Boundary Layer Theory for Momentum, Heat, and Mass Transfer, Prentice-Hall.

[152] Holman, J. P., 1968, Heat Transfer, Mcgraw-Hill, New York, NY, Chap 5.

[153] Dhanawade Hanamant, S., Vijaykumar, K., and Kavita, D., "Natural Convection Heat Transfer Flow Visualization of Perforated Fin Arrays by CFD Simulation."

[154] Cho, C., Chang, K., and Park, K., 1982, "Numerical Simulation of Natural Convection in Concentric and Eccentric Horizontal Cylindrical Annuli," Journal of Heat Transfer, 104(4), pp. 624-630.

[155] Zitzmann, T., Cook, M., Pfrommer, P., Rees, S., and Marjanovic, L., "Simulation of Steady-State Natural Convection Using CFD," Proc. Proc. of the 9th International IBPSA Conference Building Simulation 2005, Montréal: IBPSA, pp. 1449-1456.

[156] Bayón, R., Rivas, E., and Rojas, E., 2014, "Study of Thermocline Tank Performance in Dynamic Processes and Stand-By Periods with an Analytical Function," Energy Procedia, 49, pp. 725-734.

[157] Bakkar, A., 2008, "Turbulence Modeling," http://www.Bakker.org.

[158] Fiorenza, G., Sharma, V., and Braccio, G., 2003, "Techno-Economic Evaluation of a Solar Powered Water Desalination Plant," Energy Conversion and Management, 44(14), pp. 2217-2240.

[159] 2006, "Water Scarcity," http://www.un.org/waterforlifedecade/scarcity.shtml.

[160] Lindblom, J., 2009, "Solar Thermal Tehcnolgies for Seawater Desalination : State of the Art," Renewable Energy Systems.

[161] Spiegler, K. S., 1962, Salt-Water Purification, John Wiley & Sons, Inc., London.

[162] Gleick, P. H., 1996, "Basic Water Requirement for Human Activities: Meeting Basic Needs," Water International, 21(2), pp. 84-92.

[163] Catanese, C., 2012, "Virtual Water, Real Impacts: World Water Day " Healthy Waters, EPA, EPA.org.

[164] Gleick, P., 2009, "Water Contents of Things," http://water.usgs.gov/edu/sc1.html.

[165] Cooley, H. G., Peter H. ; Wolff, Gary, 2006, "Desalination , with a Grain of Salt," Pacific Institute, Oakland, CA.

[166] 2014, "Water Trivia Facts," http://water.epa.gov/learn/kids/drinkingwater/water_trivia_facts.cfm.

[167] 2014, "Fix a Leak Week," http://www.epa.gov/WaterSense/pubs/fixleak.html.

[168] 2012, "Dates In Desalination History," http://www.desalination.com/museum/key-desalination-dates.

[169] Koschikowski, J., Wieghaus, M., and Rommel, M., 2003, "Solar Thermal-Driven Desalination Plants Based on Membrane Distillation," Desalination, 156(1-3), pp. 295-304.

[170] 2009, "Total World Desalination Capacity Close to 60 Million M3/Day," Desalination.biz, D&WR.

[171] Vedachalam, S., and Riha, S. J., 2012, "Desalination in Northeastern U.S. : Lessons from Four Case Studies," Desalination, 279, pp. 104-110.

[172] Levin, T., 2004, "Turning Oceans into Tap Water," NRDC, D. S. Barasch, ed.

[173] Kalogirou, S. A., 2005, "Seawater Desalination Using Renewable Energy Sources," Progress in Energy and Combustion Science, 31, pp. 242-281.

[174] Abu-Jabal, M. S., Kamiya, I., and Narasaki, Y., 2001, "Proving Test for a Solar-Powered Desalination System in Gaza-Palestine," 137(1-3), p. 6.

[175] Marcacci, S., 2013, "Is Concentrating Solar Power The Technology That Saves Humanity?," http://cleantechnica.com/2013/06/14/is-concentrating-solar-power-the-technology-that-saves-humanity-read-more-at-httpcleantechnica-com20130614is-concentrating-solar-power-the-technology-that-saves-humanity/.

[176] Hashem, H., 2012, "CSP Secures Large Portion Of Saudi's Solar Market," CSP Today, CSP Today, onine.

[177] Tzen, E., 2003, "Renewable Energy Sources for Desalination," Solar Energy, 75(5), pp. 375-379.

[178] Greenlee, L. F., Lawler, D. F., Freeman, B. D., Marrot, B., and Moulin, P., 2009, "Reverse Osmosis Desalination: Water Sources, Technology, and Today's Challenges," Water Resources, 43(9), pp. 2317-2348.

[179] Moran, M. J., and Shapiro, H. N., 2000, Fundamentals of Thermodynamics, John Wiley & Sibs, Inc., New York.

[180] Mistry, K. H., Mitsos, A., and Kienhard V, J. H., 2011, "Optimal Operating Conditions and Configurations for Humidification-Dehumidifcation Desalination Cycles," International Journal of Thermal Sciences, 50, pp. 779-789.

[181] Burgess, G., and Lovegrove, K., "Solar Thermal Powered Desalination: Membrane Versus Distillation Technologies."

[182] Kunze, H., 2001, "A new approach to solardesalination for small- and medium-size use in remote areas," Desalination, 139(1-3), pp. 34-41.

[183] Schwarzer, K., Vieira, M. E., Faber, C., and Müller, C., 2001, "Solar Thermal Desalination System With Heat Recovery," Desalination, 137(1-3), pp. 23-29.

[184] Fath, H. E. S., 1998, "Solar Distillation: a Promising Alternative for Water Provision With Free Energy, Simple Technology and a Clean Environment," Desalination, 116(1), pp. 45-56.

[185] Ettouney, H., 2005, "Design and Analysis of Humidification Dehumidification Desalination Process," Desalination, 183(1), pp. 341-352.

[186] Millier, J. E., 2003, "Review of Water Resources and Desalinatino Technologies," Sandia National Laboratories, Albuquerque.

[187] Darwish, M. A., 2012, "MSF Engineering," DESWARE Encylopedia of Desalination and Water Resources.

[188] Howe, E. D., 1974, Fundamentals of Water Desalination, Marcel Dekker, Inc., New York.

[189] Michels, T., 1993, "Recent Achievements of Low Temperature Multiple Effect Desalination in the Western Areas of Abu Dhabi. UAE," Desalination, 93(1), pp. 111-118.

[190] Khawaji, A. D., Kutubkhanah, I. K., and Wie, J.-M., 2008, "Advances in Seawater Desalination Technologies," Desalination, 221(1), pp. 47-69.

[191] Everett, B., 2008, "Solar Thermal Energy," Renewable energy, The Open University, pp. 36-64.

[192] Glueckstren, P., 1999, "Design and operation of medium and small sie desalination plants in remote areas," Desalination, 122, pp. 123-140.

[193] Goosens, M., Sablani, S., Shayya, W., Paton, C., and Al-Hinai, H., 2000, "Thermodynamic and Economic Consdieration in Solar Desalination," Desalination, 129, pp. 63-89.

[194] El-Nashar, A. M., and Samad, M., 1998, "The Solar Desalination Plant in Abudhabi 13 Years of Performance and Operation History," Renewable Energy, 14, pp. 263-274.

[195] Garzia-rodriguez, L., 2002, "Seawater Desalination Driven by Renewable Energies: A Review," Desalination, 143, pp. 103-113.

[196] Thomas, K. E., 1997, "Overview of Village Scale Renewable Energy Powered Desalination," Midwest Research Institute, Oak Ridge.

[197] Alacron, D., Blanco, J., Malato, M. I., and Sanchez, B., 2003, "Solar Thermal Seawater Distillation Activities at the Plataforma Solar De Almeria: Increasing Thermos-Economic Process Efficiency," Plataforma Solar de Almeria, Tabernas.

[198] Alarcón-Padilla, D.-C., Blanco-Gálvez, J., García-Rodríguezz, L., Gernjak, W., and Malato-Rodríguez, S., 2008, "First Experimental Results of a New Hybrid Solar/Gas Multi-Effect Distillation System: The AQUASOL Project," Desalination, 220(1-3), pp. 619-625.

[199] Sertic, D. K. J., 2006, "Optimal Wall-Thickness of the Spherical Pressure Vessel With Respect to Creterion About Minimal Mass and Equivalent Stress," Annals of the Faculty of Engineerng Hundedoara.